

Mineralogy, Mineral Chemistry, and
Paragenesis of Gold, Silver, and Base-Metal
Ores of the North Amethyst Vein System,
San Juan Mountains, Mineral County,
Colorado

U.S. GEOLOGICAL SURVEY PROFESSIONAL PAPER 1537



AVAILABILITY OF BOOKS AND MAPS OF THE U.S. GEOLOGICAL SURVEY

Instructions on ordering publications of the U.S. Geological Survey, along with prices of the last offerings, are given in the current-year issues of the monthly catalog "New Publications of the U.S. Geological Survey." Prices of available U.S. Geological Survey publications released prior to the current year are listed in the most recent annual "Price and Availability List." Publications that may be listed in various U.S. Geological Survey catalogs (see **back inside cover**) but not listed in the most recent annual "Price and Availability List" may be no longer available.

Prices of reports released to the open files are given in the listing "U.S. Geological Survey Open-File Reports," updated monthly, which is for sale in microfiche from U.S. Geological Survey ESIC—Open-File Report Sales, Box 25286, Denver, CO 80225. Reports released through the NTIS may be obtained by writing to the National Technical Information Service, U.S. Department of Commerce, Springfield, VA 22161; please include NTIS report number with inquiry.

Order U.S. Geological Survey publications **by mail** or **over the counter** from the offices given below.

BY MAIL

Books

Professional Papers, Bulletins, Water-Supply Papers, Techniques of Water-Resources Investigations, Circulars, publications of general interest (such as leaflets, pamphlets, booklets), single copies of Earthquakes & Volcanoes, Preliminary Determination of Epicenters, and some miscellaneous reports, including some of the foregoing series that have gone out of print at the Superintendent of Documents, are obtainable by mail from

**U.S. Geological Survey, Map Distribution
Box 25286, Bldg. 810, Federal Center
Denver, CO 80225**

Subscriptions to periodicals (Earthquakes & Volcanoes and Preliminary Determination of Epicenters) can be obtained **ONLY** from the

**Superintendent of Documents
Government Printing Office
Washington, D.C. 20402**

(Check or money order must be payable to Superintendent of Documents.)

Maps

For maps, address mail orders to

**U.S. Geological Survey, Map Distribution
Box 25286, Bldg. 810, Federal Center
Denver, CO 80225**

Residents of Alaska may order maps from

**U.S. Geological Survey, Earth Science Information Center
101 Twelfth Ave. - Box 12
Fairbanks, AK 99701**

OVER THE COUNTER

Books and Maps

Books and maps of the U.S. Geological Survey are available over the counter at the following U.S. Geological Survey offices, all of which are authorized agents of the Superintendent of Documents:

- **ANCHORAGE, Alaska**—Rm. 101, 4230 University Dr.
- **LAKEWOOD, Colorado**—Federal Center, Bldg. 810
- **MENLO PARK, California**—Bldg. 3, Rm. 3128, 345 Middlefield Rd.
- **RESTON, Virginia**—USGS National Center, Rm. 1C402, 12201 Sunrise Valley Dr.
- **SALT LAKE CITY, Utah**—Federal Bldg., Rm. 8105, 125 South State St.
- **SPOKANE, Washington**—U.S. Post Office Bldg., Rm. 135, West 904 Riverside Ave.
- **WASHINGTON, D.C.**—Main Interior Bldg., Rm. 2650, 18th and C Sts., NW.

Maps Only

Maps may be purchased over the counter at the following U.S. Geological Survey offices:

- **FAIRBANKS, Alaska**—New Federal Bldg., 101 Twelfth Ave.
- **ROLLA, Missouri**—1400 Independence Rd.
- **STENNIS SPACE CENTER, Mississippi**—Bldg. 3101

Mineralogy, Mineral Chemistry, and Paragenesis of Gold, Silver, and Base-Metal Ores of the North Amethyst Vein System, San Juan Mountains, Mineral County, Colorado

By NORA K. FOLEY, STANTON W. CADDEY, CRAIG B. BYINGTON, *and*
DAVID M. VARDIMAN

U.S. GEOLOGICAL SURVEY PROFESSIONAL PAPER 1537

*A study of progressive vein-related
mineralization of structures in volcanic rocks
of the San Luis and Bachelor calderas of the
San Juan volcanic field of southwestern
Colorado and its bearing on the economic
potential of the area*



UNITED STATES GOVERNMENT PRINTING OFFICE, WASHINGTON: 1993

U.S. DEPARTMENT OF THE INTERIOR

BRUCE BABBITT, *Secretary*

U.S. GEOLOGICAL SURVEY

Dallas L. Peck, *Director*

Any use of trade, product, or firm names in this publication is for
descriptive purposes only and does not imply endorsement by the
U.S. Government

Library of Congress Cataloging in Publication Data

Mineralogy, mineral chemistry, and paragenesis of gold, silver, and base-metal ores of the North Amethyst vein system, San
Juan Mountains, Mineral County, Colorado / by Nora K. Foley . . . [et al.].

p. cm. — (U.S. Geological Survey professional paper ; 1537)

Supt. of Docs. no.: I 19.16:1537

1. Gold ores—Geology—Colorado—Mineral County. 2. Ore deposits—Colorado—Mineral County. I. Foley, N.K. II.
Series.

QE390.2.G65M56 1993

553.41'09788'38—dc20

92-40595
CIP

For sale by U.S. Geological Survey, Map Distribution
Box 25286, Bldg. 810, Federal Center
Denver, CO 80225

CONTENTS

	Page		Page
Abstract.....	1	Vein Mineralogy and Compositional Ranges—Continued	
Introduction.....	1	Quartz.....	19
Acknowledgments.....	1	Silver.....	19
Geologic Setting.....	3	Sphalerite.....	19
Age of Mineralization.....	4	Stephanite.....	20
Previous Studies.....	5	Tetrahedrite-Tennantite.....	20
Style of Mineralization.....	5	Uytenbogaardtite.....	20
Character of the Ore Zones.....	6	Discussion of Mineral Equilibria.....	21
Nature of the Veins.....	6	Gold and Silver Sulfides.....	21
Mineral Textures.....	6	Carbonate Minerals.....	21
Vein Mineralogy and Compositional Ranges.....	7	Manganese Silicate Equilibria.....	21
Ag-Sulfide and Ag-Cu-Sulfide Minerals.....	7	Mineral Associations and Assemblages.....	22
Barite.....	7	Alteration and Pre-Ore Vein Assemblages.....	22
Bournonite.....	7	Sericitic Alteration.....	22
Carbonate Group Minerals.....	9	Potassium Metasomatism and Bleaching.....	23
Chalcopyrite.....	11	Manganese-Gold Association.....	25
Chlorite.....	12	Stage Alpha.....	26
Electrum.....	13	Stage Beta.....	26
Fluorite.....	15	Transitional Breccias and Sediments.....	28
Galena.....	15	Breccia-2.....	28
Gypsum.....	16	Base-Metal-Silica Association.....	29
Hematite.....	16	Stage 1.....	30
Magnetite.....	17	Stage 2.....	32
Manganese Silicate Minerals.....	17	Stage 3.....	32
Marcasite.....	18	Correlation of Mineral Assemblages With Other Vein	
Polybasite.....	18	Systems.....	32
Potassium Feldspar.....	18	Conclusions.....	37
Pyrargyrite-Proustite.....	18	References Cited.....	37
Pyrite.....	19		

ILLUSTRATIONS

	Page
FIGURE 1. Map of the San Juan volcanic field, southwestern Colorado.....	2
2. Generalized geologic map of Creede mining district and vicinity.....	3
3. Plan map showing the levels of the North Amethyst vein system.....	5
4. Photographs of North Amethyst Mn- and Au-bearing vein assemblages.....	8
5. Photographs of North Amethyst base-metal-bearing vein assemblages.....	10
6. Cross-sectional view of mine workings, North Amethyst vein system.....	11
7. Ternary diagram showing compositions of carbonates for three stages of the North Amethyst vein mineralization.....	16
8. CaCO ₃ -MnCO ₃ binary diagram showing proposed solvii from experimental studies and from studies of naturally occurring carbonates.....	17
9. Histogram of gold content of electrum occurring in stage-beta assemblages.....	17
10. Ternary diagram showing compositions of all pyroxmangite and rhodonite analyzed for stage-alpha mineralization.....	18
11-22. Diagrams showing:	
11. Progression of events in the development of the North Amethyst ores.....	23
12. Composite paragenesis for the North Amethyst mineralization.....	24

	Page
13. Early vein assemblages	25
14. Stages alpha and beta	27
15. Two periods of Mn-carbonate and Mn-silicate mineralization of stage alpha	28
16. Relation between beta-1 and beta-2 substages	29
17. Breccia and breccia fragments	30
18. Relation of stage-1 minerals to all preceding stages and breccias	31
19. Local development of breccia-3	32
20. Reopening of vein and deposition of stage-2 minerals on preexisting mineral stages and breccias	33
21. Development of breccia cemented by pink calcite	34
22. Development of stage-3 breccia.....	35

TABLES

	Page
TABLE 1. Radiometric ages of lavas, ash-flow sheets, and mineralized veins of the central caldera cluster of the San Juan Mountains, Colo	4
2. Stages of mineralization and brecciation events of the North Amethyst vein system	6
3. Assemblages and minerals of the North Amethyst vein system	12
4. Locations and descriptions of samples from the North Amethyst vein system analyzed by electron microprobe	13
5. Representative electron microprobe analyses of carbonate minerals from the North Amethyst vein system	14
6. Representative electron microprobe analyses of electrum from the North Amethyst vein system.....	14
7. Representative electron microprobe analyses of Mn-silicate minerals from the North Amethyst vein system	15
8. Representative electron microprobe analyses of sphalerite from the North Amethyst vein system	16
9. Districtwide correlation of mineral assemblages and brecciation events.....	36

MINERALOGY, MINERAL CHEMISTRY, AND PARAGENESIS OF GOLD, SILVER, AND BASE-METAL ORES OF THE NORTH AMETHYST VEIN SYSTEM, SAN JUAN MOUNTAINS, MINERAL COUNTY, COLORADO

By NORA K. FOLEY,¹ STANTON W. CADDEY,² CRAIG B. BYINGTON,² and DAVID M. VARDIMAN³

ABSTRACT

Gold-rich adularia-sericite-type mineralization occurs near the southern margin of the San Luis caldera, at the intersection of the Equity fault and the northern extension of the Amethyst fault system. Mineralized rock is confined primarily to steeply dipping structures in silicified rhyolite and dacite. Intense sericitic alteration occurs at higher levels in the vein system, and wall rock adjacent to some veins is bleached. The ores are multiply brecciated, and vein filling locally shows sedimentary textures.

Textural, mineralogical, and chemical criteria indicate that there are at least two partially coextensive associations of mineral assemblages separated by periods of brecciation and sedimentation. An older gold-bearing association consists of two fine-grained ore stages, both of which contain electrum, uytendogaardite, tetrahedrite, silver sulfosalts, silver sulfides and base-metal sulfides, and a manganese-rich stage containing the assemblages (1) manganese silicate + manganese carbonate minerals + quartz and (2) magnetite + hematite + pyrite + quartz. A younger crosscutting association contains calcite, adularia, fluorite, and quartz, plus the assemblages (1) coarse-grained base-metal sulfides and (2) hematite + chlorite + quartz. Quartz, manganese-rich calcite, and trace pyrite line late-stage vugs.

Mineralogical, lead-isotopic, and fluid-inclusion characteristics of the younger association are similar to those of ores of the southern and central parts of the Creede mining district. In contrast, the gold and manganese-silicate assemblages of the older association are rare to absent in the southern and central parts of the district. The local and early occurrence of the manganese and gold assemblages may indicate that they formed in a small hydrothermal cell that predated the extensive hydrothermal system from which ores of the central and southern parts of the Creede district are proposed to have been deposited (Bethke, 1988). If similar early-stage cells were present in the southern and central parts of the district, they may have been replaced or overprinted by later assemblages, and they may remain to be discovered. In the latter case, mineral assemblages that formed at early stages in the paragenesis hold the most promise for gold exploration.

INTRODUCTION

The North Amethyst vein system is located just south of the Continental Divide along the southern margin of

the San Luis caldera in Mineral County, Colo. (fig. 1). The precious- and base-metal-bearing veins fill structures of the east-west-trending reverse Equity fault and steeply dipping structures related to an extension of the north-northwest-trending normal Amethyst fault system (fig. 2). These structures cut rhyolitic and rhyodacitic volcanic tuffs and flows of the central caldera cluster of the San Juan volcanic field. The veins lie just inside the northern boundary of the historic Creede mining district.

Homestake Mining Company discovered the Au-bearing ores and delineated an extensive high-grade zone adjacent to old workings of the near-surface Equity mine. Available published geologic descriptions of the mineralized rocks of the North Amethyst vein system are limited mainly to historical reports on the Equity mine (Emmons and Larsen, 1913; 1923) and some preliminary studies of the newly discovered ores (S.W. Caddey and C.B. Byington, oral commun., 1988; Plumlee and others, 1989).

This paper, part of a detailed investigation of the petrology of the complex ores of the North Amethyst vein system, concentrates on the mineralogy of the Au-rich areas exposed by underground workings. The mineralogy, mineral chemistry, and paragenesis of the ore of the North Amethyst veins, with limited petrologic interpretation, are presented here. A comparison is made with Ag- and base-metal-rich mineralization of the southern Amethyst, Bulldog Mountain, P, and OH veins of the main Creede mining district. Only a limited amount of petrologic interpretation is included in this paper; instead, the paper focuses on the mineralogy and stage assemblages. The petrology, fluid-inclusion thermometry, and lead-isotopic geochemistry of the vein system are described by Foley (1990).

ACKNOWLEDGMENTS

Homestake Mining Company discovered the veins that constitute the North Amethyst system in 1983 as the

Manuscript approved for publication October 14, 1992.

¹U.S. Geological Survey.

²Homestake Mining Company, Golden CO 80401.

³Homestake Mining Company, Lead, SD 57754.

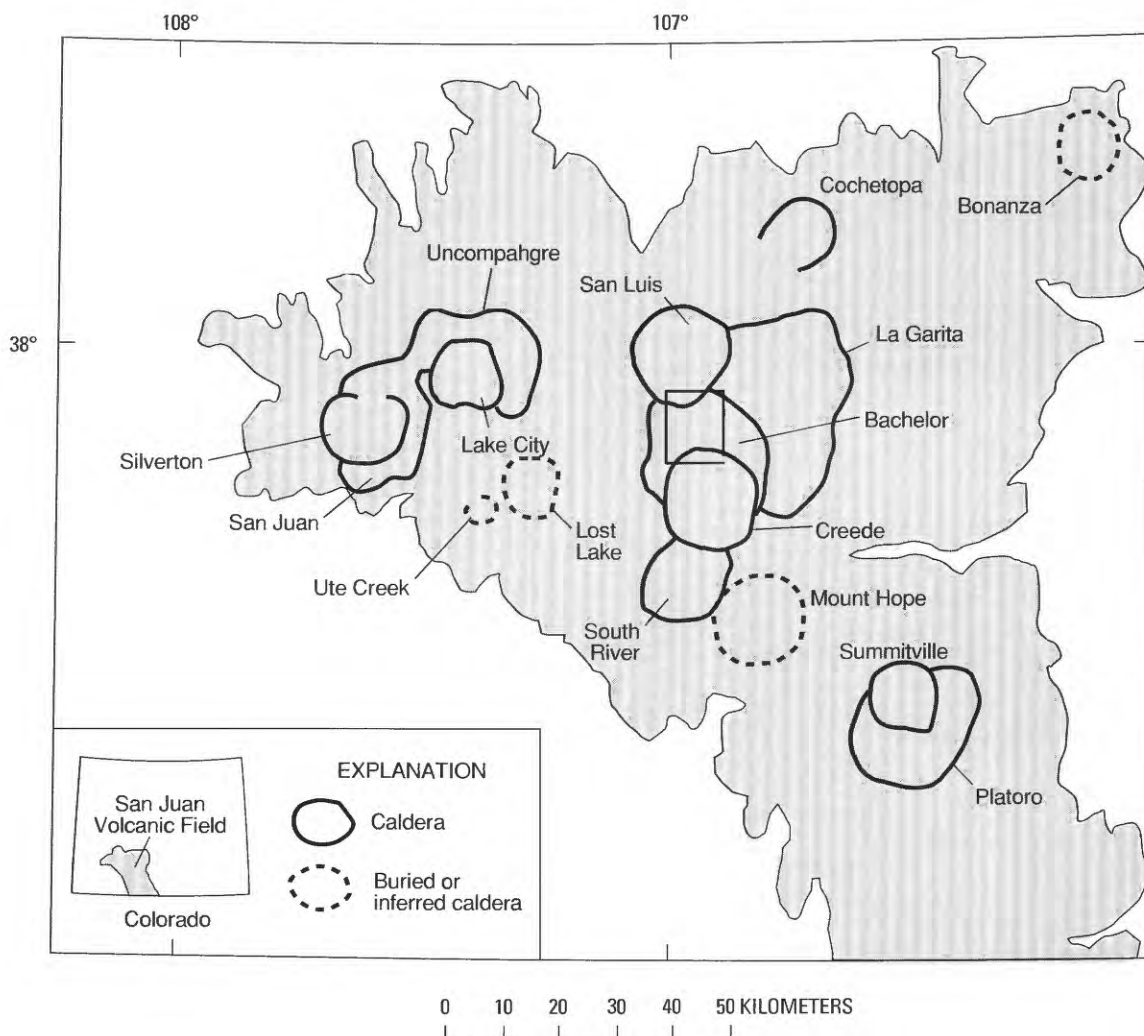


FIGURE 1.—The extent of the major ash-flow tuffs and associated calderas in the San Juan volcanic field (SJVF) in southwestern Colorado. From Plumlee (1989), after Steven and Lipman (1976), and incorporating changes suggested by Lipman and Sawyer (1988). The box in the center outlines the area of figure 2, a map of the Creede mining district and vicinity.

result of an extensive drilling program (S.W. Caddey and C.B. Byington, oral commun., 1988; Plumlee and others, 1989). Homestake Mining Company generously provided access to exploratory workings of the North Amethyst vein and the opportunity to study some aspects of the newly discovered mineralization. Stanton W. Caddey, Craig B. Byington, and David M. Vardiman, Homestake Mining Company geologists who discovered and developed the veins, contributed their time and their knowledge of the underground workings. They provided access to samples collected throughout the development of the underground workings and therefore improved the interpretations of hand-sample textures and vein relations.

The senior author would like to thank Paul B. Barton, Jr., and Philip M. Bethke of the U.S. Geological Survey (USGS) for suggesting that she undertake this project

and for providing an initial set of samples. Geoffrey S. Plumlee of the USGS also contributed samples and took some of the underground photographs. Careful reviews of this manuscript by Robert A. Ayuso (USGS), Paul B. Barton, Jr., Philip M. Bethke, James R. Craig (Virginia Polytechnic Institute and State University), Geoffrey S. Plumlee, and Gilpin R. Robinson, Jr. (USGS), have improved both its content and presentation. Much of this manuscript constitutes a part of the senior author's Ph.D. dissertation. Conversations with H.E. Belkin, J.M. Hammarstrom, D.O. Hayba, Pamela Heald, J.S. Huebner, M.J.K. Flohr, P.M. Okida, J.F. Slack, and D.S. Sweetkind, all colleagues at the USGS, were invaluable throughout the duration of the study. J.J. McGee and J.V. Emery provided guidance in use of the electron microprobe.

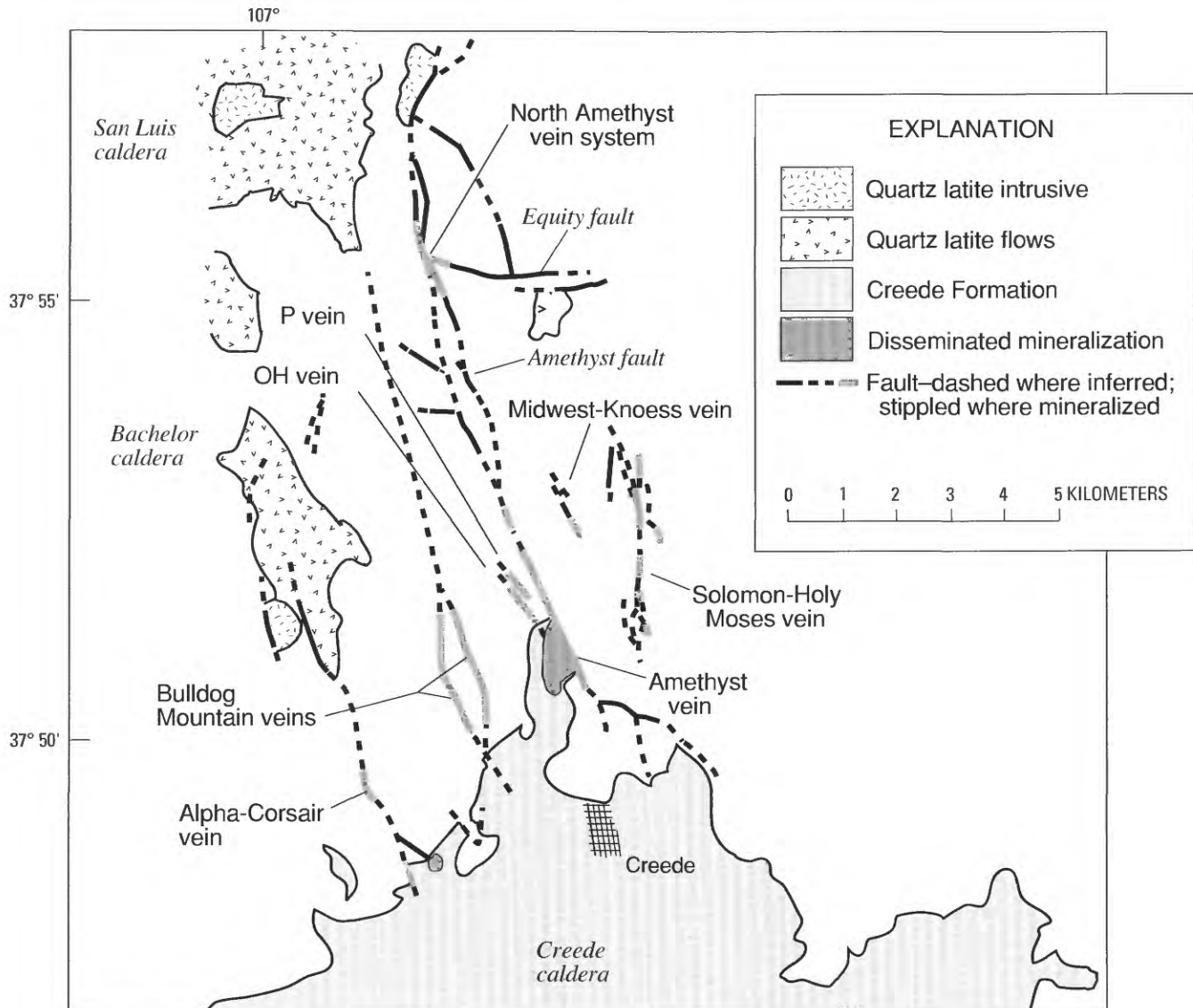


FIGURE 2.—Generalized geology of the Creede mining district and vicinity. The graben that is formed by the faults is within the Bachelor caldera and links the San Luis and Creede calderas. The North Amethyst vein system is at the intersection of the Equity fault and the Amethyst fault. From Plumlee (1989); geology after Bethke and Lipman (1987) and Lipman and Sawyer (1988).

GEOLOGIC SETTING

The San Juan volcanic field is an erosional remnant of a much larger volcanic field that covered part of the southern Rocky Mountains in the middle Tertiary (Steven, 1975; Lipman and others, 1978). The present extent of the major ash-flow tuffs and their associated calderas is shown in figure 1. The volcanic field rests upon an eroded base consisting of crystalline metavolcanic, metasedimentary, and granitoid rocks of Proterozoic age, and, possibly, remnants of Paleozoic, Mesozoic, and Tertiary sedimentary rocks (summarized by Steven and Lipman, 1976; Lipman and others, 1978; Baars and Stevenson, 1984; Gries, 1985; Bickford, 1988). The composite volcanic field consisted dominantly of andesite-

dacite lavas and associated volcanoclastic rocks erupted from precaldera-stage volcanoes in early Oligocene time, mainly between 35 and 30 Ma. A large negative Bouguer gravity anomaly underlies much of the San Juan volcanic field and is believed to reflect a large composite batholith emplaced beneath the field (Plouff and Pakister, 1972). From about 28 to 26 Ma (table 1), the central San Juan volcanic field experienced widespread silicic ash-flow eruptions and related caldera subsidence (Lipman and others, 1970, 1978; Lipman and Sawyer, 1988; Lanphere, 1988). The mineral deposits of the Creede district are located in a complex set of nested calderas formed by the pyroclastic eruptions.

The most volumetrically important sediments that accumulated within the San Juan area during the middle

TABLE 1.—Radiometric ages of lavas, ash-flow sheets, and mineralized veins of the central caldera cluster of the San Juan Mountains, Colo., given in generalized chronological order

Volcanic rock or vein mineral	Age (Ma)	Caldera	Reference
OH vein illite-smectite.....	24.8±1.3.....	Bachelor.....	Vergo (1987).
North Amethyst vein adularia.....	25.1±0.1.....	San Luis.....	Lanphere (1987, 1988).
OH vein adularia.....	25.1±0.6.....	Bachelor.....	Bethke and others (1976). ¹
OH vein sericite.....	25.3±1.4.....	Bachelor.....	Bethke and others (1976). ¹
OH vein sericite.....	25.5±0.8.....	Bachelor.....	Bethke and others (1976). ¹
OH vein sericite.....	25.7±1.2.....	Bachelor.....	Bethke and others (1976). ¹
Quartz latite of Baldy Cinco, equivalent to volcanics of Stewart Peak.	25.7±0.1.....	San Luis.....	M. Lanphere (written commun., 1989).
Nelson Mountain Tuff.....	26.1±0.1.....	San Luis.....	Lanphere (1987, 1988).
Rat Creek Tuff.....	26.4±0.1.....	San Luis.....	Lanphere (1987, 1988).
Regional K-metasomatic event.....	26.4±1.3.....	Vergo (1987).
Snowshoe Mountain Tuff.....	26.8±0.1.....	Creede.....	Lanphere (1987, 1988).
Wason Park Tuff.....	27.1±0.2.....	South River.....	Lanphere (1987, 1988).
Campbell Mountain welding zone of Bachelor Mountain Member of Carpenter Ridge Tuff.	27.2±0.2.....	Bachelor.....	Vergo (1987).
Carpenter Ridge Tuff.....	27.6±0.2.....	Bachelor.....	Lanphere (1987, 1988); Hurford and Hammerschmidt (1985).
Fish Canyon Tuff.....	27.8±0.2.....	La Garita.....	Lanphere (1987, 1988).
Masonic Park Tuff.....	28.2±0.2.....	Mount Hope.....	Lanphere (1987, 1988).

¹Revised by Hon and Mehnert (1983) using new IUGS constants.

Tertiary are those that were deposited in the moat of the Creede caldera and in channels incised in the caldera wall. They constitute the Creede Formation and consist of stream-channel gravels, landslide breccias, travertines, bedded lacustrine sediments, and water-laid tuffs (Steven and Ratté, 1965). Thin, layered sediments interbedded with volcanic units have also been found in the north-central part of the district by Chevron Resources, Inc., and Homestake Mining Company (James O'Brien, written commun., 1982; S.W. Caddey and C.B. Byington, oral commun., 1983). Within the San Luis caldera, fluvial and lakebed sediments (a few tens of meters thick) that accumulated in small depositional basins overlie the Equity Member of the Nelson Mountain Tuff.

The complex history of movement and reactivation along faults of the Creede graben has been described in detail by Steven and Ratté (1965). Normal faults are the dominant structural element controlling the location of mineralized rock in the central San Juan area, and most are related to evolution of the Oligocene calderas (fig. 2). The reverse Equity fault, which formed by fault-bounded uplift of a triangular block presumably related to a shallow underlying intrusion (Lipman and Sawyer, 1988), is also mineralized. The dominant structural features are the well-formed caldera expressions and the north-northwest-trending Creede graben, which initially formed as a keystone graben in the Bachelor caldera (fig. 1). The major faults from west to east include the Alpha-Corsair, Bulldog Mountain, Amethyst, Midwest-Knoess, and Solomon-Holy Moses faults. The OH, P, and other minor faults cut the central block of the graben, are

nearly vertical, and had primarily strike-slip motion (S.W. Caddey, written commun., 1985).

AGE OF MINERALIZATION

A single radiometric age determination (table 1) on adularia (⁴⁰Ar/³⁹Ar incremental heating ages) from drill-core from the North Amethyst vein system indicates an age of 25.1±0.1 Ma (M.A. Lanphere, written commun., 1987). The adularia is found with base-metal minerals of a late-stage hydrothermal event that occurred along the North Amethyst vein system. The Au-bearing ores predate this base-metal and vein adularia stage (Foley and Vardiman, 1988), so their age falls in the interval between that of the youngest host rock, which is the Nelson Mountain Tuff, at 26.1 Ma, and the vein adularia, at 25.1 Ma. At least five volcanic units were deposited as part of the San Luis caldera complex after deposition of the oldest host rock, which is the Carpenter Ridge Tuff, at 27.6 Ma. These include the Rat Creek Tuff at 26.4 Ma, the Nelson Mountain Tuff at 26.1 Ma, tuff of Cathedral Peak (undated), rhyolite of Mineral Mountain (undated), and volcanic rocks of Stewart Peak (undated). The youngest volcanic rock in the area is quartz latite of Baldy Cinco (25.7 Ma), a unit equivalent to the volcanic rocks of Stewart Peak in the San Luis quadrangle (Lipman and Sawyer, 1988). Radiometric ages of gangue associated with ore minerals from the main Creede mining district indicate that those minerals were deposited at about 25 Ma (table 1); this deposit is generally concurrent with base-metal mineralization of the North Amethyst veins.

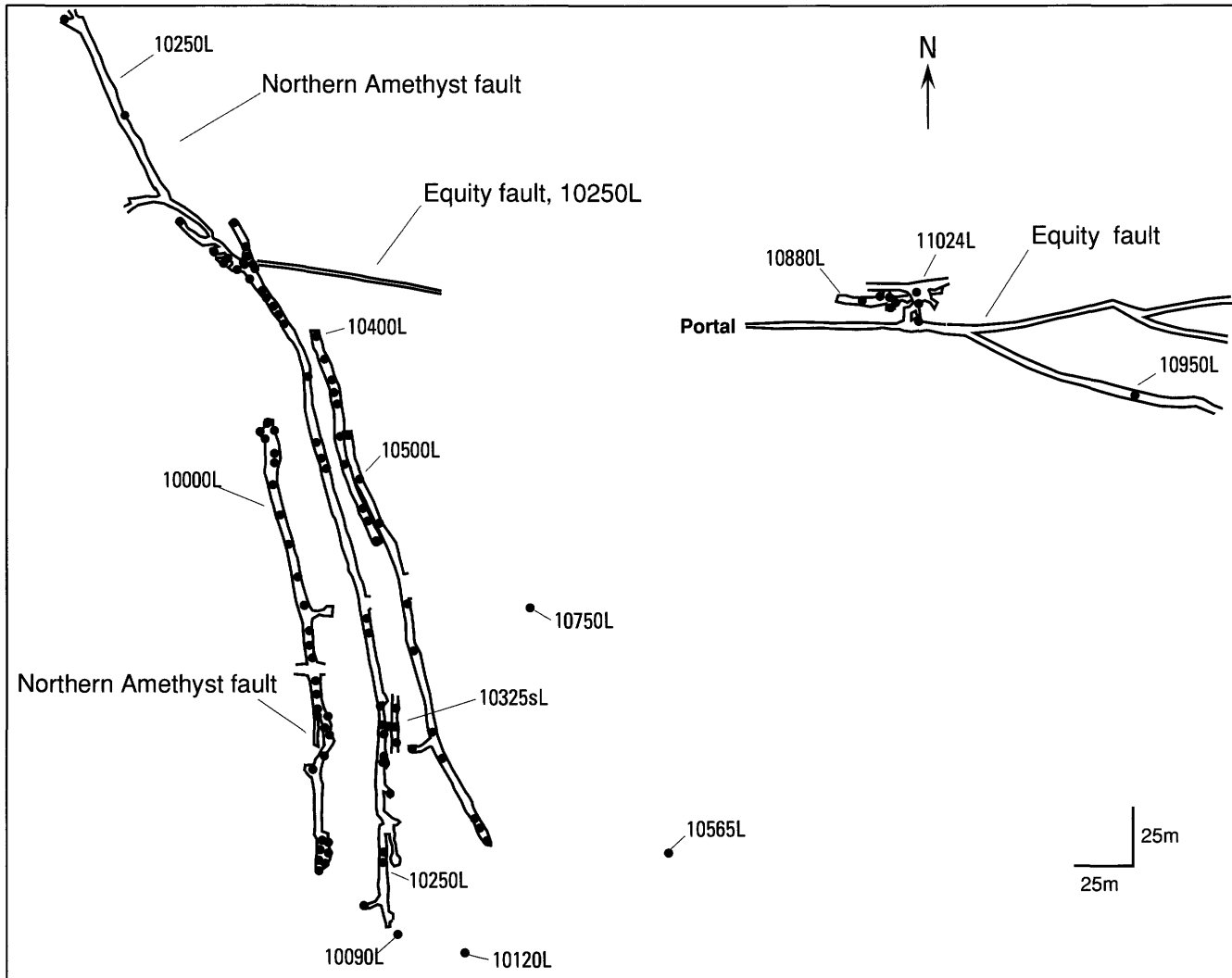


FIGURE 3.—Plan map showing the levels of the North Amethyst vein system along the northern Amethyst and Equity faults. Sample localities are shown by solid dots; localities off the vein are on the decline.

PREVIOUS STUDIES

Mineralized rock in the central part of the San Juan area has been the subject of numerous reports and papers since the area was first mined in the early 1880's. The relationship of the mineralization to regional geologic setting was first described in detail by Steven and Ratté (1960, 1965) and Steven (1968). The area in and around the Creede mining district has been the subject of continuing research since the late 1950's by the USGS and by several universities. Their work has been published in a series of papers on the Creede district (Steven and Eaton, 1975; Bethke and others, 1976; Roedder, 1977; Barton and others, 1977; Wetlaufer, 1977; Bethke and Rye, 1979; Hayba and others, 1985; Plumlee, 1989; Foley, 1990; Foley and others, 1990). Historic accounts of ores of the Equity mine and a summary of preliminary

reports of the more recently discovered North Amethyst ores are described in Foley (1990).

STYLE OF MINERALIZATION

The vertical and lateral extent, and overall shape, of ore occurrences of the North Amethyst vein system (fig. 3) is not well delineated because of the complex nature of the mineralized rock and the complex structural character of the veins. A detailed structural analysis of the North Amethyst vein system is necessary to resolve composite vein and structure relations. Some general observations, however, can be made relative to ore zones of the Bulldog and Amethyst vein systems of the main mining district at Creede as described by Plumlee (1989) and to ore zones of the OH and P veins.

TABLE 2.—*Stages of mineralization and brecciation events of the North Amethyst vein system*

[Abbreviations: >>, much greater than; >, greater than; =, approximately equal; { }, distribution unknown, local occurrence; [], molds]

Stage	North Amethyst vein mineral assemblage
<i>Base-metal-silica association:</i>	
3	Mn-calcite >> quartz > pyrite
Breccia-4	Mn-calcite cement, fragments of earlier assemblages, breccias and minerals [wall rock]
2b	Quartz > calcite > rhodocrosite > adularia > fluorite > chlorite = pyrite
Breccia-3	Quartz + chlorite cement, fragments of wall rock, and coarse stage-1 sulfides
1b	Quartz > sphalerite > galena > pyrite > chalcoppyrite > tetrahedrite
1a	Quartz > pyrite = hematite > chlorite
Breccia-2	Quartz cement, fragments of stages alpha and beta, wall rock, sedimented structures, black quartz breccia
<i>Mn-Au association:</i>	
Beta-2	Sphalerite > galena > chalcoppyrite > pyrite > tetrahedrite > Ag- and Au-bearing sulfide minerals > electrum {magnetite, hematite}
Breccia-1	Quartz cement, fragments of stages alpha and beta
Beta-1	Sphalerite > galena > chalcoppyrite > pyrite > tetrahedrite > Ag- and Au-bearing sulfide minerals > electrum {magnetite, hematite}
Alpha	Rhodocrosite = quartz > Mn-calcite = rhodonite > K-feldspar >> sphalerite > pyrite > galena > [barite]

Mineralized rock of the North Amethyst vein system fills structures related to the northern Amethyst and Equity faults. The North Amethyst veins are mineralogically complex, and the assemblages can be divided into two contrasting associations: a Mn-Au association and a base-metal-silica association. The minerals found in each association are grouped in table 2 according to the stages in which they are typically found and are discussed in greater detail herein. Both mineral associations occur along almost the entire extent of the underground workings, a distance of roughly 600 m along strike of the vein. The base-metal association is displayed over a vertical extent of about 150 m, whereas minerals of the Mn-Au association occur over an apparently larger vertical interval of 600 m.

CHARACTER OF THE ORE ZONES

Ore zones of the main mining district typically are of much greater horizontal than vertical extent. For example, the ore zone comprising the Bulldog Mountain vein system was mined for approximately 3 km laterally and 200 to 300 m vertically (Plumlee, 1989). The combined productive ore zones of the central and southern Ame-

thyst veins were of similar vertical extents and of even greater lateral extents. Mineralized zones of the OH and P structures delineated by mine workings are approximately 2,100 by 275 m and 975 by 225 m, respectively.

Only the dominantly base-metal-rich assemblages are found in core drilled just south of the North Amethyst underground workings. Farther to the south, the base-metal assemblages also occur, at least discontinuously, along much of the Amethyst fault (D.S. Sweetkind, written commun., 1990). If these assemblages are coeval, the base-metal minerals of the northern Amethyst structure may have lateral and vertical extents more like those of the main mining district.

In contrast to the base-metal-rich assemblages, the complete Au-bearing assemblages of the North Amethyst system are not found in drillcore to the south of the North Amethyst workings, nor are they reported to occur in underground workings. (As discussed in the section "Electrum," isolated occurrences of electrum have been reported in ore of the main mining district.) These findings suggest that the Au-bearing assemblages may have a more restricted lateral extent compared to ore zones of the main mining district.

NATURE OF THE VEINS

The veins of the North Amethyst system vary in width and mineral content because of their complex structural character and the high degree of structural activity contemporaneous with, and occurring after, mineralization. Veins can vary from a few centimeters to greater than 2 m in width, and they contain multiple assemblages that record different stages of mineralization.

Most vein assemblages are brecciated, and some vein fillings show sedimentary textures. Fracturing events are recorded in crosscutting vein relations and in breccias that developed at sites of intense structural activity. Multiple periods of movement resulted in many generations of breccias with characteristic fragment types and cements; these can be used to demonstrate timing relations.

MINERAL TEXTURES

Minerals were deposited in a number of stages that are characterized by distinctive textural styles. Extensive brecciation and recrystallization overprint the earlier stages, but a striking textural contrast between stages of the earlier, Mn-Au association and those of the later, base-metal association is retained in many veins.

The minerals of the Mn-Au association were deposited in two stages that show a variety of textures (fig. 4). The earliest stage of sulfide-bearing mineralization, desig-

nated here as stage alpha, was deposited primarily in open fractures, in some cases around preexisting barite and quartz crystals. The cryptocrystalline material shows a faint but clearly visible mineralogic banding on aged surfaces that is due to manganese oxidation. Stage alpha also shows some evidence for replacement of volcanic wall rock. Embayed remnant feldspar grains are caught up in a fine-grained "frozen mush" consisting dominantly of rhodocrosite, manganese pyroxenoids and other carbonate minerals, and quartz. The second stage of the Mn-Au association, stage beta, consists of fine-grained precious- and base-metal-sulfide-rich seams that cut and recrystallized the stage-alpha minerals.

The later, base-metal-silica association minerals filled open spaces in fractures and breccias (fig. 5). Although many veins filled completely, some large vugs lined with crystals of the latest stages remained open. Minerals of this association are generally coarser grained than those of the Mn-Au association and show crustification sequences. Dissolution and replacement textures are also common.

VEIN MINERALOGY AND COMPOSITIONAL RANGES

Detailed descriptions of ore and gangue minerals are given here for common or economically important minerals and for those used to constrain conditions of ore formation. The minerals are listed in alphabetical order and grouped by type for convenience; sample locations are shown in figure 6. Table 3 describes the relative abundance and distribution of minerals in each assemblage and includes all minerals reported for the deposit. Compositional ranges for carbonate minerals, electrum, manganese silicates, and sphalerites described in table 4 are listed in tables 5 through 8. Sample distribution, selection method, analytical details, and analyses are described by Foley (1990). Ore minerals were identified on the basis of descriptions presented by Ramdohr (1969) and Craig and Vaughan (1981).

Ag-SULFIDE AND Ag-Cu-SULFIDE MINERALS

Four Ag- and Cu-bearing sulfide minerals occur in the Au-rich stage of mineralization: acanthite, jalpaite, mckinstryite, and, possibly, stromeyerite. These phases were identified on the basis of optical properties and analysis by an energy dispersive system but were not examined by X-ray diffraction. Where possible, the compositions were estimated by energy dispersive analysis and electron microprobe analysis. The Cu-Ag-S minerals do not yield reliable temperatures of specific conditions of ore deposition because of their exceedingly fast reequilibration rates (Skinner, 1966) but are

included in this discussion because of their economic importance.

Acanthite (Ag_2S)-*Argentite* (Ag_2S).—Small (<0.03 mm), irregularly shaped grains of acanthite occur alone in quartz gangue and at the margins of galena, pyrrargyrite, and chalcopyrite grains and as inclusions in pyrite and galena. The Ag sulfide is contemporaneous with chalcopyrite and pyrrargyrite. It is also found both alone and with polybasite, in association with galena, with chalcopyrite and electrum, and rimming and enveloping rounded grains of galena. Some small (<0.01 mm), rounded grains are contained within galena; however, no clearcut exsolution textures were observed.

Jalpaite (Ag_3CuS_2).—Soft, light-gray, Ag- and Cu-bearing sulfide mineral grains, 10 to 25 μ m in width, are intergrown with or are enclosed by acanthite that is in turn bordered by chalcopyrite and galena. This mineral is tentatively identified as jalpaite on the basis of an absence of Sb or As, high Ag relative to Cu, good polish, and distinct anisotropism without the striking blue-violet tints of stromeyerite. The mineral also occurs in aggregates with acanthite and Ag-bearing tetrahedrite that are enclosed by gangue.

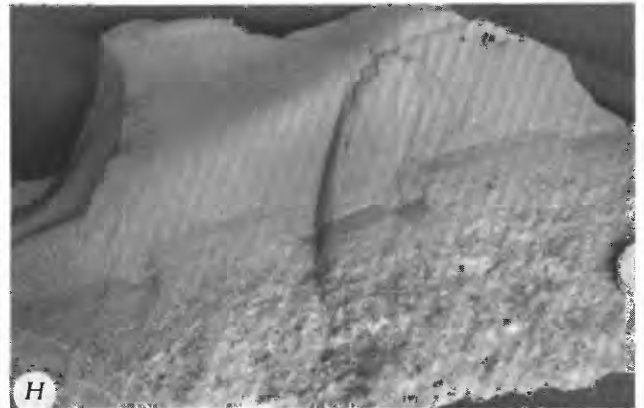
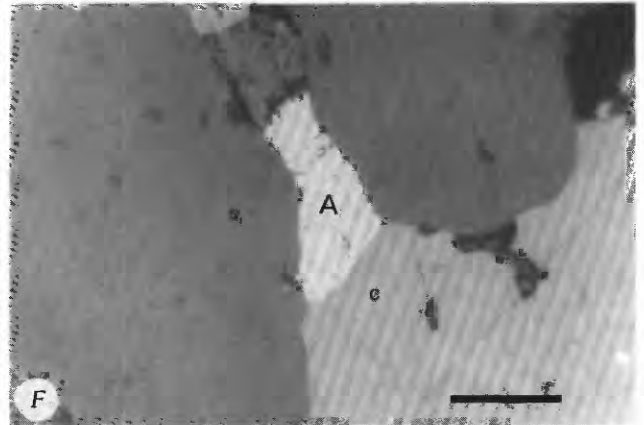
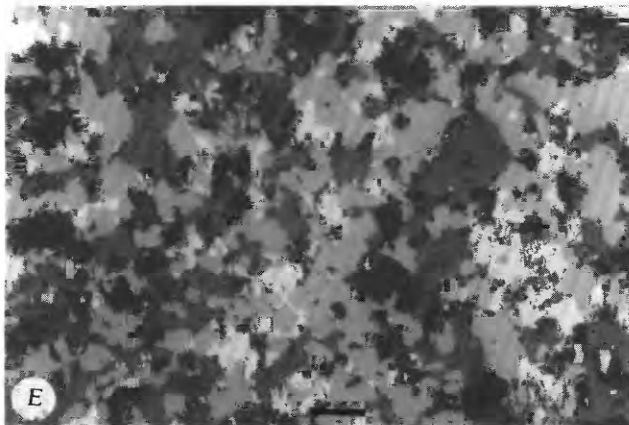
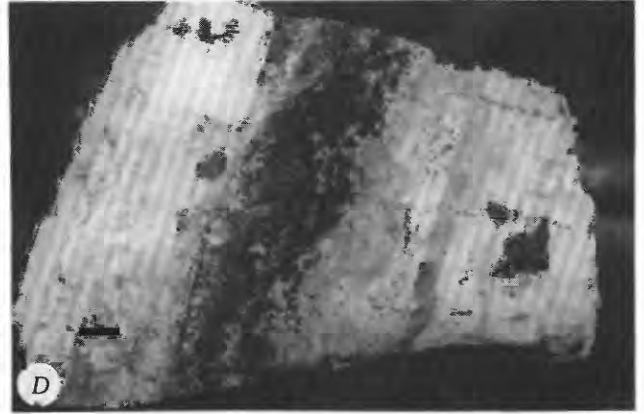
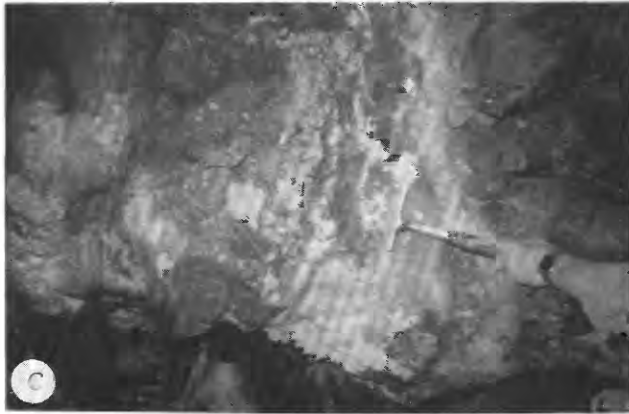
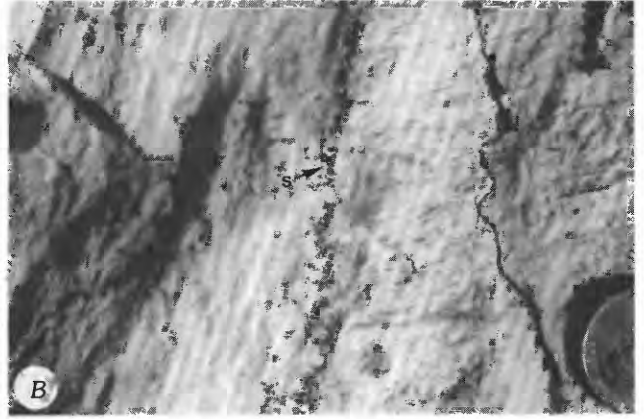
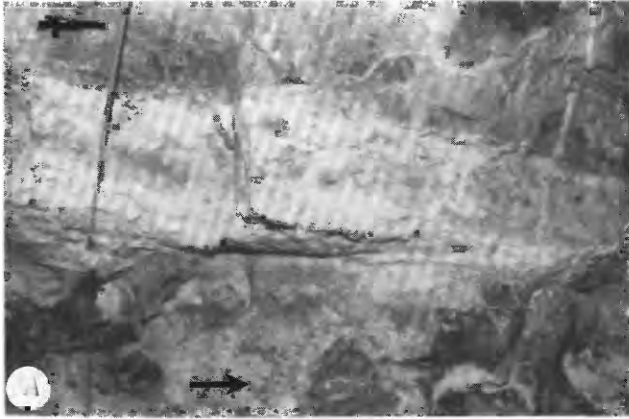
Mckinstryite ($Ag_{1.3}Cu_{0.7}S$).—Anhedronal crystals of mckinstryite (15 μ m wide) are intergrown locally with acanthite, jalpaite, uytenbogaardtite, and, possibly, stromeyerite. The mineral also occurs as small <20- μ m-wide anhedronal grains in aggregates intergrown with chalcopyrite and acanthite, and with wire silver the mckinstryite fills cavities and microfractures that cut sulfide-rich zones. Although optical properties of this phase closely resemble those of stromeyerite, the two Cu-Ag sulfides can be distinguished optically when intergrown. Identification was confirmed by electron microprobe where possible.

BARITE

Barite ($BaSO_4$) was not found in samples collected from underground workings. However, tabular molds up to 3 cm in length resembling the crystal habit of barite do occur in samples from the lower elevations in the workings, especially to the south. The mineral is found in drillcore samples from the southern end of the underground workings and in core drilled to the south of the exploratory workings. Tabular and bladed crystals of colorless to pale-cream barite ranging in length from 1 to 10 mm occur in veinlets with quartz, calcite, and minor pyrite.

BOURNONITE

A gray-white phase ($PbCuSbS_3$) occurs with galena rimming corroded sphalerite and as small aggregates of



equant to slightly platy grains (<100 μm) associated with acanthite, electrum, tetrahedrite, chalcopyrite, and galena. Twinning, distinctive color adjacent to galena, very slight anisotropy, and lack of internal reflections are indicative of bournonite.

CARBONATE GROUP MINERALS

Carbonate minerals are abundant in all stages of the North Amethyst paragenesis, and each stage is characterized by carbonate minerals of different composition, color, and texture. The earlier, Mn-Au association is characterized by three fine-grained carbonate minerals: a manganian calcite, kutnahorite,⁴ and a calcian rhodocrosite. The later, base-metal-silica association contains coarser grained manganian calcite, manganosiderite (oligonite), and a calcian rhodocrosite. Each mineral has a range of compositions. Representative analyses are given in table 5; all analyses are plotted in figures 7 and 8.

Calcite ($\text{Ca}_{.73-.91}\text{Mn}_{.26-.09}\text{CO}_3$).—Three calcites are distinguished on the basis of paragenetic position, color, and grain size; however, they overlap in part in composition. Calcite associated with the Mn-Au stages is very fine grained (crystals <50 μm in width) and is intergrown with microcrystalline Mn-silicates, kutnahorite, rhodocrosite, and quartz. Calcite of this stage shows a range in manganese contents from about 10 to about 30 mole percent MnCO_3 .

Calcite that occurs in the early stages of the base-metal-silica association is colorless to pale yellow and generally has lower manganese contents than other analyzed carbonate minerals (9 to 15 mole percent

MnCO_3). The crystals range in size from a few millimeters to 2 to 3 cm and are intergrown with 0.1- to 1.0-mm-wide grains of oligonite, the manganian siderite. The calcite contains virtually no magnesium and generally less than 1 mole percent FeCO_3 .

The last stage of the base-metal-silica association is composed dominantly of a pink to pale-cream manganian calcite, especially in the northern part of the ore zone. Thick crusts of crystalline carbonate, up to 15 cm in thickness, are found mainly lining late-stage vugs and open spaces in the vein. The crusts are dominantly pale cream in color and contain thin bands of darker tan to rust-colored carbonate. The compositional range for this calcite is similar to calcite of the Mn-Au stages.

Kutnahorite ($\text{Ca}_{.47}\text{Mn}_{.52}\text{CO}_3$).—A Mn- and Ca-bearing carbonate mineral having a composition equivalent to kutnahorite, the manganese analog of dolomite, has been identified intergrown with fine-grained rhodocrosite, Mn-calcite, and Mn-silicates of the Mn-Au association (table 5). X-ray diffraction analyses of the mixture suggest primarily quartz, rhodonite, pyroxmangite, and carbonate minerals having a wide range of Ca-Mn solid solution. Microprobe analyses of the carbonate minerals yield some compositions in the range $\text{Cc}_{46}\text{Rc}_{54}$ to $\text{Cc}_{53}\text{Rc}_{47}$ with less than 1 percent $(\text{Fe,Mg})\text{CO}_3$. The material is too fine grained to permit single-crystal X-ray study to determine if the kutnahorite is ordered; long-range cation ordering of kutnahorite is not detectable by conventional powder X-ray diffraction techniques (Pearce and others, 1987).

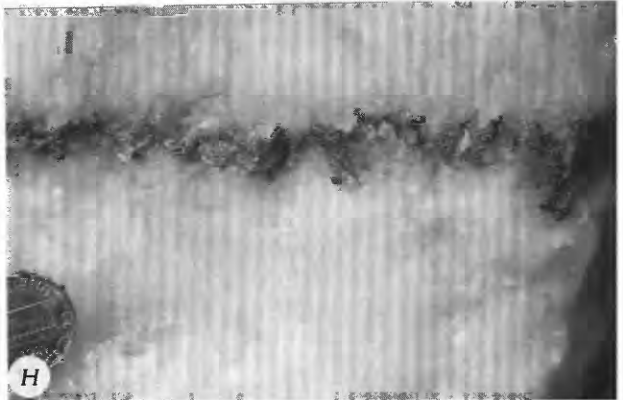
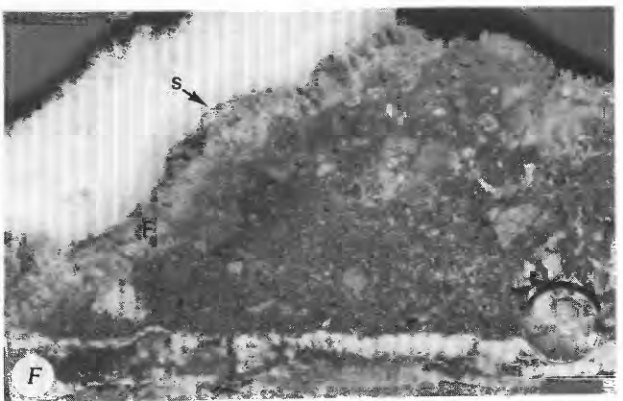
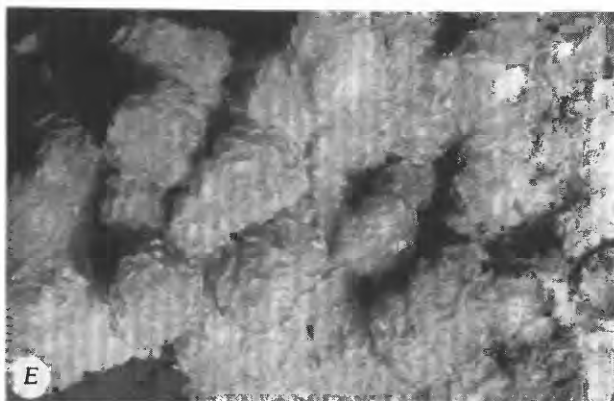
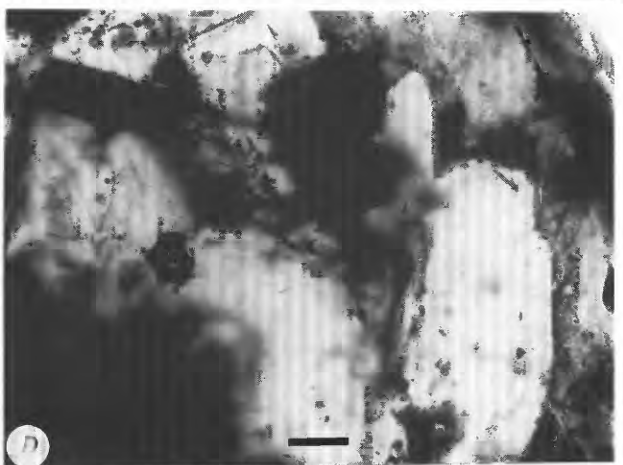
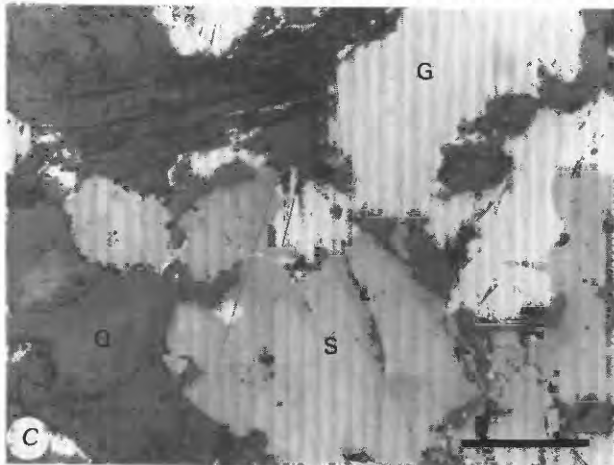
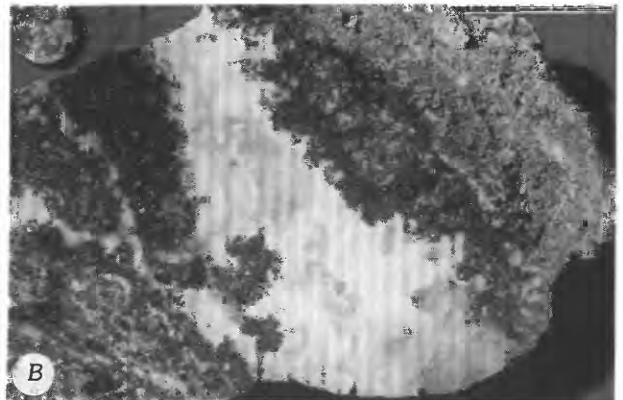
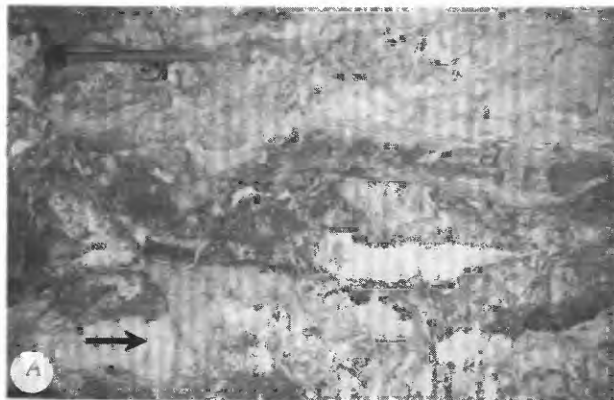
Rhodocrosite ($\text{Mn}_{.86-.76}\text{Ca}_{.13-.24}\text{CO}_3$).—In the Mn-Au association, rhodocrosite is the most abundant carbonate mineral and occurs in a microcrystalline (<50 μm) admixture composed mainly of rhodonite, quartz, and Mn-calcite. The admixture is zoned mineralogically on the scale of hundreds of micrometers. Coarser rhodocrosite (up to 0.5 mm in width) occurs in some of the zones and in patches that cut across zones; the patches consist of mats of intergrown curls that resemble poodle hair. Compositions of the poodle-hair rhodocrosites are similar to, and as calcic as, those of the finer grained material (up to $\text{Cc}_{24}\text{Rc}_{76}$).

In the base-metal-silica association, rhodocrosite is associated with amethystine quartz and fluorite. Rhodocrosite also occurs in most later stages of the North Amethyst paragenesis in small (<5 mm wide) veinlets, and as 1- to 5-mm-wide, near-gem-quality crystals that line small vugs and are perched on minerals from earlier stages.

Siderite, manganian.—Fe- and Mn-bearing oligonite ($\text{Fe}_{.54}\text{Mn}_{.32}\text{Ca}_{.12}\text{Mg}_{.02}\text{CO}_3$) is found in one assemblage of the base-metal-silica association. The mineral occurs as discrete crystals 0.1 to 1.0 mm wide within a coarser calcite. The carbonate minerals are intergrown primarily

⁴Capobianco and Navrotsky (1987) recommend that the name kutnahorite be applied to the 50:50 phase having dolomite-type ordering and that naturally occurring phases lacking dolomite-type ordering be termed pseudokutnahorite. The fine-grained nature of these samples hindered their characterization; hence, ordering (or the lack of ordering) is not implied by the use of the name kutnahorite.

◀ FIGURE 4.—Photographs of North Amethyst Mn- and Au-bearing vein assemblages. A, Vein of stage-alpha Mn-carbonates, Mn-silicates, and quartz cutting volcanic wall rock. Field of view is 1 m. Arrow points up. B, Closeup of bleached wall rock, sphalerite grains (s), and stage-alpha material. C, View of Au-rich stage-beta sulfide vein cutting fine-grained Mn-carbonates and Mn-silicates of stage alpha. Photograph by G.S. Plumlee. D, Closeup of Au-bearing stage-beta sulfide vein cutting fine-grained banded Mn-carbonates, Mn-silicates, and quartz. Scale bar equals 1 cm. E, Equigranular sulfide assemblage of stage beta. Scale bar equals 25 μm . F, Closeup of electrum (A), sphalerite (s), and chalcopyrite (c) of stage beta. Scale bar equals 15 μm . G, View of sedimented vein. Photograph by G.S. Plumlee. H, Graded bedding in siliceous sediment. Note small offsets in bedding, fine-to-coarse texture, clasts of altered volcanics, rounded quartz crystals, and small sulfide aggregates.



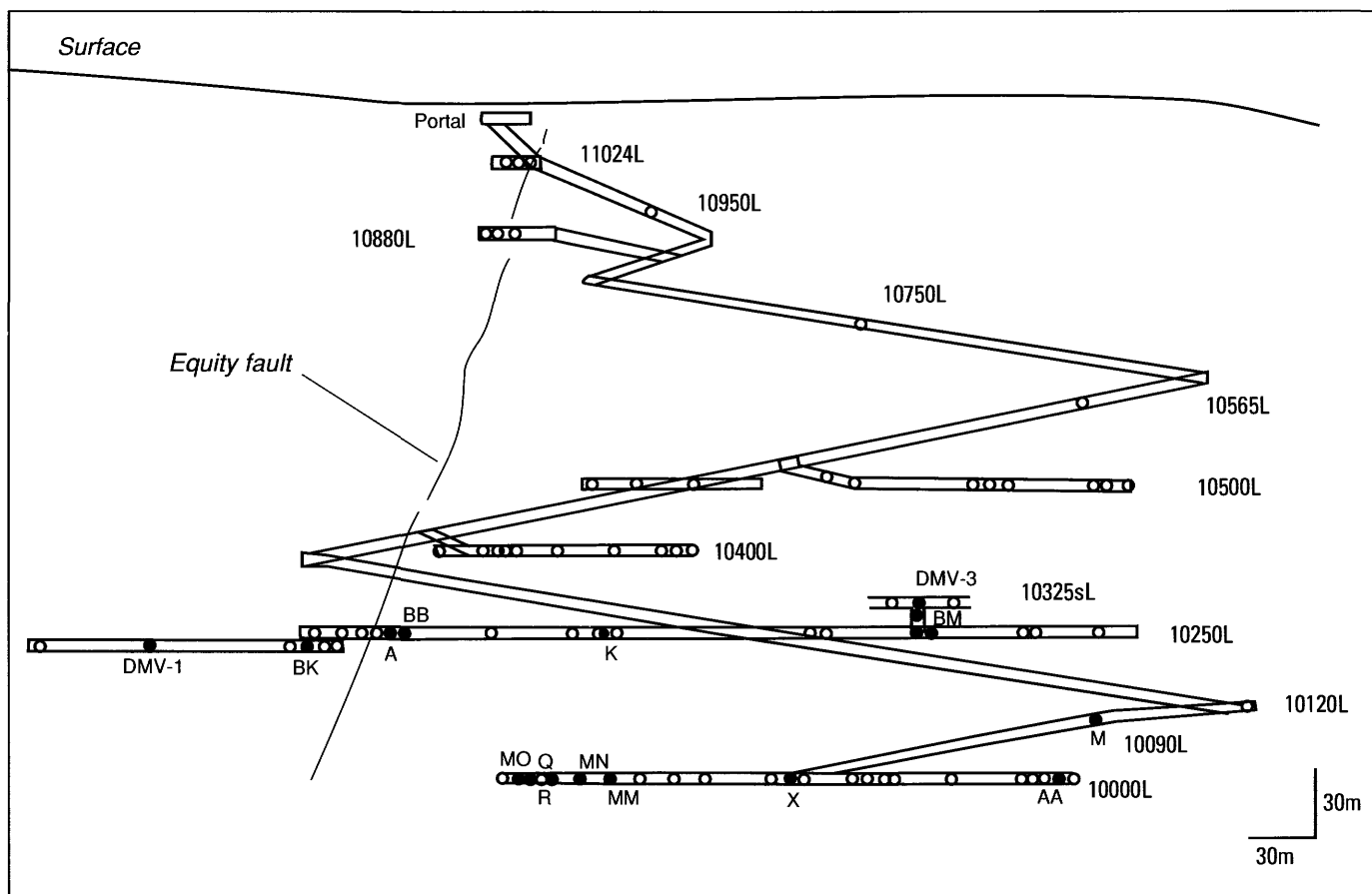


FIGURE 6.—Cross-sectional view of mine workings, North Amethyst vein system. Locations of samples used in the electron microprobe study are labeled. See table 4 for sample descriptions.

with chlorite, quartz, hematite, and minor adularia and sphalerite and were deposited just after a major period of base-metal mineralization.

Wetlauffer (1977), in a study of carbonate minerals occurring in the southern part of the Creede district, documented significant compositional variations in rhodocrosite and siderite. She found that Bulldog Mountain rhodocrosite compositions from the early pre-ore

stage lie along the $\text{FeCO}_3\text{-MnCO}_3$ join and typically contain 68 to 93 mole percent MnCO_3 . CaCO_3 contents vary from 2 to 15 mole percent, and MgCO_3 contents are generally less than 4 mole percent. A later intra-ore siderite-manganosiderite stage was found to contain 33 to 94 mole percent FeCO_3 , 6 to 67 mole percent MnCO_3 , 1 to 13 mole percent CaCO_3 , and 1 to 10 mole percent MgCO_3 .

◀ FIGURE 5.—Photographs of North Amethyst base-metal-bearing vein assemblages. A, Meter-wide vein of coarse base-metal sulfides of stage 1, base-metal-silicate association. Arrow points up. Photograph by G.S. Plumlee. B, Closeup of base-metal sulfide of stage 1 and quartz, calcite, and chlorite of stage 2. C, Reflected-light photograph of sphalerite (S), galena (G), and quartz (Q) of the stage-1 assemblage. Scale bar equals 5 mm. D, Transmitted-light photograph of sphalerite. Note color banding paralleling growth zones defined by fluid inclusions. Scale bar equals 1 cm. E, 2- to 3-cm-long stage-2 quartz crystals coated by stage-3 calcite; calcite is dusted with tiny pyrite cubes. F, Brecciated stage-1 sulfides coated with fluorite (F) of stage 2. Note pockets of quartz sediment (s) between fluorite and calcite of stage 3. G, 15-cm-wide crusts of cream- to pink-colored Mn-rich calcite of stage 3 lining late vugs. Photograph by G.S. Plumlee. H, Pink calcite (light) and pyrite (dark) of stage 3.

CHALCOPYRITE

Chalcopyrite (CuFeS_2) is abundant in three sulfide-bearing stages of mineralization and is not found in stages composed dominantly of gangue. Size is highly variable; diameters of the irregular grains range from a few micrometers to a few millimeters. Earlier stage occurrences are generally finer grained than later stage occurrences.

Chalcopyrite is generally formed later than and replaces sphalerite. Extensive chalcopyrite disease textures (Barton and Bethke, 1987) are present in all sphalerite-bearing stages. The disease consists of

TABLE 3.—Assemblages and minerals of the North Amethyst vein system

[Abbreviations: ×, present; —, not present; A, wall-rock alteration; ?, previously reported by Homestake Mining Company (C.B. Byington, S.W. Caddey, D.M. Vardiman, oral commun., 1987) but not found in this study]

Mineral	Stage									
	Pre-ore	Alpha	Beta 1	Beta 2	1-a	1-b	2-a	2-b	3	Post-ore
Sericite	×	×	—	—	×	×	×	—	—	—
K-feldspar	A	×	—	—	—	—	×	×	—	—
Quartz	×	×	×	×	×	×	×	×	×	—
Barite	?	?	—	—	—	—	—	—	—	—
Pyrite	×	×	×	×	×	×	—	×	×	—
Hematite	—	—	—	×	×	×	—	—	—	—
Magnetite.....	—	×	×	×	—	—	—	—	—	—
Chlorite.....	—	—	—	—	×	×	×	—	—	—
Rhodocrosite.....	—	×	—	—	—	—	—	×	—	—
Rhodonite	—	×	—	—	×	—	—	—	—	—
Mn-calcite	—	×	—	—	—	—	×	—	×	—
Kutnahorite.....	—	×	—	—	—	—	—	—	—	—
Alleganyite	—	?	—	—	—	—	—	—	—	—
Bustamite	—	?	—	—	—	—	—	—	—	—
Pyroxmangite.....	—	×	—	—	—	—	—	—	—	—
Inesite	—	×	—	—	—	—	—	—	—	×
Sphalerite	—	×	×	×	—	×	—	—	—	—
Galena	—	×	×	×	—	×	—	—	—	—
Chalcopyrite.....	—	—	×	×	—	×	—	—	—	—
Marcasite.....	—	—	—	×	—	—	—	—	×	—
Acanthite	—	—	×	×	—	—	—	—	—	—
Pyrrargyrite.....	—	—	×	×	—	—	—	—	—	—
Electrum	—	—	×	×	—	—	—	—	—	—
Uytenbogaardtite.....	—	—	×	×	—	—	—	—	—	—
Polybasite	—	—	?	×	—	—	—	—	—	—
Tetrahedrite.....	—	—	×	×	—	×	—	—	—	—
Jalpaite.....	—	—	×	×	—	—	—	—	—	—
Stephanite.....	—	—	—	×	—	—	—	—	—	—
Bournonite.....	—	—	—	×	—	—	—	—	—	—
Siderite.....	—	—	—	—	—	—	—	×	—	—
Fluorite.....	—	—	—	—	—	—	×	—	×	—
Stromeyerite	—	—	—	—	—	—	—	—	—	×
Native Ag	—	—	—	—	—	—	—	—	—	×
Gypsum.....	—	—	—	—	—	—	—	—	—	×

micrometer-sized chalcopyrite grains that are rounded to rod shaped; they are generally concentrated at the rims of sphalerite crystals.

In earlier stages, chalcopyrite is found in sphalerite and as somewhat larger separate grains bordering and corroding sphalerite. Xenomorphic grains of chalcopyrite are intergrown with galena, tetrahedrite, silver minerals, and electrum, and together these minerals fill interstices around crystals of sphalerite and pyrite (fig. 4E and F).

In the later stages, chalcopyrite occurs as anhedral grains bordering sphalerite and as common intergrowths with galena. It also occurs as isolated grains that are entirely surrounded by quartz and carbonate gangue.

Oxidation of the chalcopyrite to chalcocite and covellite has been reported for some samples of the North

Amethyst ores (S.W. Caddey and D.M. Vardiman, oral commun., 1988); this type of oxidation was not observed in any of the samples examined in this study.

CHLORITE

In the North Amethyst veins, chlorite ($A_{5-6}Z_4O_{10}(OH)_8$, where $A=Al, Fe^{2+}, Fe^{3+}, Mg, Mn$ and $Z=Al, Fe^{3+}, Si$) occurs primarily in the later, base-metal-silica association where it is intergrown with hematite, quartz, and pyrite. Assemblages containing the green, fine-grained (<100- μ m-wide flakes) layer silicate formed just prior to, and concurrently with, the period of major base-metal-sulfide mineralization in the later association. Some chlorite is also intergrown with quartz and calcite deposited after the base-metal sulfides.

TABLE 4.—Locations and descriptions of samples from the North Amethyst vein system analyzed by electron microprobe

[Samples collected by: DMV, D.M. Vardiman, Homestake Mining Co.; GSP, G.S. Plumlee, U.S. Geological Survey; NKF, N.K. Foley, U.S. Geological Survey]

Sample no.	Location	Description
DMV-1	10250 level, E-126+75'N	Coarse-grained (up to 1 cm wide) stage-1 lemon-yellow crystals of sphalerite intergrown with galena and chalcopyrite in veinlets 2 mm to 1 cm wide cutting bleached volcanic rock.
DMV-3	10325 level, 2' south	Seam of fine-grained electrum-bearing sulfide at contact of volcanic wall rock with breccia of stage beta.
GSP-MM-10-86	10000 level, E-125	20-cm-wide seam of gold-bearing fine-grained sulfides of stage beta in fracture cutting vein of stage alpha. Rounded grains of sphalerite intergrown with chalcopyrite, galena, electrum, and other precious- and base-metal minerals of stage beta.
GSP-MN-87	10000 level, E-125+35'N	Large (up to 1 cm wide) color-banded crystals of sphalerite of stage 1 intergrown with quartz and chlorite, coated by stage-3 pink calcite.
GSP-MO-2-86	10000 level, E-126+50'N, in scam off vein.	Coarse veins of honey-brown sphalerite, galena, chalcopyrite, pyrite, and quartz of stage 1 cutting a meter-wide brecciated vein of Mn-carbonate, Mn-silicate, and quartz.
NKF-A-1-87	10250 level, E-127+140'N	Coarse- to medium-grained sulfides of Zn, Pb, and Cu of stage 1; quartz and calcite of stage 2.
NKF-K-11-87	10250 level, E-85	Fluorite at base overlain by thick crust of calcite color banded from pink to pale-cream.
NKF-M-13-87	10090 level, E-120	Small (1 to 2 mm wide) rounded sphalerite grains of stage alpha rimmed with chalcopyrite disease, contained in fine-grained admixture of rhodonite, rhodocrosite, and quartz.
NKF-Q-17-87	10000 level, 25 ft from north face	Meter-wide vein of Mn-carbonates and Mn-silicates containing disseminated galena (stage alpha), sulfides, quartz, and rhodocrosite.
NKF-R-18-87	10000 level, E-126+25'S	Banded hematite, magnetite, sulfides, quartz, and electrum (stage alpha). Cut by fractures containing coarse-grained sulfides of stage 1.
NKF-X-24-87	10000 level, below 1S orebody, 30'N	Coarse-grained sulfides (stage 1), quartz, and carbonate on chlorite + pyrite alteration. Yellow to red-brown sphalerite intergrown with other stage-1 minerals, overgrown by quartz, fluorite, and calcite of stage 2.
NKF-AA-24-87	10000 level, E-125	15-cm-wide seam of high-grade ore in vein of Mn-carbonates and Mn-silicates. Galena taken from Au-bearing zone (stage beta).
NKF-BB-54-87	10250 level	Fine-grained carbonate, Mn-silicate, and quartz material of stage alpha.
NKF-BK-63f-87	10250 level, No. 2 dogleg	Disseminated sulfides in recrystallized Mn-carbonates and Mn-silicates. Fine-grained minerals of stage alpha cut by veins containing red-brown to yellow sphalerite of stage 1, pyrite, chalcopyrite, and quartz and calcite gangue.
NKF-BM-65-87	10250 level, S2 raise	Rounded cobble of fine-grained sulfide containing gold and sphalerite (stage beta) in breccia.

No quantitative compositional data are available for North Amethyst chlorites. They are iron rich like other Creede chlorites (Barton and others, 1977) and contain substantial manganese (by energy dispersive analysis).

ELECTRUM

Electrum ($\text{Au}_{0.3-0.5}\text{Ag}_{0.7-0.5}$) is characteristic of the early, Mn-Au association of the North Amethyst paragenesis. The mineral is intricately intergrown with a variety of base- and precious-metal sulfides and generally formed late with respect to the base-metal sulfides (fig. 4F). The whitish-yellow Ag-rich grains occur most

frequently as small rounded inclusions (3 to 25 μm) in chalcopyrite and uytenbogaardtite, although they are also found in acanthite, pyrargyrite, and galena. More rarely, electrum occurs as small (3 to 30 μm) separate grains in quartz gangue and occurs adjacent to sphalerite aggregates rimmed with galena and chalcopyrite. Larger grains, up to 75 μm in diameter and visible in hand specimen, occur with pyrargyrite, chalcopyrite, and galena. They fill interstices between, and in part replace, sphalerite grains at lower elevations in the mine. Representative electrum compositions are given in table 6 and plotted in figure 9. Analyzed electrum contained entirely within pyrite (Nos. 6, 7, table 6) has slightly higher Au

TABLE 5.—*Representative electron microprobe analyses of carbonate minerals from the North Amethyst vein system*
 [Values in weight percent unless otherwise indicated; m%, mole percent; collected by: NKF, Nora K. Foley; GSP, Geoffrey S. Plumlee]

	1	2	3	4	5	6	7
CaO	46.90	24.08	11.75	6.10	48.31	5.83	39.13
MgO25	.00	.01	.00	.01	.86	.11
FeO65	.59	.77	.83	.23	34.36	.50
MnO	8.64	34.63	47.20	53.16	8.25	19.93	17.21
SrO14	.01	.01	.03	.08	.04	.09
BaO08	.00	.09	.08	.09	.12	.01
CO ₂	42.91	39.53	38.49	38.31	43.24	38.98	41.41
Total	99.57	98.84	98.32	98.51	100.21	100.12	98.46
Ca	1.72	.94	.47	.25	1.75	.23	1.46
Mg01	.00	.00	.00	.00	.05	.01
Fe02	.02	.02	.03	.01	1.08	.01
Mn25	1.05	1.51	1.72	.24	.63	.52
Sr00	.00	.00	.00	.00	.00	.00
Ba00	.00	.00	.00	.00	.00	.00
CO ₃	2.00	2.00	2.00	2.00	2.00	2.00	2.00
m% Ca	85.77	46.81	23.31	12.50	87.68	11.73	73.14
m% Mg63	.00	.03	.00	.02	2.40	.30
m% Fe93	.91	1.23	1.33	.33	54.00	.62
m% Mn	12.49	52.26	75.35	86.09	11.84	31.73	25.85

1. NKF-M-13-87, fine-grained pale-pink calcite from stage alpha-1.
2. NKF-BB-54-87, fine-grained "kutnahorite" from stage alpha-2.
3. NKF-BB-54-87, medium-grained "poodle-hair" rhodocrosite from stage alpha-2.
4. NKF-BB-54-87, medium-grained pink rhodocrosite of stage alpha-1.
5. GSP-MN-24-87, colorless to pale-cream calcite of stage 2 (intergrown with no. 7).
6. GSP-MN-1-87, yellowish manganian siderite of stage 2 (intergrown with no. 6).
7. NKF-K-11-87, true pink manganian calcite of stage 3.

TABLE 6.—*Representative electron microprobe analyses of electrum from the North Amethyst vein system*

[Values in weight percent; collected by: NKF, Nora K. Foley; GSP, Geoffrey S. Plumlee]

	1	2	3	4	5	6	7
Ag	57.52	49.33	42.77	36.76	38.80	33.40	32.90
Au	40.74	49.31	56.02	61.31	59.65	64.34	65.73
Total	98.26	98.64	98.79	98.07	98.45	97.74	98.63
Atomic proportion							
Ag ⁺¹72	.65	.58	.52	.54	.49	.48
Au ⁺¹28	.35	.42	.48	.46	.51	.52

1. NKF-AA-27-87, silver-rich electrum grain contained in matrix of siliceous quartz.
2. NKF-AA-27-87, electrum contained in chalcopyrite.
3. NKF-AA-27-87, electrum rimmed by acanthite and uytenbogaardtite.
4. NKF-BM-65-87, electrum grain intergrown with sphalerite, galena, and chalcopyrite.
5. NKF-BM-65-87, electrum rimmed by silver minerals including acanthite and uytenbogaardtite.
6. GSP-MM-10a, gold-rich electrum grain entirely rimmed by pyrite.
7. DMV-3, gold-rich electrum grain contained in pyrite.

TABLE 7.—*Representative electron microprobe analyses of Mn-silicate minerals from the North Amethyst vein system*
 [Values in weight percent; —, not detected; collected by: NKF, Nora K. Foley; GSP, Geoffrey S. Plumlee; EQ, David M. Vardiman]

	1	2	3	4	5	6	7
SiO ₂	45.41	45.64	45.35	47.10	47.06	46.49	45.00
Al ₂ O ₃13	.27	.13	.55	.20	.25	.32
Fe ₂ O ₃00	.00	.00	.00	.00	.00	—
FeO	1.91	5.87	2.70	2.21	2.98	1.03	1.73
MnO	47.95	47.01	47.79	45.22	43.23	41.79	37.48
MgO42	.31	.56	.39	.71	.03	.47
CaO	3.65	1.51	1.73	6.02	6.32	10.59	6.78
Total	99.47	100.61	98.26	101.49	100.50	100.18	91.78
Number of ions on the basis of 6 or 36 oxygen							
Si IV	1.98	1.98	2.00	1.99	2.00	1.98	9.88
Al IV01	.01	.00	.01	.00	.01	.08
T site	1.98	1.99	2.00	2.00	2.00	1.99	10.00
Al VI	—	—	.00	.01	.01	—	—
Fe ⁺³	—	—	—	.00	—	—	—
Fe ⁺²07	.21	.10	.08	.11	.04	.32
Mn ⁺²	1.77	1.72	1.78	1.61	1.55	1.51	6.97
Mg03	.02	.04	.02	.04	.00	.15
Ca17	.07	.08	.27	.29	.48	1.60
M1,M2	2.04	2.03	2.00	2.00	2.00	2.03	9.00

1. NKF-AA-27-2-87, colorless to pale-pink crystals of rhodonite having relatively low calcium contents.
2. NKF-AA-27-2-87-3M, pyroxmangite crystal adjacent to no. 1.
3. NKF-AA-27-2-87-3M, pyroxmangite crystal adjacent to no. 1.
4. EQ-16-1, fine crystals of rhodonite intermixed with rhodocrosite, calcite, and quartz.
5. NKF-Q-17-87, colorless to pink crystals of rhodonite adjacent to vuggy quartz.
6. NKF-M-13-87, calcian rhodonite.
7. Inesite from the Equity vein, Equity mine; FeO determined colorimetrically, MnO by XRF, and all other elements by gravimetrics (Van Loenen, 1980).

contents than electrum rimmed by chalcopyrite or Au-Ag sulfides.

FLUORITE

Large cubes of fluorite (CaF₂) up to 13 mm on a side are found lining vugs, veins, and cavities in the North Amethyst vein system. The crystals are most frequently green; purple and colorless varieties are less common. No clear-cut relation between color and paragenetic position was discerned. Fluorite generally forms late in the paragenesis and usually grows on quartz; however, the fact that the bases of many late-stage quartz crystals contain numerous small octahedra of colorless to pale-green fluorite indicates near-contemporaneous deposition. Fluorite crystals are sometimes dusted with fine-grained quartz sediment that is overgrown by coarse cream-to-pink, manganese-rich calcite and (or) pyrite (fig. 5F). In small vugs, fluorite may follow quartz and adularia.

GALENA

Galena (PbS) occurs in both of the principal sulfide stages of the North Amethyst paragenesis. It generally

is intergrown with chalcopyrite and is similar to chalcopyrite in size and texture where they are found together.

In the Mn-Au association, galena is found as both isolated anhedral grains and aggregates bordering and corroding sphalerite and pyrite in a gangue of fine-grained Mn-carbonate minerals, Mn-silicates, and quartz. In sulfide-rich assemblages, galena is usually in mutual contact with chalcopyrite, pyrargyrite, acanthite, uytenbogaardtite, and polybasite. Bournonite rims are present on some galena. Micrometer-wide rounded grains of galena occur along fractures in the outer zones of sphalerite crystals, and larger grains (10 to 100 μm wide) occur in an almost equigranular mix of sphalerite and chalcopyrite.

In the base-metal-mineral association, anhedral grains and aggregates of 2- to 3-mm-wide galena grains are found bordering sphalerite or enclosed by gangue. The galena is often intergrown with chalcopyrite or tetrahedrite. The generally xenomorphic texture of galena and the occurrence along cracks in sphalerite crystals suggest that it may have formed later than did sphalerite and pyrite. Skeletal crystals of galena also grow on sphalerite and project into quartz- and calcite-filled vugs.

TABLE 8.—*Representative electron microprobe analyses of sphalerite from the North Amethyst vein system*
[Values in weight percent; collected by: NKF, Nora K. Foley; GSP, Geoffrey S. Plumlee]

	1	2	3	4	5	6	7	8	9
Fe ⁺²	0.22	0.80	0.60	1.58	0.67	0.59	4.78	2.12	0.78
Cd ⁺²32	.34	.31	.28	.53	.34	.43	.34	.33
Mn ⁺²19	.80	.63	.69	.24	.06	.57	.56	.16
S ⁻²	32.69	33.11	32.88	33.03	32.77	33.10	32.96	32.73	32.59
Zn ⁺	66.86	64.99	65.98	64.08	66.56	66.90	61.27	63.48	66.67
Total.....	100.28	100.04	100.40	99.66	100.77	100.99	100.01	99.23	100.53
Fe ⁺²00	.01	.01	.03	.01	.01	.08	.04	.01
Cd ⁺²00	.00	.00	.00	.00	.00	.00	.00	.00
Mn ⁺²00	.01	.01	.01	.00	.00	.01	.01	.00
S.....	.99	1.01	.99	1.01	.98	.99	.99	1.00	.98
Zn ⁺²99	.97	.98	.96	.98	.99	.90	.95	.98
Total.....	1.98	2.00	1.99	2.01	1.97	1.99	1.98	2.00	1.97

1. NKF-M-13-87, core of sphalerite crystal occurring in sulfide stringer in fine-grained admixture of rhodocrosite, rhodonite, and quartz.
2. NKF-AA-27-87, core of sphalerite crystal occurring in sulfide stringers in fine-grained admixture of rhodocrosite, rhodonite, and quartz.
3. NKF-BM-65-87, sphalerite crystal occurring in fine-grained gold-bearing sulfide seam containing pyrite.
4. NKF-BM-67-87, sphalerite crystal occurring in fine-grained gold-bearing sulfide seam containing pyrite + magnetite + hematite.
5. NKF-X-24-87, coarse-grained lemon-yellow sphalerite crystal of late base-metal mineralization.
6. NKF-R-18-87, colorless sphalerite in coarse-grained banded crystal occurring in veinlet cutting earlier gold-bearing sulfide seam.
7. NKF-R-18-87, red-brown sphalerite in coarse-grained banded crystal occurring in veinlet cutting earlier gold-bearing sulfide seam.
8. NKF-R-18-87, sphalerite from earlier gold-bearing seam containing magnetite + hematite + pyrite, cut by veinlet containing coarser sphalerite (nos. 6 and 7).
9. GSP-MN-87, coarse crystals of late-stage yellow sphalerite rimmed with minor chalcopyrite.

GYPSUM

Large curls of gypsum ($\text{CaSO}_4 \cdot 2\text{H}_2\text{O}$) ranging in size from a few to tens of centimeters are found in open vugs and cavities along the vein structures. Gypsum having a fine-grained spongelike texture also occurs in vugs and cavities. These crystals certainly formed later than all of the ore-stage minerals and probably are of recent (modern) age.

HEMATITE

Hematite (Fe_2O_3), the most abundant iron oxide mineral, occurs in both mineral associations of the North Amethyst paragenesis. It is intergrown with precious- and base-metal sulfides and other iron oxides in the earlier association and with quartz, chlorite, and base-metal sulfides in the later association. Much of the hematite is coated with iron oxides; microprobe analyses of visually unoxidized grains indicate that they contain less than 1 weight percent combined $\text{MnO} + \text{SiO}_2 + \text{Al}_2\text{O}_3 + \text{MgO}$.

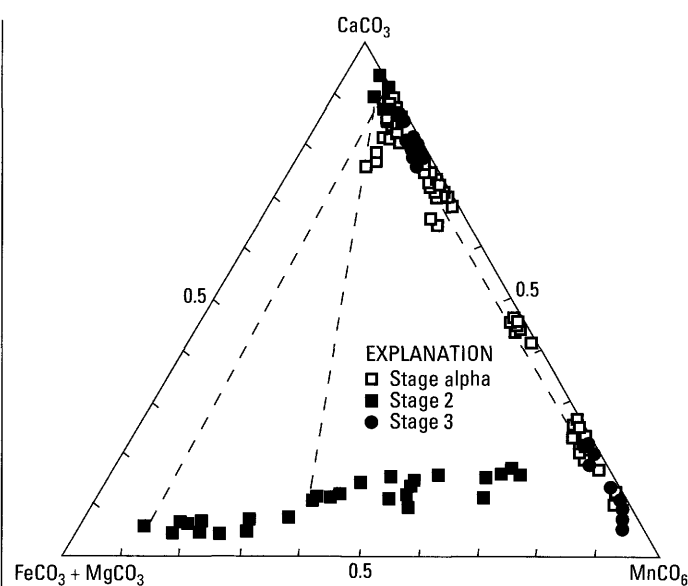


FIGURE 7.—Ternary diagram showing compositions of carbonates for three stages of the North Amethyst vein mineralization. Bars show range of compositions for carbonates present in more than one stage. Possible tie-lines are dashed.

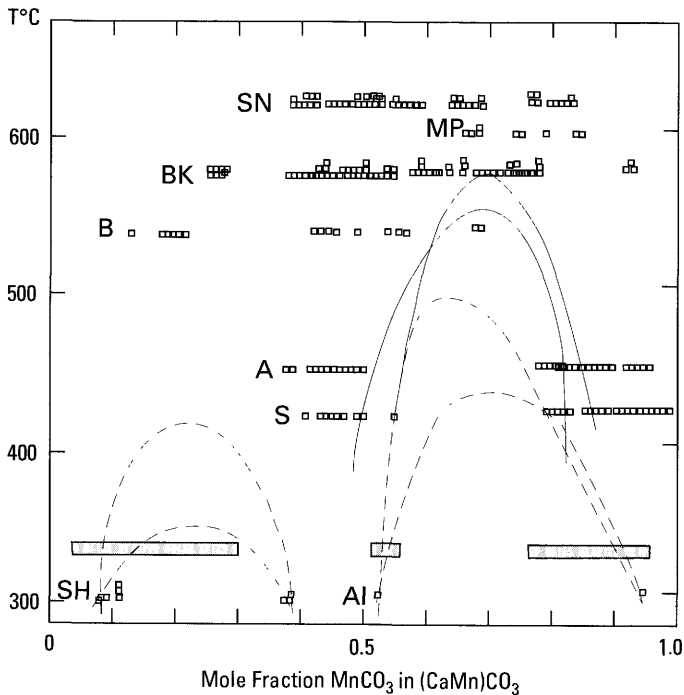


FIGURE 8.— $\text{CaCO}_3\text{-MnCO}_3$ binary diagram of the proposed solvii from experimental studies (solid lines) of Goldsmith and Graf (1957) and deCapitani and Peters (1981) and from studies of naturally occurring carbonates (dashed lines) by Peacor and others (1987). Compositions of carbonates from stage-alpha mineralization are plotted as bands at 330°C , the temperature estimated for coexisting Mn-silicate minerals (see text for discussion). This figure is after Peacor and others (1970) and includes analyses from the following areas: SN, Serra do Navio (Brazil) (Scarpelli, 1973); S, Scerscen (Bernina, Switzerland); A, Alagna (Italy); MP, Muretta Pass (Switzerland) (Peters and others, 1978); B, Buritirama (Parana, Brazil) (Peters and others, 1977); BK, Bald Knob (North Carolina, U.S.A.) (Winter and others, 1981); AI, Andros Island (Greece); and SH, Sterling Hill (New Jersey, U.S.A.) (Peacor and others, 1987).

Blades of hematite, 0.1 to 1.0 mm long, in electrum-bearing samples of the earlier association are intergrown with rounded anhedral magnetite grains ($<50\ \mu\text{m}$ in diameter) and cubes of pyrite. In some sections, the hematite is replaced by magnetite, while in other areas, the hematite has been altered to fine-grained iron oxides. Abundant hematite colors some ore samples a deep red hue.

Thin, transparent-red hematite flakes having well-developed hexagonal outlines occur in the later association as fine- to medium-grained crystals ($<60\ \mu\text{m}$ wide) intergrown with quartz, chlorite, pyrite, sphalerite, galena, and chalcopyrite. The flakes are also included in sphalerite and quartz crystals, where they frequently are clustered along colored growth zones.

MAGNETITE

Magnetite (FeFe_2O_4) is found in the earlier mineral association of the North Amethyst paragenetic sequence

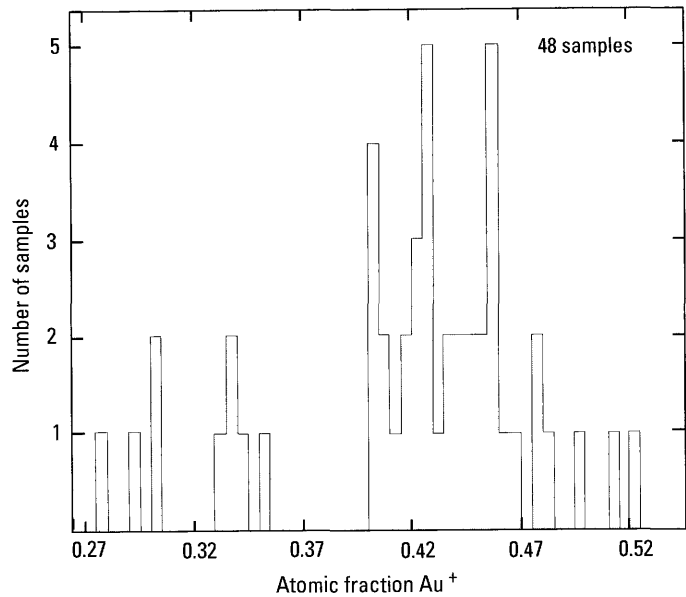


FIGURE 9.—Histogram of gold content of electrum occurring in stage-beta assemblages.

and is primarily associated with hematite and pyrite in a quartz-rich gangue. It occurs as equant grains ($<0.5\ \text{mm}$ wide) intergrown with euhedral pyrite and laths of hematite, and as a replacement of hematite. Some magnetite contains blebs of electrum several micrometers wide. Electron microprobe analyses of magnetite intergrown with hematite indicate virtually no substitution of MnO , Al_2O_3 , SiO_2 , ZnO , or MgO . Magnetite is not found with chlorite. In general, magnetite appears to be restricted to the earlier mineral association, whereas chlorite characterizes the later, base-metal association.

MANGANESE SILICATE MINERALS

At least four Mn-silicate minerals occur in the earliest stage of the North Amethyst ores. Rhodonite is the most abundant, and pyromangite, caryopillite(?), and inesite occur in much smaller quantities. The complete assemblages include rhodocrosite and quartz. Kutnohorite and Mn-calcite are also present in small amounts.

Caryopillite ($\text{Mn}_6\text{Si}_4\text{O}_{10}(\text{OH})_8$).—Fine-grained intergrown aggregates of a pleochroic yellow to brown hydrated layer silicate ($\sim <0.01 \times 0.05\ \text{mm}$) are found in small, matted, 2-mm-wide clumps in the early, Mn-Au association. The mineral fills in around earlier formed-quartz crystals and rims pyrite, chalcopyrite, and sphalerite stringers in a rhodonite + quartz admixture. The mineral clearly formed late, probably by retrograde alteration of rhodonite, pyroxmangite, and inesite. The mineral has been tentatively identified as caryopillite on the basis of petrographic characteristics as described in Abrecht (1989) and energy dispersive analysis.

Inesite ($\text{Ca}_2\text{Mn}_7\text{Si}_{10}\text{O}_{28}(\text{OH})_2 \cdot 5\text{H}_2\text{O}$).—Acicular crystals of inesite (table 7) up to 2 cm in length form radiating

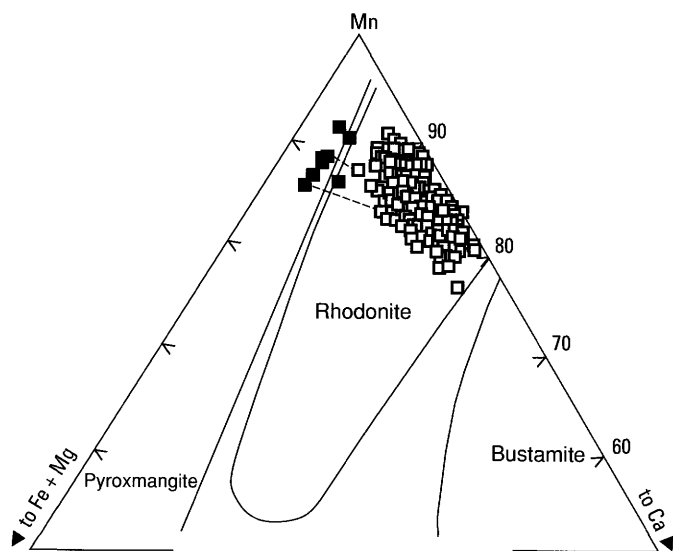


FIGURE 10. — Compositions of all pyroxmangite and rhodonite analyzed for stage-alpha mineralization. See table 4 for sample descriptions and text for discussion. Possible tie-lines are dashed. Stability fields shown are consistent with well-characterized, naturally occurring pyroxenoids in metamorphic environments (estimates at $650 \pm 100^\circ\text{C}$ for all occurrences); presented in Peacor and others (1978), after Ohashi and others (1975).

sheaths that fill fractures cutting silicified wall rock and early Mn-carbonate- and Mn-silicate-bearing assemblages in higher levels of the North Amethyst workings. Minerals intergrown with the coarse pale-pink to cream-colored crystals include quartz, rhodocrosite, Mn-calcite, galena, sphalerite, pyrite, and pyrargyrite.

Pyroxmangite ($\text{Ca}_{.01-.02}\text{Mn}_{.86-.92}\text{Fe},\text{Mg}_{.1-.06}\text{SiO}_3$). — Pyroxmangite (table 7, fig. 10) is present in the earliest stage of mineralization. The mineral ranges in size from a few micrometers to, at most, 100 μm in length and is tentatively identified by X-ray diffraction analysis, petrographic study, and electron microprobe analysis but has not been confirmed by single crystal techniques. It is intergrown primarily with rhodocrosite, rhodonite, and quartz. Microprobe analyses of the mineral (table 7) show a small variation in calcium, iron, and manganese.

Rhodonite ($\text{Ca}_{.08-.2}\text{Fe},\text{Mg}_{0-.08}\text{Mn}_{.92-.76}\text{SiO}_3$). — Rhodonite is the most abundant Mn-silicate present in the early stages of the paragenesis (table 7, fig. 10). The mineral occurs primarily in a cryptocrystalline admixture of quartz, carbonate minerals, and other Mn-silicates and as coarser crystals edging small quartz-filled vugs. The coarser grained crystals range up to 50 μm in width and 200 μm in length.

MARCASITE

Characteristic reflection pleochroism and strong anisotropy distinguish marcasite (FeS_2) from other iron

sulfides. The mineral occurs primarily as 50- to 100- μm -wide tabular or carrot-shaped crystals growing on pyrite and, at times, is coated with chalcopyrite. Anhedra marcasite is found coating and filling cracks in pitted crystals of pyrite. Marcasite generally appears to have formed late in the base-metal-silica association, as carrot-shaped crystals resting on pyrite, as anhedra fillings, and as small fragments caught up in a fine quartz sediment matrix. Distribution of marcasite within the veins is difficult to define because of the fine grain size and scarcity of this mineral.

POLYBASITE

Polybasite ($(\text{Ag},\text{Cu})_{16}\text{Sb}_2\text{S}_{11}$) is most commonly associated with acanthite and generally formed late with respect to other Ag-bearing minerals. The sulfosalt is admixed with galena and sphalerite and intergrown with chalcopyrite; it also replaces sphalerite. The softness of the mineral, light etching, and darker color adjacent to galena help to distinguish it from pyrargyrite.

POTASSIUM FELDSPAR

Feldspar ($\text{K}_{.98-.92}\text{Na}_{.02-.08}\text{AlSi}_3\text{O}_8$) occurs as anhedra to subhedra grains extensively replaced by fine-grained Mn-carbonate, rhodonite, and other Mn-silicates and by quartz in the earliest Mn-rich vein stage. The feldspars vary in composition from Or_{93} to Or_{96} and have barium contents that vary from ~ 0.1 to 2.4 weight percent BaO. These feldspars are compositionally similar to wall-rock phenocrysts of sanidine or orthoclase adjacent to the veins but locally have higher barium contents. The feldspars may have been incorporated into the vein during formation of the earliest stages of mineralization by metasomatic alteration of the volcanic wall rock.

Potassium feldspar also occurs as 0.1- to 1.0-mm-long euhedral barium-rich crystals of adularia intergrown with amethystine quartz and filling small vugs, cavities, and fractures in most vein material. The adularia is associated with minerals of the base-metal association and is relatively common throughout the ore zone. Adularia ranges in content from Or_{92} to Or_{93} and contains 0.4 to 1.6 weight percent BaO.

PYRARGYRITE-PROUSTITE

Pyrargyrite (Ag_3SbS_3)-proustite (Ag_3AsS_3) primarily occurs alone in small ($>10 \mu\text{m}$) anhedra grains scattered through a silicious gangue and in aggregates with acanthite that border galena and sphalerite. It also is intergrown with acanthite and native silver in aggregates that border or are enclosed by chalcopyrite. Other grains are

intergrown with acanthite and uytenbogaardtite and rim chalcopyrite, tetrahedrite, and galena. Subhedral prismatic to anhedral crystal aggregates are enclosed by rhodochrosite and quartz and occur along cracks in broken pyrite cubes.

PYRITE

Pyrite (FeS_2) is the most abundant and ubiquitous sulfide mineral, as it occurs in almost all stages of both mineral associations. It is primarily associated with either quartz-chlorite-hematite assemblages or other base-metal sulfides. The pyrite shows idiomorphic habit, and cubes are the most common shape, although some overgrowths and aggregates are anhedral. Thin botryoidal crusts of pyrite occur late in the paragenetic sequence in places.

In the early association, subhedral equant pyrite crystals are bordered by sphalerite, rimmed by chalcopyrite and galena, and contain inclusions of all three sulfides. The crystals range in size up to a millimeter on edge; however, most are in the range 0.1 to 0.3 mm. Some of these crystals also contain rounded blebs of electrum. Grain margins of the pyrite crystals are often corroded and replaced by sphalerite and galena.

Some crystals are isotropic to faintly anisotropic and twinned. There is often a zonal arrangement with sphalerite, acanthite, and pyrargyrite crystals, which suggests that pyrite began to crystallize early, and its deposition continued as other sulfides and sulfosalts began to form. Later pyrite overgrowths on these crystals do not show inclusions. Rarely, marcasite crystals sit on pyrite. Pyrite also occurs as isolated equant cubes in quartz and carbonate gangue.

In the later association, euhedral pyrite is found in mixtures of quartz, hematite, and chlorite and is also intergrown with euhedral sphalerite and anhedral galena and chalcopyrite. The pyrite crystals of the late association are much larger in size, and cubes up to a centimeter on edge do occur. However, most pyrite crystals in this association are a millimeter or less on a side. Pyrite crystals in the size range 0.1 to 0.5 mm dust singly terminated quartz crystals and coarse crystalline calcite (fig. 5E) in the latest stage. They also occur as millimeter-thick layers within crusts of carbonate minerals. At times, 50- to 100- μm -sized carrot-shaped marcasite crystals overlie this latest stage pyrite.

QUARTZ

Quartz (SiO_2) occurs in all mineralogical stages and shows a variety of textures ranging from cryptocrystalline interlocking grains to large, terminated euhedral

crystals. Quartz also occurs as a chalcedonic cementing medium in many breccias.

In the early stages of mineralization, quartz $< 50 \mu\text{m}$ in size is intergrown in a microcrystalline mix of Mn-silicate and Mn-carbonate minerals. It fills barite molds and small vugs that occur within the mix.

In later stages, quartz occurs most often as larger (0.2 cm to 5 cm) crystals intergrown with base-metal sulfides, fluorite, and calcite. Where they project into vugs, the crystals are euhedral and terminated. Much of the quartz is amethystine, especially the outer parts of crystals. The larger crystals contain solid inclusions, including fluorite octahedra, laths of rhodonite(?), and carbonate crystals. Fluid and solid inclusions often are found decorating acicular structures that radiate from the bases of the quartz crystals.

Quartz also forms the cement for many of the breccias and sediments found within the ore zones. The siliceous cements are generally gray and chalcedonic. Coarser areas of cement show a granular texture with overgrowths of quartz. In some samples, the quartz has sutured grain boundaries. One of the breccias has a distinctive black quartz cement; the color apparently results from fine sulfides and electrum admixed with the quartz. Some vein sediment areas consist of fine parallel laminations distinguished by subtle variations in color and grain size. The chalcedonic laminations have a mosaic texture, with sutured grain boundaries between fine crystalline quartz, that may reflect recrystallized amorphous silica sediment.

SILVER

Native silver (Ag^0) occurs primarily as scarce, lone 10- to 100- μm -sized grains in fractures and as millimeter-long wire aggregates in cavities or resting on broken surfaces. It is also found as scarce grains bordering galena that are enclosed by gangue and are rarely bordered by acanthite. In some samples, native silver borders sphalerite in aggregates that include chalcopyrite, jalpaite, and possibly stromeyerite. Textural relations indicate that native silver occurs much later in the paragenetic sequence than most other silver minerals.

SPHALERITE

Sphalerite ($(\text{Zn}, \text{Fe}, \text{Mn}, \text{Cd})\text{S}$) is one of the most abundant sulfide minerals in the deposit. The mineral is found in two stages of the early, Mn-Au association and in one stage of the later, base metal-silica association. Sphalerites in different stages vary in grain size, color, and composition.

Stage alpha.—Small (<2 mm) rounded grains of intensely chalcopyritized sphalerite occur in small stringers within the cryptocrystalline admixture of Mn-silicates, carbonate minerals, and quartz that make up the earliest stage. The sphalerite is intergrown with cubes of pyrite and anhedral galena and contains generally low and subequal amounts of iron, cadmium, and manganese (table 8, Nos. 1 and 2).

Stage beta.—Abundant sphalerite is present also in the precious- and base-metal seams of the Mn-Au association. It is often rimmed and replaced by electrum, pyrargyrite, acanthite, chalcopyrite, uytenbogaardtite, and galena. Sphalerite corrodes and sometimes replaces pyrite. Small equant grains also occur in siliceous gangue, with sparse micrometer-sized exsolution blebs of chalcopyrite. Sphalerite is bordered and corroded by all of the other sulfides, especially galena and chalcopyrite, and by tetrahedrite. All sphalerite of the Au-bearing stage is extensively chalcopyritized, and most crystals (table 8, No. 3) have a composition similar to that of the sphalerite described above. An important exception to this is that sphalerite intergrown with magnetite and hematite has a more iron rich composition (table 8, Nos. 4 and 8), generally containing around 2 percent iron by weight.

Stage 1.—Sphalerite crystals of the later, base-metal stage range in width from about a millimeter to a maximum of about 2 cm and range in hue from colorless to greenish to pale yellow to dark red-brown. The subhedral, equant crystals form aggregates that are intergrown with galena, euhedral pyrite, chalcopyrite, and minor tetrahedrite. All sphalerite of this association is chalcopyritized; it contains numerous microscopic inclusions of chalcopyrite that are especially abundant at the rims. Some grains also contain abundant minute blebs of tetrahedrite that are concentrated at grain boundaries.

While most grains are uniform in color, many larger crystals of sphalerite are color banded on a simple scale. The colors fall into three groups—red-brown, yellow, and colorless—that show only minor color variation. On the scale of individual crystals, the contact between colors is sharp rather than gradational.

The majority of the banded samples studied have colorless or yellow cores and red-brown rims (thin-section thicknesses ranging from 60 μm to 1 mm). Rims, in shades ranging from moderate red-brown to deep red-brown, are more finely banded than cores; however, they still do not show the beautifully well-developed banding of samples typical of the OH vein in the main Creede district as described by Barton and others (1977) and Roedder (1977). Other samples show an alternating set of color bands, from red-brown to yellow to red-brown, but these are less common. No attempt was made

to correlate color banding in the sphalerite, because possible marker horizons lacked continuity.

Analyzed sphalerite from the later, sulfide-rich stage displays higher and more variable iron contents (up to 8 mole percent FeS) than earlier sphalerites (table 8, Nos. 5–8). Some of the darkest sphalerites were not analyzed, so the true range may be higher. Measured iron contents are not as high as those of sphalerite from the OH vein of the main mining district (Barton and others, 1977), which contains up to 16 mole percent FeS. However, the most typical iron contents of North Amethyst sphalerite (~1 mole percent FeS) are similar to the most typical iron contents of OH sphalerite (~1 to 2 mole percent FeS).

STEPHANITE

A silver sulfosalt resembling stephanite (Ag_5SbS_4) is intergrown with pyrargyrite and polybasite in aggregates in a siliceous matrix. It is also found alone filling cavities and fractures in the siliceous matrix.

TETRAHEDRITE-TENNANTITE

Tetrahedrite-tennantite ($(\text{Cu,Fe,Ag,Zn})_{12}(\text{Sb,As})_4\text{S}_{13}$) occurs in all sulfide-bearing stages, usually in association with sphalerite, galena, pyrite, and chalcopyrite. Reported to be Ag-rich (S.W. Caddey, C.B. Byington, and D.M. Vardiman, written commun., 1988), energy dispersive analysis confirms that much of the tetrahedrite contains appreciable amounts of silver and arsenic.

In the early association, tetrahedrite is most often adjacent to sphalerite and galena and also is in aggregates with chalcopyrite and acanthite. Scarce anhedral grains of tetrahedrite occur marginal to, and intergrown with, chalcopyrite and acanthite. Tetrahedrite also occurs with polybasite, intergrown with pyrargyrite and acanthite, alone, and intergrown with galena and chalcopyrite in cavity fillings.

In the later association, 50- to 70- μm -sized grains of tetrahedrite most often are with contemporaneous chalcopyrite and galena in aggregates that border sphalerite. Rounded micrometer-sized grains of tetrahedrite occur in sphalerite in a texture similar to that of chalcopyrite disease.

Growth banding was not observed in any of the samples, possibly because of their small grain size. Growth banding in tetrahedrite from the Bulldog vein of the Creede district is described by Plumlee (1989). He found that the growth bands reflected compositional variations in Ag, As, and Sb.

UYTENBOGAARDTITE

Uytenbogaardtite (Ag_3AuS_2) most often is intergrown with acanthite containing micrometer-sized electrum

($\text{Au}_{3-4}\text{Ag}_{7-6}$) grains. When intergrown with acanthite, uytenbogaardtite can be distinguished readily from the acanthite, and from many other silver minerals, by its extremely rapid light etching. Small and irregularly shaped anhedral grains of uytenbogaardtite also occur alone or in contact with other minerals such as pyrrargyrite, and, especially, chalcopyrite.

DISCUSSION OF MINERAL EQUILIBRIA

GOLD AND SILVER SULFIDES

Experimental work by Barton (1978) demonstrated that uytenbogaardtite is stable at relatively low temperatures (<200°C) with Au-bearing argentite but that only below 113°C can uytenbogaardtite coexist with acanthite. Barton (1978) also showed that uytenbogaardtite is stable with relatively Au-rich electrum compositions (0.8–0.9 atomic fraction Au). The intergrowth textures described in this study for uytenbogaardtite, acanthite, and electrum are similar to those described by Barton and others (1978) for uytenbogaardtite from the Comstock lode. For that deposit, they suggested that the textures may reflect exsolution during cooling of a higher temperature Au-bearing argentite + Ag-rich electrum assemblage. Upon cooling, the argentite would exsolve uytenbogaardtite and leave the original Ag-rich electrum with acanthite and uytenbogaardtite. Thus, the Au- and Ag-sulfide equilibria for the North Amethyst ores most likely reflect subsolidus reequilibration at quite low temperatures and, like the Cu-Ag-sulfides, cannot be used to yield reliable temperatures of specific conditions of ore deposition because of their fast reaction rates.

CARBONATE MINERALS

Peacor and others (1978, 1987) have suggested possible solvii between calcite and kutnahorite and kutnahorite and rhodocrosite to account for the compositions of some naturally occurring carbonate minerals. Comparison of those solvii with the North Amethyst carbonate data suggests temperatures of formation above 350°C for the calcite-kutnahorite compositions of the early assemblage and temperatures in excess of 425°C, and possibly in excess of 500°C, for rhodocrosite intergrown with kutnahorite in the early assemblage (fig. 8). The most Ca-rich rhodocrosite of the earliest carbonate-bearing stage has a composition of $\text{Cc}_{23}\text{Rc}_{75}$ and contains less than 2 mole percent combined $\text{FeCO}_3 + \text{MgCO}_3$. This composition is somewhat less calcic than the critical point of the $\text{CaCO}_3\text{--MnCO}_3$ solvus as reported by deCapitani and Peters (1981) at 540°C and a composition of $\text{Cc}_{32}\text{Rc}_{68}$. (Experiments were run at 2 and 10 kbar, and no significant differences due to pressure were detected.) These

temperatures are exceedingly high and, as discussed below, unreasonable for this environment.

Temperatures above 300°C are unusual for mineralization occurring in the typically shallow epithermal environment (Heald and others, 1987) where depths are generally on the order of 500 m. However, for the North Amethyst vein, about 1,500 m of volcanic and volcanoclastic rock may have overlain the base of Au-rich mineralized rock (Lipman and Sawyer, 1988; Foley, 1990). A simple analysis based on temperature-depth calculations of Haas (1971) indicates that the boiling point of a nonsaline fluid at 1,500 m is about 320°C; fluids that are more saline would boil at higher temperatures. Temperatures as high as those suggested by carbonate mineral equilibria are unlikely, however, because they would require formation at unreasonably great depths. The excessively high temperatures suggest that compositions of rapidly deposited carbonates of the early stage may be metastable.

Rhodocrosites and calcites from all later stages of mineralization have more restricted compositional ranges and lie outside experimental solvii (Goldsmith and Graf, 1957; diCapitani and Peters, 1981) at temperatures of less than 400°C.

MANGANESE SILICATE EQUILIBRIA

Pyroxmangite and rhodonite are polymorphs of MnSiO_3 . Rhodonite is the high-temperature form and is stable above about 350°C at pressures of 1 to 2 kbar, whereas pyroxmangite of MnSiO_3 composition is the stable phase at low pressures below 350°C (Maresch and Mottana, 1976). The presence of both rhodonite and pyroxmangite can be used to constrain temperature if the compositions do not depart markedly from MnSiO_3 and if pressure is known. In this case, because up to 11 weight percent CaO and 2 weight percent FeO + MgO replaces MnO, and because pressures are not well constrained (Foley, 1990), the assemblage can be used only qualitatively. To a first approximation based on ionic radii, the substitution of Mg^+ and Fe^+ would stabilize pyroxmangite at higher temperatures, whereas the substitution of Ca^+ should stabilize rhodonite to lower temperatures (Maresch and Mottana, 1976).

If an ideal ionic activity model is used as a first approximation to describe the activity of MnSiO_3 in rhodonite and pyroxmangite and the phase equilibria data of Maresch and Mottana (1976) are used, the free energy of reaction can be written as:

$$\begin{aligned} \Delta G_r = & \Delta H_r - \Delta S_r + P\Delta V_r + RT\ln K_r = 1347(\pm 100) \\ & - 2.069(\pm 0.2)T(^{\circ}\text{K}) + 0.0418(\pm 0.025)P(\text{bars}) \\ & + 8.3143T(^{\circ}\text{K})\ln(X_{\text{Mn,rhodonite}}/X_{\text{Mn,pyroxmangite}}) \end{aligned}$$

where ΔG_r = Gibbs free energy of formation for the reaction

ΔH_r = enthalpy of formation of the reaction

ΔS_r = entropy of formation of the reaction

P = pressure

ΔV_r = change in volume of the reaction

R = gas constant

T = temperature of the reaction

K_r = equilibrium constant for the reaction

X = mole fraction

This can be further recast to define temperature:

$$T(^{\circ}\text{C}) = \frac{162(\pm 12) - 5.027(\pm 3.0)P(\text{kbars})}{0.2488(\pm 0.025) - \ln(X_{\text{rhodonite}}/X_{\text{pyroxmangite}})} - 273$$

When data for coexisting rhodonite-pyroxmangite pairs ($P = 0.5$ kbar) are used, an approximation to the temperature of equilibrium can be calculated:

X_{MnSiO_3} pyroxmangite	X_{MnSiO_3} rhodonite	$T^{\circ}\text{C}$ (estimated)
0.89 ± 0.01	0.875 ± 0.01	$327 \pm 58^{\circ}\text{C}$
0.86	0.85	$339 \pm 58^{\circ}\text{C}$

Temperatures at the middle to lower range of this approximation to the temperature of equilibrium ($\sim 330 \pm 60^{\circ}\text{C}$) are in general agreement with mineral assemblages, fluid-inclusion data, and other geologic considerations for the Mn-Au association of the North Amethyst vein system.

MINERAL ASSOCIATIONS AND ASSEMBLAGES

The ore and gangue minerals of the North Amethyst vein system are paragenetically complex; they fall into two mineralogically, texturally, and chemically distinct associations. The associations overlap spatially but were separated in time by a period of extensive brecciation and sedimentation. The earlier association is characterized by two mineralogic stages, whereas the second, later association is subdivided into three stages on the basis of mineralogy and textural relations. Successive stages in each association are generally marked by relatively sharp rather than gradational changes in mineralogy and by periods of movement, brecciation, sedimentation, or replacement. In only a few instances are the transitions characterized by intergrowths or interbanding between mineral assemblages of adjacent stages.

Figure 11 describes the sequence of events relating to formation of mineralized rock in the North Amethyst area. The general sequence of mineral deposition is shown in figure 12. Temporal and spatial relationships

between mineralization, brecciation, and sedimentation are shown in a series of diagrams beginning with figure 13.

ALTERATION AND PRE-ORE VEIN ASSEMBLAGES

Several types of wall-rock alteration have been observed in the North Amethyst vein system. These include intense sericitic alteration at higher levels in the system, two stages of potassium metasomatism of the wall rock at depth, and a bleaching of the wall rock adjacent to some vein structures at all levels (figs. 11, 13). A detailed examination of the alteration assemblages was beyond the scope of this study and is unwarranted because of existing regional studies of alteration relations in the Creede area. However, certain observations can be made on the basis of field relations, hand-sample study, geochemical variations, and some X-ray diffraction analyses.

SERICITIC ALTERATION

Intense sericitic alteration characterized by illite-smectite clay minerals is generally restricted to above the 10400 level of the North Amethyst vein workings (see fig. 6). Geochemical analysis of selected material by the WDXRF and graphite AA techniques outlined in Baedeker (1987) (N.K. Foley, unpub. data, 1990) shows that the most intense sericitically altered rock consists of about 90 percent $\text{SiO}_2 + \text{Al}_2\text{O}_3$, 4 percent K_2O , and 2.5 percent combined $\text{Fe}_2\text{O}_3 + \text{FeO} + \text{MgO}$; measured precious-metal values (~ 5 ppm Au) are much higher than those of typical unaltered volcanic rock but lower than those of substantially less-altered wall rock adjacent to veins lower in the workings (20 to 40 ppm Au).⁵

The light-colored sericitic alteration is cut by seams of fine-grained dark-colored clay (mixed illite-smectite by X-ray diffraction). Quartz veins also cut the sericitic material; sharp contacts suggest that the veins formed when the rock was more competent, prior to the peak alteration event. Clear-cut paragenetic relations between ore mineralization and this intense alteration were not found; however, the alteration zone appears to overlie the zone of base-metal-rich mineralized rock and cuts across the zone of Au-bearing mineralized rock. Au- and Mn-silicate-bearing assemblages occur at elevations above and below the intense alteration zone, but the base-metal-rich later stages are only below, as is true for veins in the main Creede district. No information is available on the presence or absence of alteration assem-

⁵ Average gold values are notoriously difficult to determine because of the effect of a single nugget of electrum on a bulk analysis, so these values are given only for general discussion. They do not reflect actual modes or means.

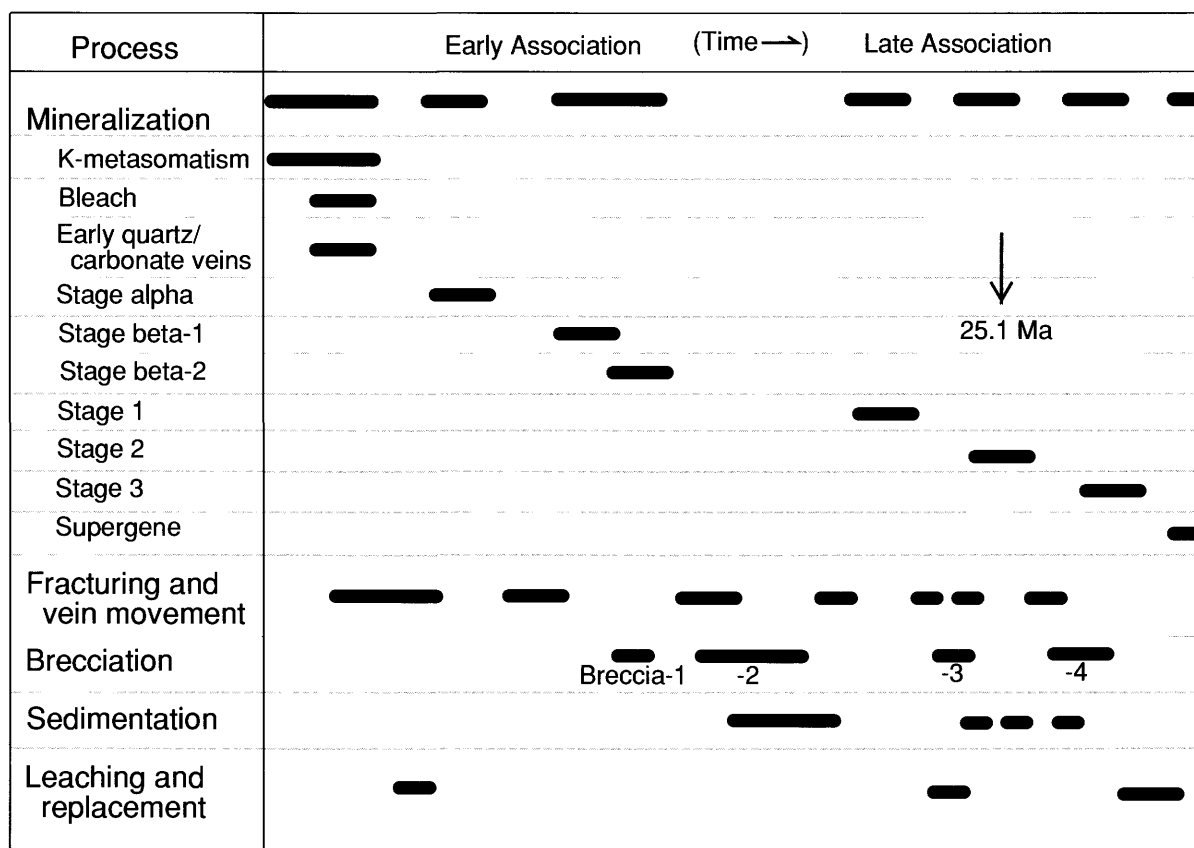


FIGURE 11. —Progression of events in the development of the North Amethyst ores. See text for description of stages and named breccias. Arrow locates interval containing dated adularia.

blages above the highest elevations of gold mineralization. Rocks cropping out on the hillside above the North Amethyst portal are stained by iron oxides all along the trace of the Equity fault.

Well-developed clay alteration zones cap vein structures throughout much of the central and southern Creede district (Steven and Eaton, 1975; Barton and others, 1977; Horton, 1983). Barton and others (1977) and Bethke and Rye (1979) proposed that the caps formed primarily as a result of reaction of the wall rock with acidic fluid that resulted from condensation of ore fluid that boiled at depth. An age date on illite-smectite from the cap material in the OH vein of the southern part of the district is in agreement with dates measured on vein adularia and sericite (table 1). A similar interpretation could explain the relation between overlying alteration-zone and base-metal mineralization in the North Amethyst area; however, any relation to gold mineralization is left unexplained.

POTASSIUM METASOMATISM AND BLEACHING

Wall rocks of the North Amethyst vein are potassium metasomatized at depth. A general increase in potassium content of the wall rock with depth is reported by

Sawyer and others (1989), who suggest that the intensity of potassium metasomatism may increase with depth in the vein system. This pattern may be influenced by type and distribution of veins within the wall rock, because bleached wall rock has elevated potassium contents over adjacent unbleached wall rock at all depths (N.K. Foley, unpub. data, 1990). Moreover, the barium contents of potassium feldspar in the bleached wall rock are higher than barium contents of unbleached wall rock, a fact suggesting that the bleaching event was chemically distinct from the regional pre-ore potassium metasomatic event (N.K. Foley, unpub. data, 1990). Sharp contacts between bleached and unbleached wall rock, coupled with the chemical distinctions cited above, suggest that the bleaching event postdated the potassium metasomatism; however, this needs to be substantiated by studies that delineate the extent of the metasomatism within the Nelson Mountain Tuff and that determine mass transfer among the alteration zones and vein mineral assemblages. Within the central and southern Creede district, a bleaching event confined to wall rock adjacent to a vein does postdate the regional potassium metasomatism of the Carpenter Ridge Tuff (P. Barton and P. Bethke, oral commun., 1989).

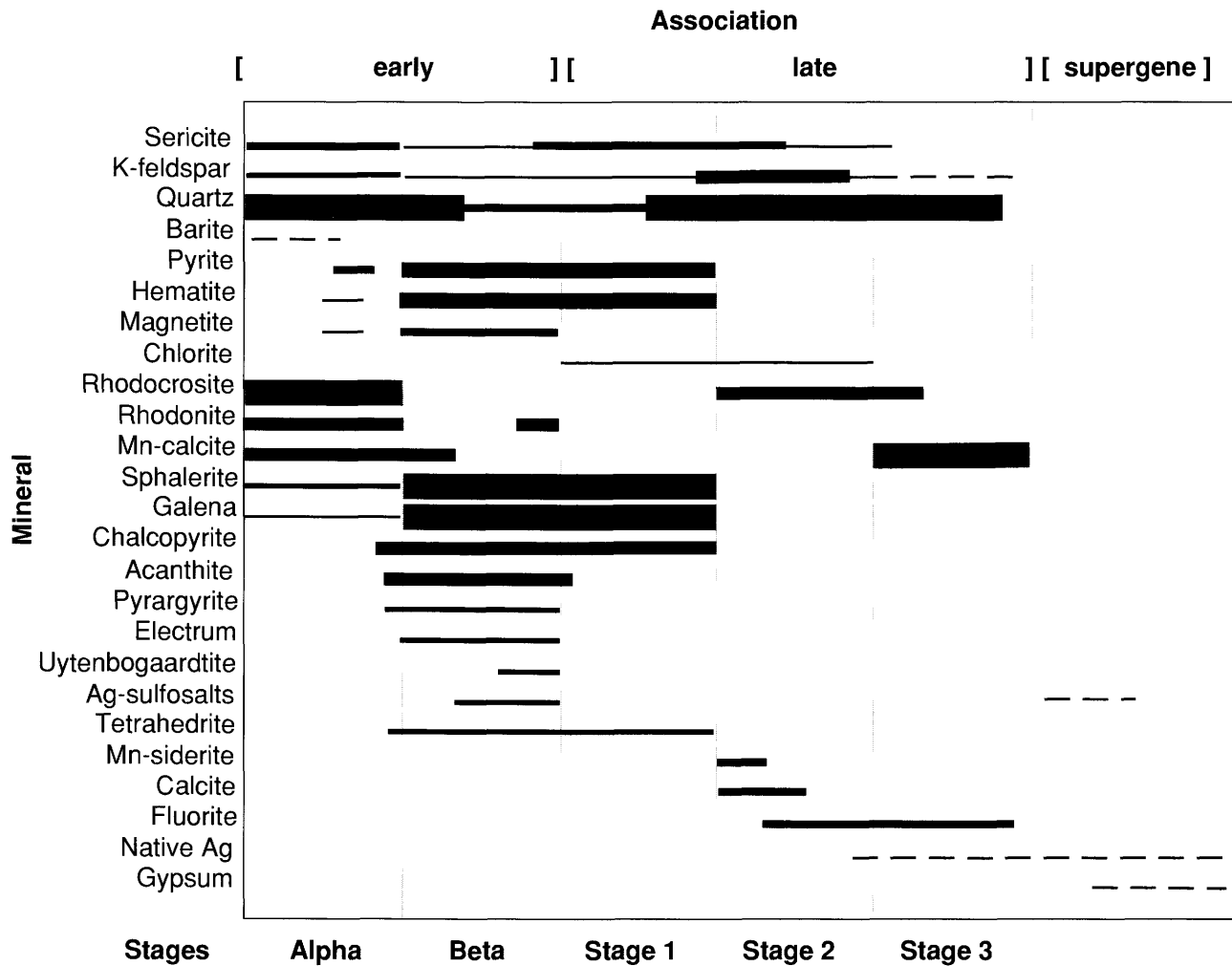


FIGURE 12. —Composite paragenesis diagram for the North Amethyst mineralization. Mineral deposition is shown in black. Leaching is not shown because of its local character. The thickness of a bar for a given mineral is proportional to its abundance. Dashed vertical lines show temporal boundaries for stages. Most transitions are defined by brecciation (see fig. 11).

The bleaching event (fig. 13A) resulted in a color change from gray and gray-tan to off-white of widths ranging from a few centimeters to tens of centimeters in wall rock adjacent to some veins. The event apparently predates all mineralization because vein minerals of both associations fill structures that cut both bleached and unbleached wall rock. In drillcore away from the underground workings, similar bleached fractures are filled with a fine-grained mixture of pyrite, quartz, and, at times, hematite and (or) chlorite.

Unbleached Nelson Mountain Tuff forms the wall for many of the mineralized veins. In general, the rock is hard and brittle, medium to dark gray, and retains volcanic textures consisting of phenocrysts (<2 mm) and flattened pumice in a very fine groundmass. The brittle nature indicates that the Nelson Mountain Tuff is silicified adjacent to veins, although chemical analyses of the rock show that SiO_2 and total alkali contents are not

much elevated over values typical for volcanic rocks of dacitic-rhyolitic composition, on the basis of the IUGS classification scheme (LeMaitre, 1989; N.K. Foley, unpub. data, 1990). In the northern part of the workings, the veins cut slightly coarser grained rocks, possibly intrusive dacitic Nelson Mountain Tuff (Equity Member; Lipman and Sawyer, 1988), that are propylitized; they contain epidote, calcite, and abundant chlorite.

Most of the wall rock visible underground is cut by small (<3 cm) fractures that are crosscut in turn by minerals of the two main sulfide-bearing associations—the Mn-Au and base-metal-silica. These fractures are filled primarily with quartz and calcite and cut both bleached and unbleached wall rock. In drillcore away from the intensely mineralized area, bleached fractures contain mainly quartz, calcite, and pyrite, and occasionally barite and minor amounts of base-metal sulfides. In drillcore south of the exploratory workings, barite has

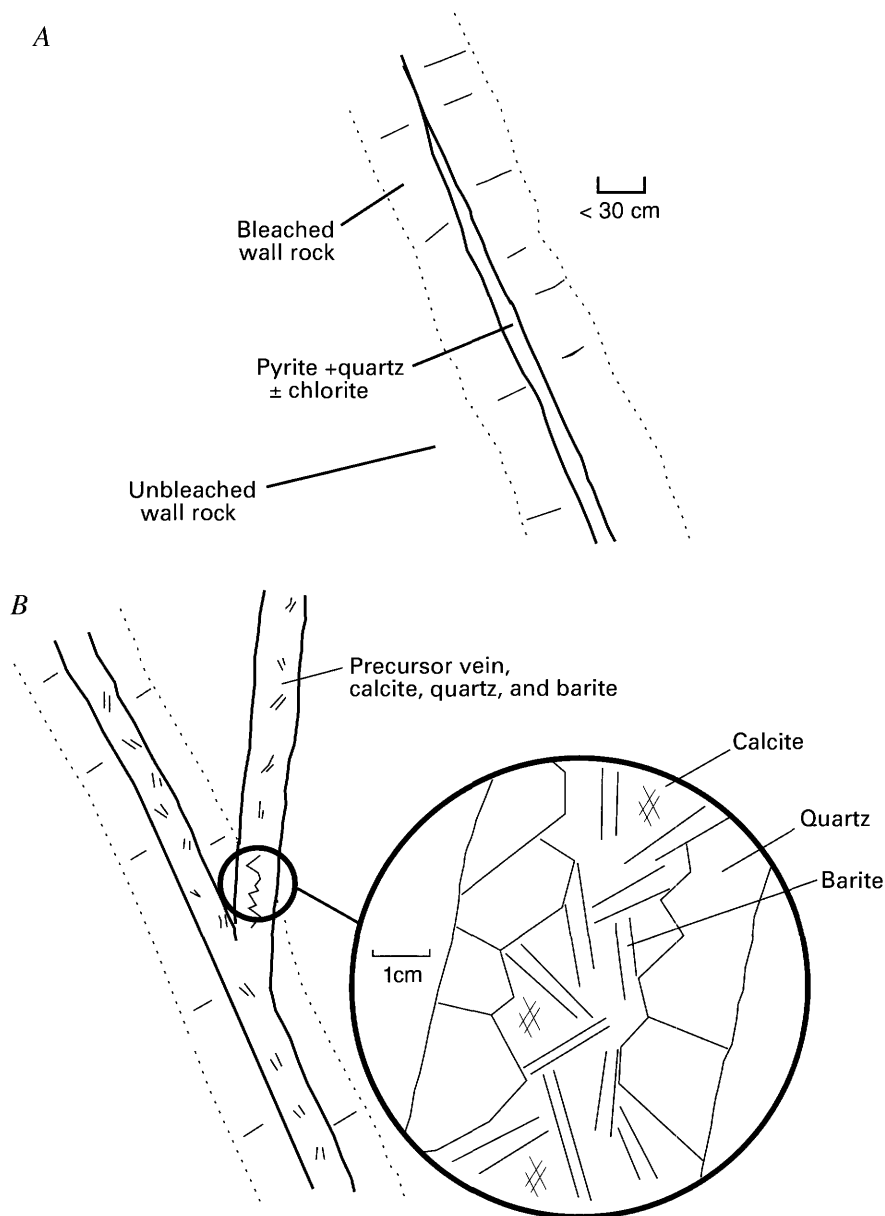


FIGURE 13.—A, Bleached and unbleached wall rock adjacent to early pyrite + chlorite + quartz vein; these veins are found in drillcore away from main ore zones. B, Relation between precursor veins and bleached and unbleached wall rock within the main ore zone.

also been identified in similar fractures (D. Sweetkind, written commun., 1990). Barite was not found in samples collected underground and examined in this study, although it has been reported (S.W. Caddey, C.B. Byington, D.M. Vardiman, oral. commun., 1987). As described earlier, possible barite molds have been identified in samples of early assemblages collected from the underground workings.

MANGANESE-GOLD ASSOCIATION

The Mn-Au association is so named because of the presence of electrum and Au-Ag sulfide in one stage and

because of the abundance of Mn-bearing minerals in the other stage. The occurrence and proportion of these two elements and the textural character of the minerals distinguish this association from the later, base-metal-rich association of the North Amethyst vein system and from other mineralized veins found throughout the Creede district.

The first stage, alpha, is characterized by Mn-carbonate minerals, Mn-silicates, and minor base-metal sulfides. The second stage, beta, has abundant precious- and base-metal minerals and minor quartz and carbonate gangue. Each stage has two mineralogically similar

substages identified by crosscutting relations. The sulfide-rich substages were separated by a period of fracturing and the development of a breccia having characteristic fragments.

STAGE ALPHA

The first vein-filling event that is directly related to ore development in the North Amethyst area occurred during faulting and fracturing of the volcanic wall rock. This event introduced Mn-rich fluids that deposited a fine-grained, almost cryptocrystalline, banded mineral mixture consisting predominantly of rhodocrosite, manganese calcite, rhodonite, pyroxmangite, and quartz (figs. 11, 14A). Locally, this fine-grained material of stage alpha coated a platy, tabular mineral (barite?) that was subsequently leached; the molds are filled with coarser adularia and quartz (probably stage-2 minerals; see below). Minor sulfides, primarily pyrite, sphalerite, and galena, occur in stringers in the Mn-carbonate, Mn-silicate, and quartz matrix. Retrograde alteration of this material produced a complex suite of hydrated Mn-silicate and Mn-carbonate minerals.

Vein widths of stage alpha vary from a few centimeters to more than a meter. Features that characterize this stage are best preserved in the narrower veins; wider veins show multiple fracturing events and recrystallization of minerals.

Alpha-1 substage veins cut bleached and unbleached wall rock and precursor veins, indicating that both the bleaching event and the development of precursor veins predated this stage. In general, contacts of vein and wall rock are sharp; however, the occurrence of embayed and partially replaced grains of potassium feldspar in the Mn-rich matrix suggests that some metasomatic replacement of wall rock may have occurred.

Deposition appears to have progressed from the walls in toward the center of the veins, leaving open spaces in the center. The walls of the spaces have a rounded, bulbous texture and were filled later with 1- to 2-mm-long adularia rhombs, coarse amethystine quartz (~2 to 3 cm long), rhodocrosite (1 to 5 mm wide), and, in places, fluorite (1 to 2 mm wide) and sphalerite (1 to 2 mm wide; probably stage-2 minerals).

The alpha-2 substage consists of a fine-grained mixture of quartz, rhodocrosite, and Mn-silicate minerals deposited around fragments of alpha-1 substage and wall rock (fig. 15). This substage is more quartz rich than the earlier alpha substage and has a greater proportion of base-metal sulfides. Definition of this stage and its exact position in the paragenesis is complicated by evidence that most fluids of later stages reacted with or recrystallized stage alpha to some extent. Alpha-2 substage is probably a product of the local reaction of later stage fluids with fragments of the alpha-1 substage; however,

a second influx of Mn-rich fluids may have contributed to the mineralization.

STAGE BETA

Continued movement of the North Amethyst vein and fracturing of the stage-alpha assemblage caused the vein system to open up again. Precious- and base-metal-rich fluids invaded the fractures and precipitated a complex suite of Au-, Ag-, Cu-, Zn-, Pb-, and Fe-bearing sulfides and sulfosalts (figs. 12, 14B). The location of the sulfide-rich seams may have been controlled in part by the structurally weak vuggy zones in the core of stage-alpha vein material. Seam widths vary from a few millimeters to tens of centimeters, although most samples studied had widths of 2 to 3 cm. The ore seams are reasonably intact in some areas, but most show minor offsets. In other areas, the seams are stretched and broken, and sulfide-rich pods are more strongly deformed.

Stage-beta fluids appear to have irregularly altered stage-alpha minerals from a dominantly Mn-carbonate, Mn-silicate, quartz assemblage to a Mn-carbonate and quartz assemblage. During the retrograde alteration, hanging-wall sides of the sulfide-rich seams are often recrystallized to a coarse Mn-calcite, whereas footwalls are altered to a dusty fine-grained mixture of rhodocrosite and quartz (fig. 4D).

The complex suite of precious- and base-metal sulfides precipitated by stage-beta fluids is listed in table 3, and the paragenetic sequence for the most common stage-beta minerals is shown in figure 12. The intergrowth of gangue, sulfides, and sulfosalts shows that, in general, deposition within stage beta was initiated by precipitation of pyrite and sphalerite, followed by galena, chalcocopyrite, electrum, and other Au and Ag minerals. Although the depositional sequence was interrupted by minor periods of dissolution (for example, replacement of pyrite crystals; chalcocopyrite, and tetrahedrite disease in sphalerite; corroded sphalerite crystals), stage-beta precipitation was generally continuous. Native silver, stromeyerite, and other minerals are found mainly in tiny late-stage veinlets that cut the stage-beta seams or as rims on earlier phases, and may be supergene.

Stage-beta seams show a mineralogic zonation that is discontinuous along strike of the seams and irregularly distributed across the vein widths. Zn, Fe, and Pb minerals occur across the width of all seams, while chalcocopyrite and other Cu-bearing minerals are concentrated toward the center of the seams. In general, electrum and Au- and Ag-sulfides and sulfosalts occur with, or are generally formed later than, chalcocopyrite.

The iron-oxide and -sulfide assemblage of stage beta consists of magnetite, hematite, and pyrite. This relatively oxidizing assemblage occurs locally along the

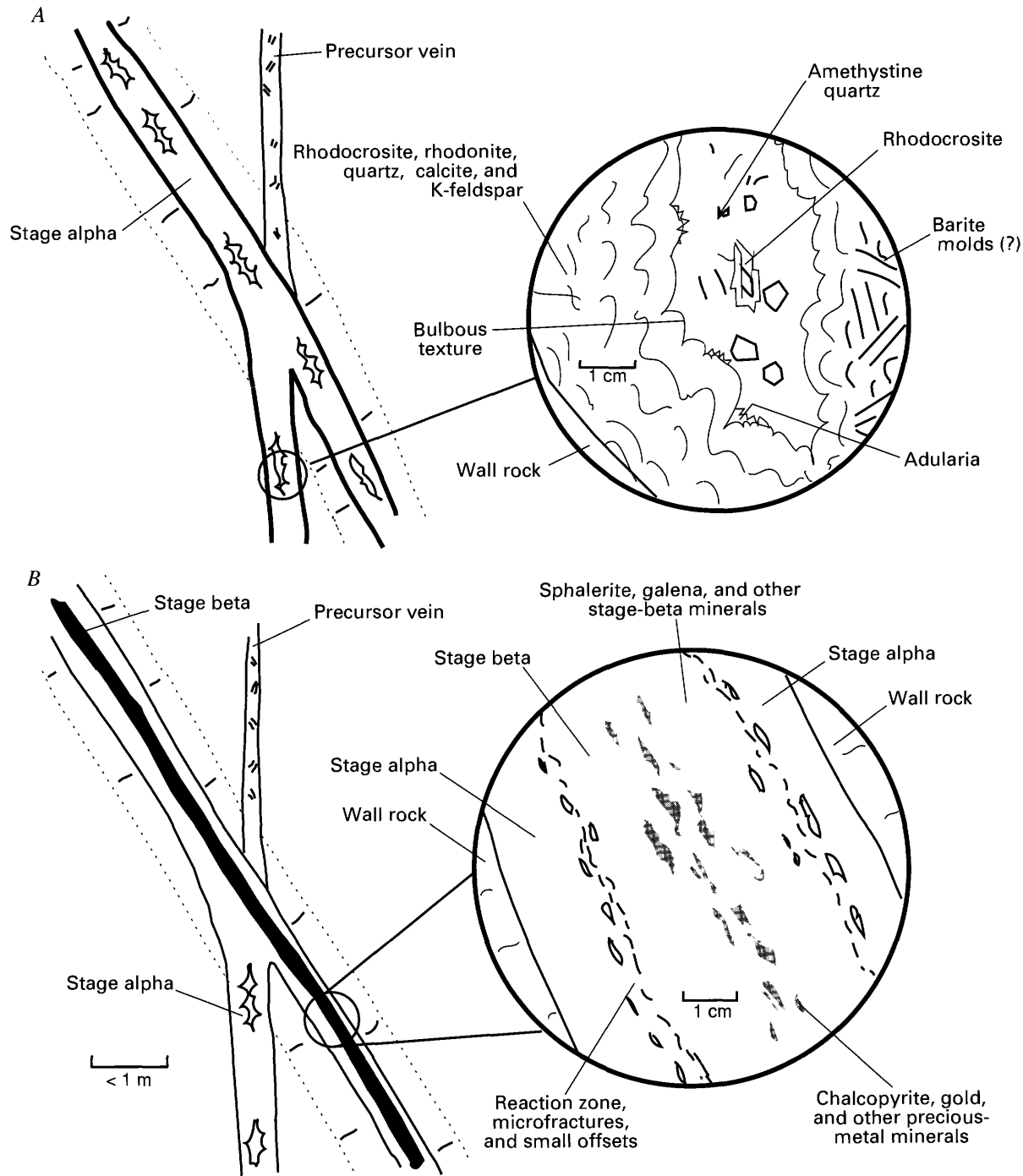


FIGURE 14. —A, Relation among stage alpha, precursor vein, and bleached and unbleached wall rock. Inset shows banded nature of fine-grained Mn-carbonates, Mn-silicates, quartz, sulfides. B, A stage-beta sulfide seam. The location of the seam was probably controlled by a structurally weak, vuggy zone at the core of stage alpha.

stage-beta seams and is most frequently found at depth in the system. The irregular distribution of the iron-oxide minerals, in contrast to the pervasive occurrence of pyrite, may indicate local change from pyrite equilibria to pyrite-hematite equilibria or a pyrite-magnetite-hematite buffer by an oxidative process such as boiling (Foley, 1990).

The pyrite, hematite and magnetite are intergrown with fine-grained Zn-, Pb-, and Cu-sulfides and abundant quartz. Electrum is the only precious-metal mineral commonly found with the iron-rich assemblage; it is intergrown with magnetite and pyrite and compositionally is similar to electrum in other assemblages. Euhe-dral magnetite is intergrown with pyrite and hematite in

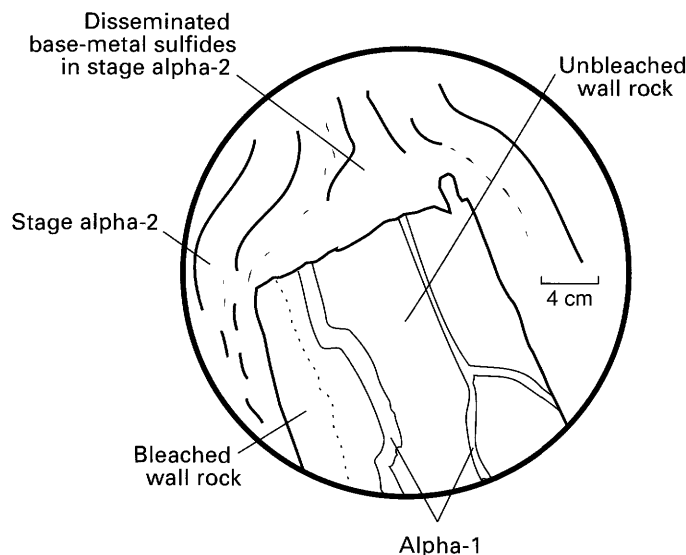


FIGURE 15.—Two periods of Mn-carbonate and Mn-silicate mineralization of stage alpha are shown by the occurrence of one in the other.

apparent equilibrium, and magnetite also replaces hematite blades; the contrasting textures support a change from pyrite to pyrite-hematite-magnetite and locally to pyrite-magnetite or magnetite equilibria, as noted previously. Hematite appears, in some cases, to be altered to limonite; this alteration probably is supergene in origin.

The occurrence of rounded cobbles of stage beta in breccias and sedimented zones cut by later competent seams of stage-beta sulfides was the basis for defining two substages (beta-1 and beta-2). The two have essentially identical mineralogies and differ only in their occurrence (fig. 16). Lead-isotopic compositions of galenas from the two substages are identical within analytical error (Foley, 1990). Electrum compositions and sphalerite compositions are also virtually identical for the two substages (tables 6 and 8).

Breccia-1.—Precious-metal minerals were deposited in two pulses separated by a period of brecciation and sedimentation along parts of the vein. The breccia that developed between the two beta substages is characterized by an unsorted mix of subangular to rounded pieces of fine-grained Au-bearing ore, angular fragments of bleached and unbleached wall rock, and fragments of stage alpha held together with a microcrystalline, dominantly quartz cement (fig. 16).

TRANSITIONAL BRECCIAS AND SEDIMENTS

The transition between deposition of the Mn- and Au-rich assemblages and assemblages of the base-metal-silica association is marked by extensive breccia-

tion of, and sedimentation in, the veins. The movement along the veins may have been a continuation, on a much larger scale, of the fracturing that formed breccia-1. Most of the breccias and sediments formed during this period are lumped together under the category breccia-2, with the exception of a matrix-supported, quartz-cemented breccia referred to as the “black quartz breccia.” The different breccias types record a short history of the transition period from the initial dynamic hydrology that reworked fragments and deposited them as fragment-supported breccias in large shoots and sediment “dumps” to the more quiescent hydrologic setting that resulted in graded bedding and chemically cemented, matrix-supported breccias.

BRECCIA-2

Breccias that are lumped together in this group have fragments that range in width from a few millimeters to 15 cm and in shape from angular to rounded (fig. 17). The fragments consist of all earlier stages of mineralization and wall rock; most fragments were derived from points close to the site of deposition.

Large breccia zones, resembling “shoots” of sedimented material with local graded bedding and quartz cement, formed as the fluids dumped their sediment load. The unsorted material forming the breccia zones consists mainly of subangular to rounded, bleached and unbleached fragments of volcanic wall rock, rounded and altered pieces of stage alpha, rounded to subrounded cobbles up to 15 cm in width of sulfide-rich stage beta, and fragments of earlier breccias (fig. 17A,B). The pieces are held together with quartz-rich cement. Interstitial sediment between larger fragments has graded bedding, soft-sediment deformation, and other textures indicating that the material settled out of solution after the larger cobbles and blocks were dumped (fig. 17B).

In another area, silt- to gravel-sized fragments settled out in large graded beds of at least four cycles that extend for 30 m along a vein wall and are greater than 3 m in height (tops and bottoms were not visible; fig. 4G, 17C). The water-deposited beds show minor soft-sediment deformation and an occasional sulfide-bearing cobble (up to 8 cm in width) that has fallen into finely graded sediment (fig. 4H). The graded beds are truncated at one end by a mineralized linking fault, and at the other end they appear to drape against hanging-wall volcanic rocks.

Black quartz breccia.—Late in this transition period, veins of “black quartz breccia” developed along planes of movement (fig. 17D). The black quartz breccias consist of 50 to 90 volume percent microcrystalline quartz-rich matrix and 10 to 50 percent fragments of stage-beta and stage-alpha material, earlier breccias, and wall rock. The

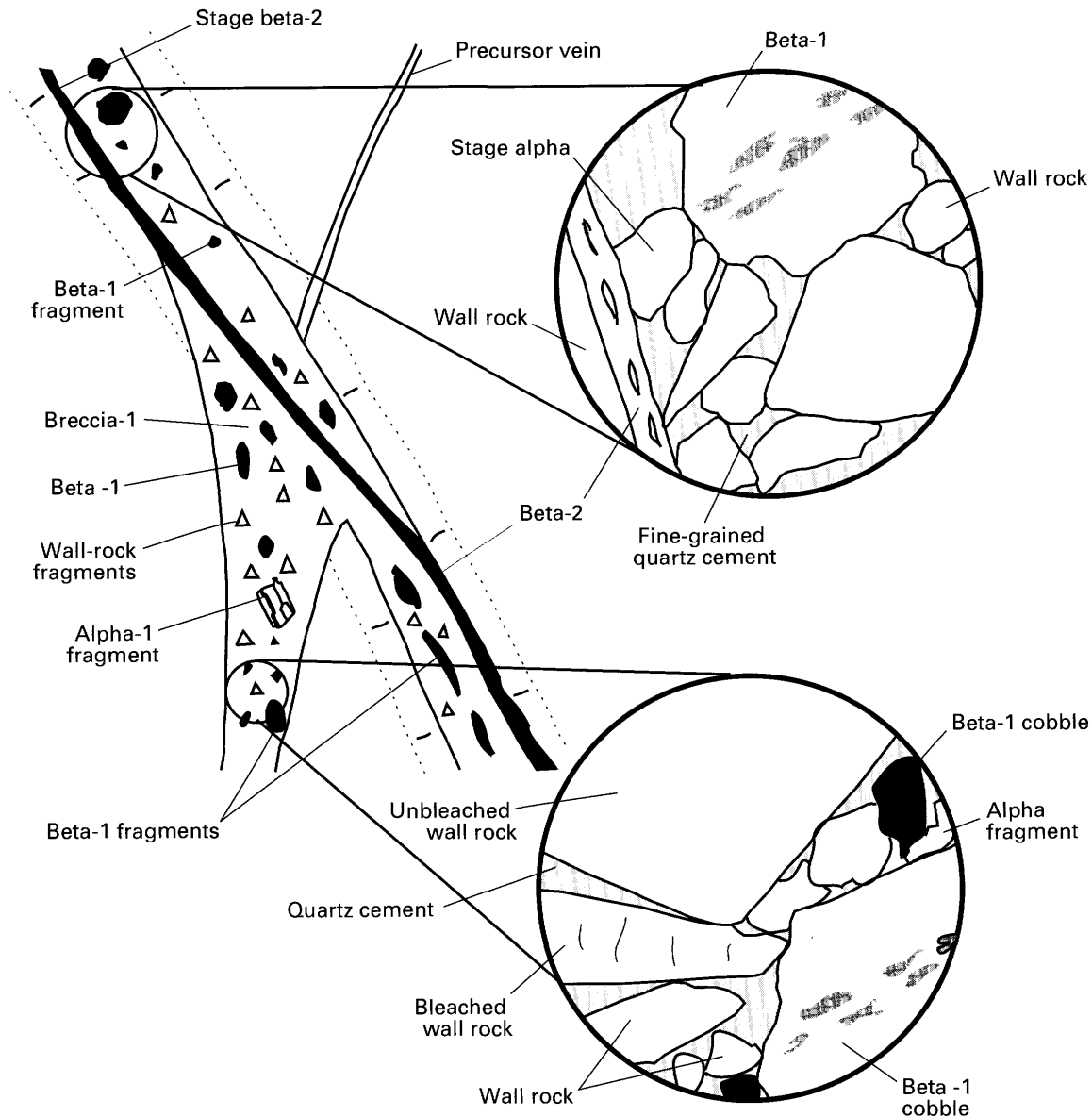


FIGURE 16. — Relation between beta-1 and beta-2 substages. Insets show development of breccia-1, which contains cobbles of beta-1 substage and is cut by a seam of beta-2 substage.

cement is composed dominantly of microcrystalline quartz having a granular texture with sutured grain boundaries. The cements grade in color from light gray to black, apparently in relation to the amount of fine sulfides and electrum contained therein. It has not been possible to ascertain whether the sulfide aggregates are clastic or if they formed as precipitates, but the shapes of the grains suggest that they were broken and ground. They may be finely ground dust from earlier stage-beta sulfide seams.

BASE-METAL-SILICA ASSOCIATION

This association has three mineralogical stages: (1) an interval consisting dominantly of base-metal sulfides, iron oxides, and quartz; (2) an interval of Ca-, Mn-, and Fe-bearing carbonate minerals, fluorite, and quartz; and (3) a Mn-calcite, quartz, and pyrite interval. The association is named after the most abundant constituents, base-metal sulfides and quartz. Complete mineralogical listings of all stages are given in table 3.

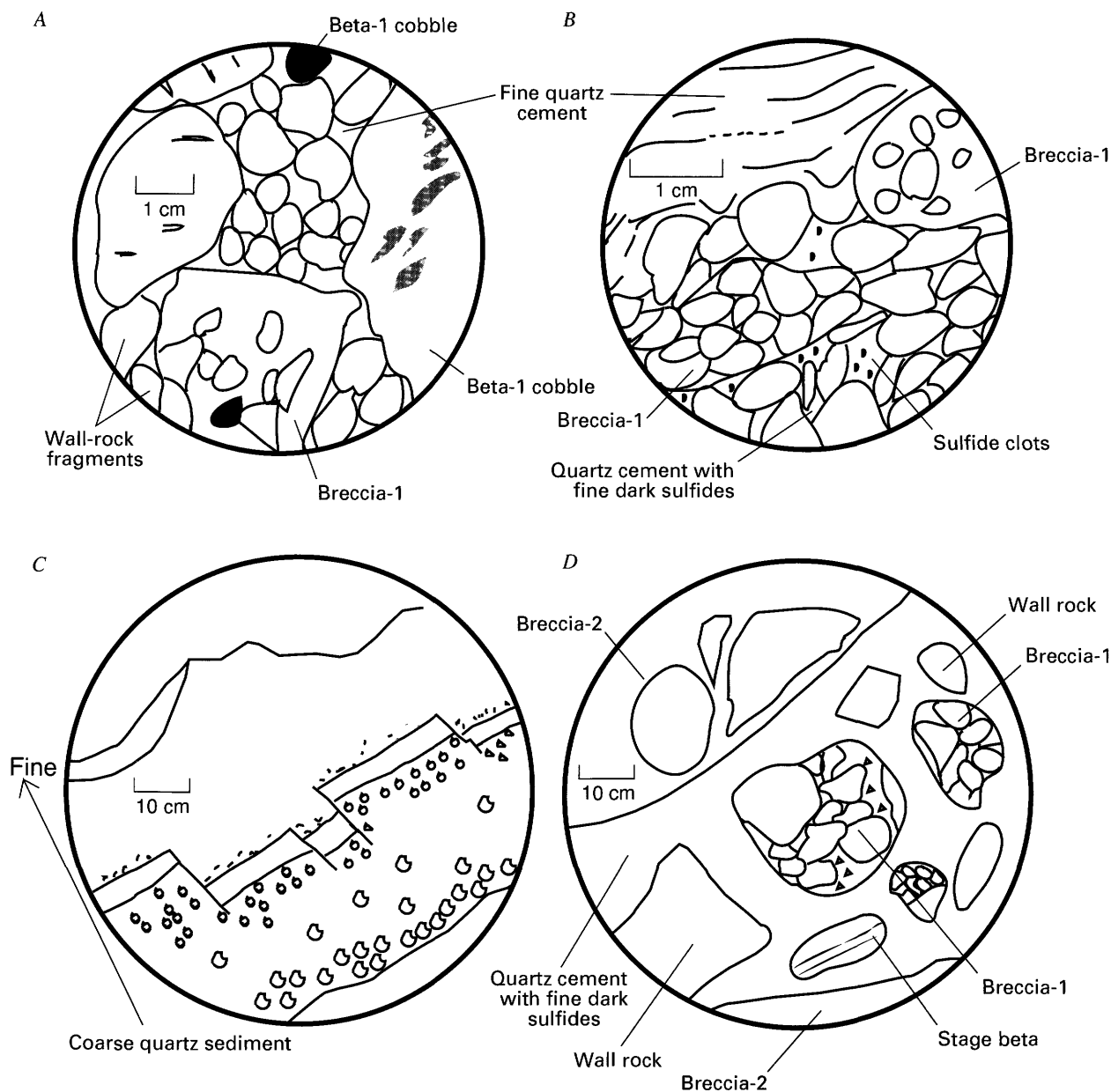


FIGURE 17.—A, Breccia containing wall rock and sulfide cobbles cemented with a quartz slurry. B, Detail showing bedding in fine-grained quartz cement surrounding breccia fragments. C, Graded bedding from fine-grained quartz cement to coarser breccia fragments. D, Black quartz breccia (see text); breccia fragments in quartz colored by sulfide dust.

STAGE 1

The first stage of the base-metal-silica association (fig. 18) is characterized by abundant base-metal sulfides, argentian tetrahedrite, hematite, chlorite, and quartz. Two mineralogically distinct substages are recognized: a chlorite, hematite, and quartz assemblage was deposited prior to, and concurrently with, the major period of base-metal mineralization that resulted in a crustified sequence of sphalerite, galena, pyrite, chalcopryrite, and tetrahedrite.

The fine-grained chlorite, hematite, and quartz assemblage was deposited on blocks of earlier breccias and in fractures cutting earlier assemblages of the Mn-Au association. Isolated crystals of sphalerite appear in the siliceous mixture. Some of the siliceous mixture was fragmented and recemented before the fluids began depositing relatively coarse base-metal sulfides. In other areas, the sulfides are intergrown with chlorite, hematite, and quartz without obvious breaks, so a gradual shift in dominant mineralogy is suggested.

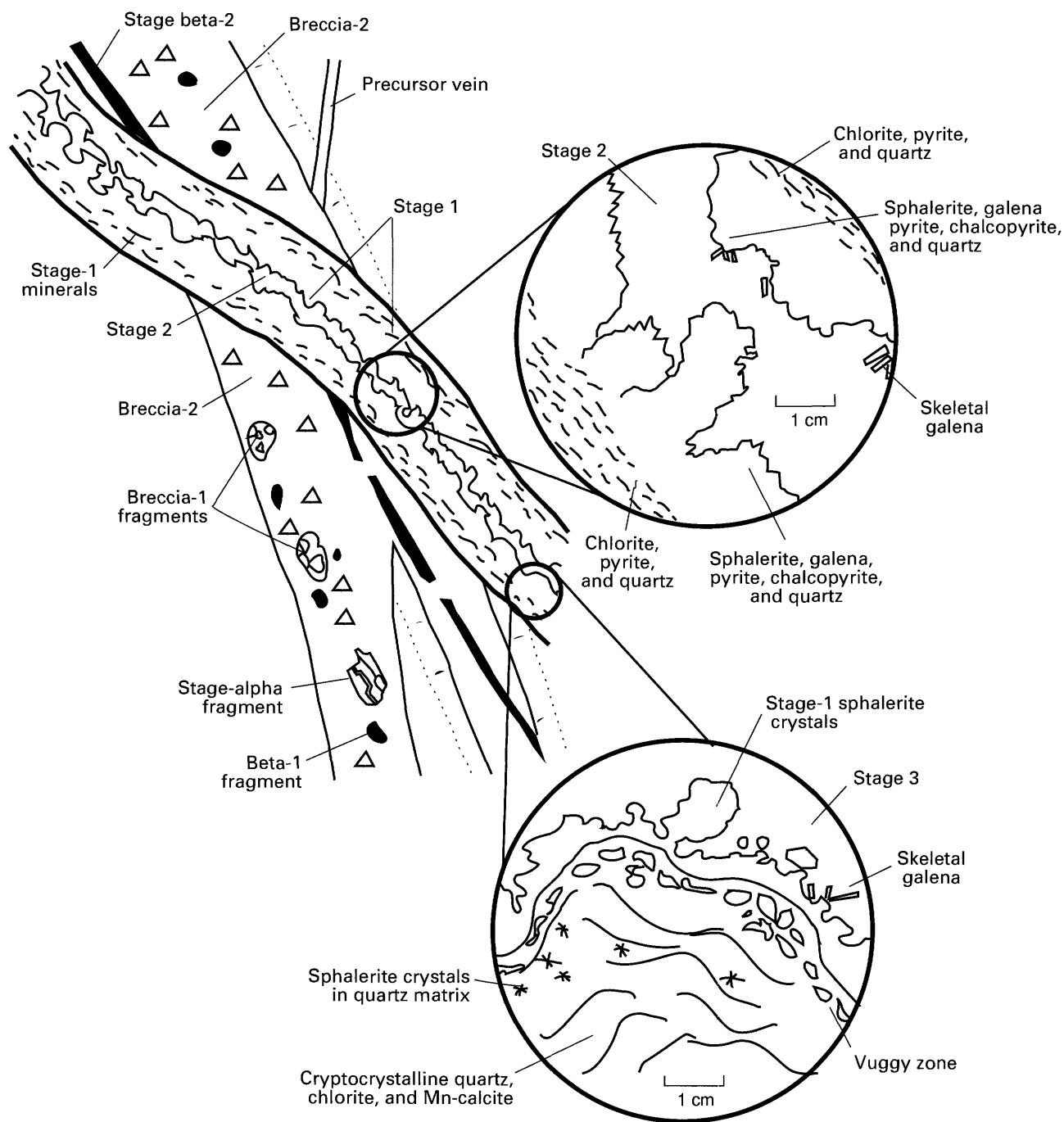


FIGURE 18.—Relation of stage-1 minerals to all preceding stages and breccias. Insets show textures typical of stage 1. See figure 5A–D.

The coarse-grained sphalerite, galena, pyrite, and chalcopryite assemblage of stage 1 contains interstitial quartz, chlorite, and hematite. Hematite flakes also are included in the sphalerite crystals. No clear-cut paragenetic relations are apparent among the minerals, with the exception that fluid reacted with sphalerite along fractures and grain boundaries to form chalcopryite- and tetrahedrite-disease textures (Barton and Bethke, 1987). Sphalerite crystals are corroded, and periods of dissolu-

tion and reprecipitation are identifiable through studies of thin sections. Late-forming galena of stage 1 occurs as skeletal crystals in vugs that were subsequently filled with minerals of stage 2 (fig. 18).

Breccia-3.—Continued local fracturing of stage-1 minerals formed a breccia that is characterized by fragments of coarse base-metal sulfide and chloritized wall rock cemented by a slurry of cryptocrystalline quartz, chlorite, and pyrite (figs. 5F, 19). The chlorite gives the

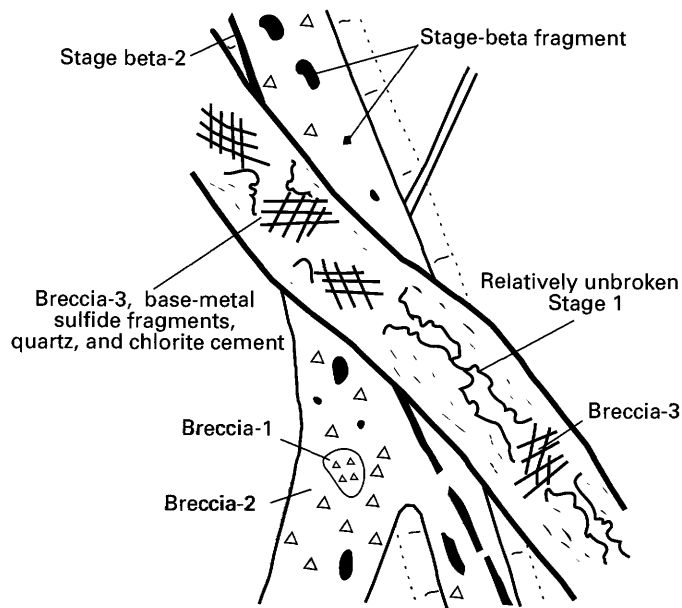


FIGURE 19.—Local development of breccia-3, characterized by fragments of stage-1 sulfides and a green, chlorite-rich cement.

cement a green hue. Minor amounts of base-metal sulfides were deposited on this brecciated material. Fragments of the base-metal sulfide are angular to subangular, and the wall-rock fragments are rounded. The breccia is most frequently found where stage-1 vein widths are greatest.

STAGE 2

The second stage of mineralization in the base-metal-silica association (fig. 20) is characterized by coarse-grained quartz, calcite, rhodocrosite, and fluorite, all intergrown with minor amounts of adularia, chlorite, and pyrite. Locally, manganosiderite occurs within the calcite. Stage 2 was deposited on breccia-3 and stage 1. The minerals are coarse grained; quartz crystals grew up to 40 mm in length, while green fluorite cubes attained 13 mm on a side. Smaller octahedra of fluorite (<3 mm) are colorless or pale green or purple. In general, quartz, chlorite, and calcite were deposited before fluorite and additional quartz. Quartz crystals are zoned from colorless and white to amethystine and contain solid inclusions of calcite, adularia, and fluorite. Occasionally, a small amount of fine gray quartz sediment was deposited in vugs on crystals of stage 2.

Quartz and adularia that fill barite(?) molds in stage alpha probably crystallized from stage-2 fluids. The minerals are texturally identical to stage-2 minerals and have fluid-inclusion salinities and homogenization temperatures that are similar to those of other stage-2 minerals (Foley, 1990). Rhodonite crystals (up to 0.5 mm in length) that form selvages and project into some of the

quartz-filled molds, and are intergrown with some rhodocrosite, may have formed from recrystallization of finer grained stage-alpha material.

Breccia-4.—This breccia contains angular fragments of all earlier assemblages, some breccias, and broken crystals and is cemented with a pale- to light-pink calcium-rich carbonate having a composition of $Cc_{95}Rc_5$ (fig. 21). It is especially prevalent in the north parts of the vein system. The fragile and vuggy nature of the breccia suggests a late formation, probably concurrent with the development of stage 3.

STAGE 3

The last clearly defined mineralization in the paragenetic sequence was deposition of quartz or manganocalcite, with pyrite, along the North Amethyst structure (fig. 22). Movement along the structure created vugs, cavities, and brecciated zones that cut all of the earlier stages. This movement was accompanied by, or followed by, leaching of earlier vein material along the entire length of the North Amethyst workings.

In the northern part of the ore zone, extensive crusts of pink to pale-yellow Mn-bearing calcite, interlayered with thin layers of crustiform pyrite, were deposited in the vugs and on material leached earlier. The carbonate crusts ranged in total thickness from millimeters to a meter. The carbonate minerals were selectively leached and now contain large, open vuggy zones.

Leaching of earlier stages, especially the extensive breccias, appears to have been more extensive in the southern workings. Samples of breccia-2 exhibit gradations in the degree of leaching ranging from bleaching of fragments to alteration of phenocrysts to clay minerals to samples that consist entirely of a foamlike siliceous material containing molds possibly of leached blocks of wall rock and rare specks of dark sulfides. Geochemical analysis of the most altered and leached material indicates that, of the major elements, only SiO_2 (~94 percent), and minor Al_2O_3 (~3 percent) and K_2O (~1 percent) remain. Relatively high values of base and precious metals also persist (~90 ppm Au, 30 ppm Ag). This leached material is overgrown by large terminated crystals of quartz in the southern part of the ore zone. The quartz crystals are included in stage 3 because they overgrow the leached base; however, their formation may predate the manganocalcite. Minute cubes of pyrite dust the quartz surfaces; timing of this pyrite relative to the crustiform occurrence within manganocalcite is not clear.

CORRELATION OF MINERAL ASSEMBLAGES WITH OTHER VEIN SYSTEMS

The relation of the North Amethyst ores to those of the main Creede district 5 km to the south is of great

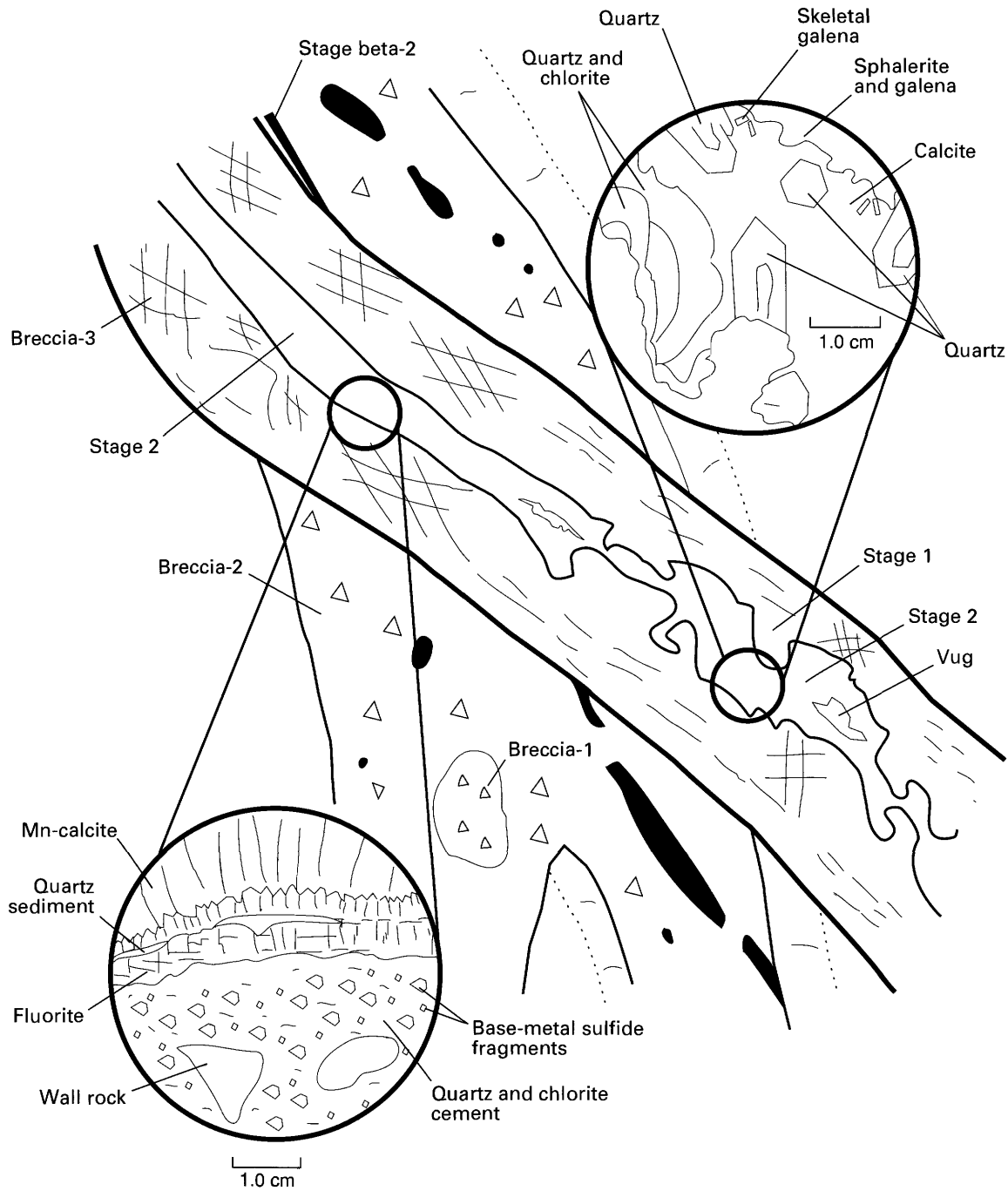


FIGURE 20.—Reopening of vein and deposition of stage-2 minerals on preexisting mineral stages and breccias. Insets show textures of stage-2 minerals.

importance in assessing the nature, extent, and timing of mineralization. The mineralogy, textures, and paragenetic sequences established in this study can be used to compare the North Amethyst veins to veins of the main mining district at Creede. Paragenetic relations for the North Amethyst vein system and some veins of the main mining district are summarized in table 9. Mineral stages

defined for the North Amethyst vein system can be correlated, in part, with mineral stages defined in previous studies for the southern Amethyst vein (Guidice, 1981; Robinson, 1981; and Robinson and Norman, 1984), the Bulldog Mountain vein system (Plumlee, 1989), and the OH and P veins (Barton and others, 1977; Bethke and Rye, 1979; P.B. Barton, Jr., oral commun., 1989). Most

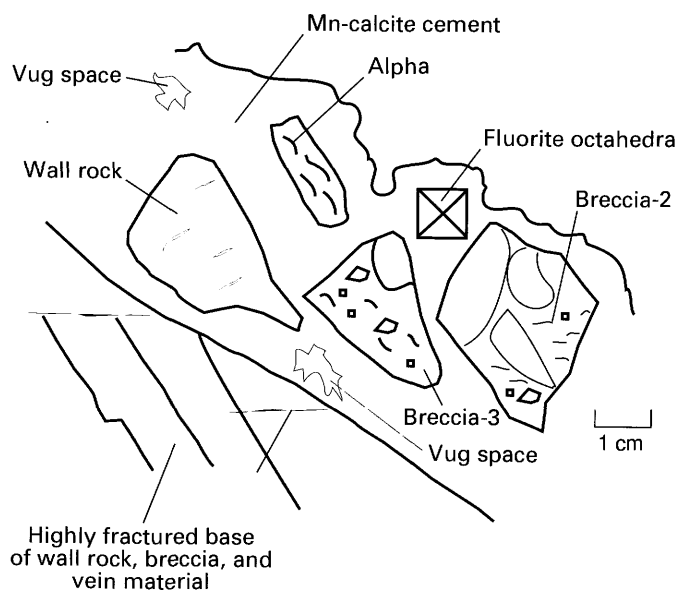


FIGURE 21.—Development of breccia cemented by pink calcite just prior to, or concurrently with, stage-3 mineralization.

of the corresponding stages are mineralogically similar and occur throughout the district; however, there are some important exceptions.

At present, stages alpha and beta of the Mn-Au association have been found only in the North Amethyst area. The assemblages have not been described elsewhere within the boundaries of the Creede mining district. Mn-silicates and uytenbogaardtite are not found south of the North Amethyst workings, although rare occurrences of electrum have been reported for a couple of localities. An occurrence of dark-yellow gold with a high degree of fineness contained in a gangue of manganese oxides has been described by Emmons and Larsen (1913, 1923) from the Happy Thought and Amethyst mines of the Amethyst vein. The gold occurred in cracks and veinlets cutting older ore and was said to be a common supergene occurrence in near-surface workings. Gold also has been reported as inclusions in pyrite, galena, sphalerite, and other minerals (Emmons and Larsen, 1923); however, no additional details are available. P.M. Bethke and P.B. Barton, Jr. (oral commun., 1989), note the occurrence of abundant finely disseminated gold in early chalcopryrite in a single sample from the OH vein (their stage A or B, table 9). Galenas from North Amethyst gold-bearing stage beta are distinct in their lead-isotopic character from galenas of stage 1 of the North Amethyst veins and from most veins of the main Creede mining district (Foley, 1990; Foley and Ayuso, in press); this distinctness lends support to their unique occurrence in the north.

The three stages of the base-metal-silica association of the North Amethyst vein system can be correlated

directly with mineralogically similar stages of the OH and P veins (table 9; defined as stages A through E). Stage A of the northern OH and P veins consists primarily of massive chalcedonic quartz intergrown with rhombs of adularia. This stage is not found in the North Amethyst ores; however, in the interval of brecciation and sedimentation between the two sulfide-rich North Amethyst stages (stage beta and stage 1), quartz was deposited as chalcedonic cement in breccia. Although not defined as a vein-filling stage, the quartz cement may correlate with OH vein stage-A quartz, and this correlation would indicate a districtwide period of silica deposition.

Stage B of the OH and P veins is dominated by fine-grained base-metal sulfides—sphalerite, galena, chalcopryrite, and lesser amounts of Ag-rich tetrahedrite—contained in a chlorite, pyrite, hematite, and quartz gangue assemblage. This stage correlates directly with stage 1 of the North Amethyst vein (table 9). Sphalerites of the North Amethyst, OH, and P vein assemblages show extensive chalcopryrite- and minor tetrahedrite-disease textures. Zoned sphalerites from the OH stage B and North Amethyst stage 1 are compositionally similar; light zones have generally low iron contents (<2 mole percent), and dark bands are iron rich (up to 8 mole percent for North Amethyst stage 1, up to 16 mole percent for OH stage B). Galenas (stage 1B) from all three veins also have similar lead-isotopic compositions (Foley, 1990; Foley and Ayuso, in press). The composition of OH and P vein tetrahedrite is variable but generally is silver rich (L.B. Wiggins and T.L. Woods, unpub. data, 1980), similar to that of the North Amethyst ore.

Stage 2 of the North Amethyst vein correlates mineralogically with stage C of the OH and P veins (table 9). Both stage 2 and stage C contain fluorite, quartz, and carbonate minerals. The North Amethyst stage-2 carbonate minerals consist of intergrown calcite and manganosiderite, whereas the OH and P veins contain only manganosiderite (Wetlaufer, 1977).

OH and P vein stage D ores are apparently absent in the North Amethyst vein system (table 9). Stage D consists largely of coarsely crystalline sphalerite, galena, quartz, chalcopryrite, and hematite. D-stage sphalerite is free of chalcopryrite disease and is color zoned from core to rim with yellow-white to red-brown to yellow-white zones having iron contents of less than 3 mole percent FeS (Barton and others, 1977).

Stage 3 of the North Amethyst vein system can be correlated with stage E of the OH and P veins mainly on the basis of the occurrence of pyrite in all of these stages (table 9). Pyrite in North Amethyst stage 3 is volumetrically minor compared to stage E, and quartz and

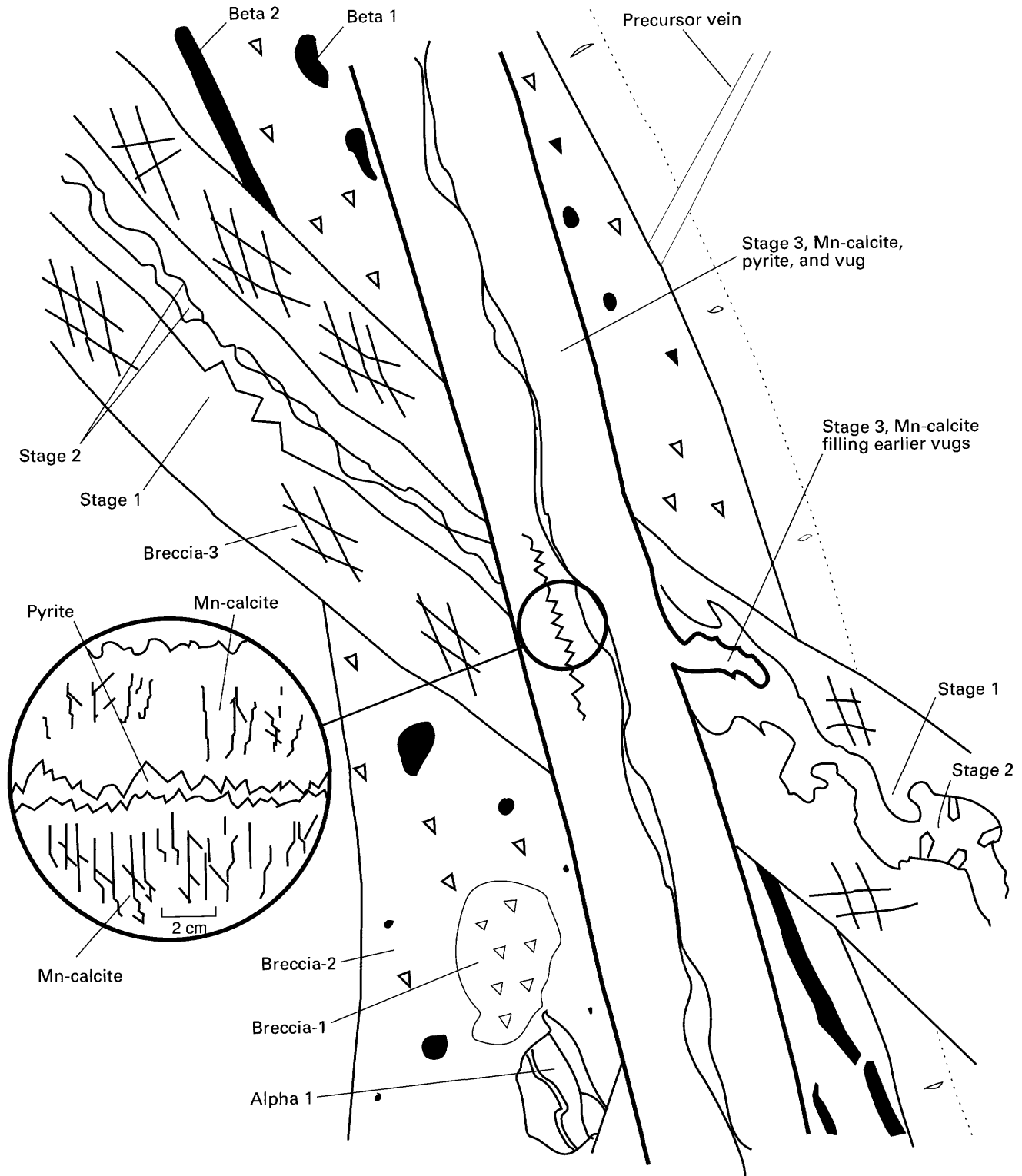


FIGURE 22.—Stage 3 is marked by deposition of thick crusts of a coarse pink calcite, pyrite, and quartz. Inset shows calcite and pyrite occurrence.

TABLE 9.—*Districtwide correlation of mineral assemblages and brecciation events*

[Stage designations for each vein are shown in parentheses. For example, (II) is stage II of Plumlee (1989). Abbreviations: Ac, acanthite; Ad, adularia; Ag, silver; Au, electrum; Bar, barite; Cc, calcite; Chl, chlorite; Cpy, chalcopyrite; Fl, fluorite; Gn, galena; Hm, hematite; Mn, manganese; Pear, pearcite; Px, pyroxmangite; Py, pyrite; Pyr, pyrrargyrite; Qz, quartz; Rc, rhodocrosite; Rh, Rhodonite; Sp, sphalerite; Sid, siderite; Stib, stibnite; Td, tetrahedrite-tennantite; Uyt, uytenbogaardite]

North Amethyst vein (Foley and Vardiman, 1988; Foley, 1990)	OH and P veins (Bethke and Rye, 1979)	Bulldog vein (Plumlee, 1989)	Southern Amethyst vein (Robinson, 1981)	Disseminated ore, OH and Amethyst veins (Guidice, 1981)
(3) Mn-Cc + Qz + Py	(E) Py + Stib	(V) Py + Stib + Pyr	Absent?	(2) Py + Qz.
Breccia-4	Absent?	Absent?	Absent?	Absent?
Absent	(D) Sp + Gn + Qz + Cpy + Hm	(IV) Sp + Gn + Cpy + Td + Pear + Ac	Absent?	Absent?
(2) Qz + Mn-Cc + Fl + Rc + Mn-sid + Chl + Py + Ad	(C) Fl + Qz + Mn-sid	(III) Qz + Fl + Mn-sid + Sp + Gn	Absent?	Included in (1)?
Breccia-3	Absent?	Absent?	Absent?	Absent?
(1) Sp + Gn + Py + Cpy + Qz + Hm + Chl + Td	(B) Qz + Sp + Chl + Gn + Hm + Td + Au	(II) Bar + Qz + Sp + Gn + Td	(2) Qz + Sp + Gn + Py + Td + Hm + Ac + Ag	(1) Sp + Gn + Py + Cpy + Chl + Rc + Bar + Ag + Td + Ac
Breccia-2	(A) Qz + Ad	(I) Rc + Qz + Sp + Gn + Ad	(1) Rc + Qz + Bar + Cc + Sp + Gn + Py + Cpy	Absent?
(Beta-2) Gn + Sp + Cpy + Py + Td + Ac + Uyt + Au	Absent?	Absent?	Absent?	Absent?
Breccia-1	Absent?	Absent?	Absent?	Absent?
(Beta-1) Gn + Sp + Cpy + Py + Td + Ac + Uyt + Au	Absent?	Absent?	Absent?	Absent?
(Alpha) Rc + Qz + Mn-Cc + Rh + Px + Sp + Gn + Py + Ad	Absent?	Absent?	Absent?	Absent?

manganian calcite occur in relatively greater proportions.

The sequence of mineral stages defined for the Bulldog Mountain vein system has been correlated with mineral stages of the OH and P veins by Plumlee (1989). The comments and ideas presented in that study may hold true for comparing the North Amethyst and Bulldog Mountain paragenetic sequences because of the mineralogical similarities between the OH and North Amethyst assemblages (table 9). As in the case of the OH vein, chalcidony of Bulldog Mountain stage I may correspond to chalcidonic cements of North Amethyst breccia-2. The North Amethyst stage 2 is more like the sphalerite- and galena-rich, Ag-poor assemblages of the northern Bulldog Mountain stage II than the barite and Ag-rich assemblages of the southern half of the Bulldog system. However, in contrast to the North Amethyst stage 2, northern Bulldog Mountain stage II does contain some barite and does not have abundant chlorite-pyrite-hematite-quartz gangue. Compositions of carbonate minerals of North Amethyst stage 2 (table 5) are similar to those of Bulldog Mountain stage III (Wetlaufer, 1977).

Thus, Bulldog Mountain stage III may correlate with North Amethyst stage 2. Bulldog Mountain stage IV, which correlates with OH stage D, is not found in the North Amethyst area. Pyrites appear in both Bulldog Mountain stage V and North Amethyst stage 3.

Correlations between mineralogical stages of the North Amethyst vein system and mineralized segments of the southern part of the Amethyst vein are difficult because paragenetic relations for some of those areas are less well known. Two main stages of mineralization along the southern Amethyst vein system have been defined by Robinson (1981), and he has correlated the two assemblages with the A and B stages defined by Bethke and Rye (1979) for the OH vein. Minerals of southern Amethyst vein stage 2 correlate mineralogically with stage 1 of the North Amethyst vein (table 9). Galenas from the southern Amethyst stage-2 assemblage have lead-isotopic values that overlap the field defined by lead-isotopic compositions of galenas from the North Amethyst stage 1 (Foley, 1990).

Disseminated ore present in the hanging wall of the Amethyst fault at the southern end of the mineralized

structure, in the vicinity of an on-strike projection of the OH vein, has been examined by Guidice (1981). He has described two main hypogene stages and a supergene stage for disseminated minerals in volcanic rock located between the two veins. The first hypogene stage of mineralization may correlate with a combination of stages 1 and 2 of the North Amethyst vein and, as described by Plumlee (1989), with a combination of stages A through C of the OH vein and stages I through III of the Bulldog Mountain vein. This lumping of stages clearly reflects a lack of clear-cut paragenetic relations in the disseminated ore. The second hypogene stage for the disseminated ore correlates well with stage 3 of the North Amethyst vein.

The detailed paragenetic studies (table 9) demonstrate that base-metal minerals of the North Amethyst stage 1, OH and P vein stage B, and Bulldog Mountain stage II constitute the most widely distributed and persistent mineralogical stage, occurring in some form in all veins. Later stages of mineralization are more local and were interrupted by periods of dissolution. The North Amethyst vein retains the most complete record of mineralogical stages deposited anywhere in the district (table 9). In some of the other veins, only certain mineralogical stages are well developed, and many stages are absent or unrecognized. Thus, the North Amethyst vein probably has the most complete record of the changing chemical composition of the hydrothermal fluids.

CONCLUSIONS

1. The paragenesis of ore minerals of the North Amethyst vein system can be divided into two multistage associations separated by periods of intense brecciation. The earlier association has two stages, the first of which is characterized by abundant manganese minerals and the second by high gold content. The later association has three stages that consist primarily of base-metal sulfides, chlorite, quartz, carbonate minerals, and fluorite, in varying proportions.
2. Complete assemblages of the earlier Mn-Au stages of the North Amethyst system are not found elsewhere in the central San Juan region. In contrast, mineralogical stages and breccias identified in the base-metal-silica association can be correlated with paragenetic stages defined for veins of the central and southern Creede mining district.
3. The local and early occurrence of the Mn and Au assemblages may indicate that they either formed in a small hydrothermal cell that predated the extensive hydrothermal system from which ores of the Creede district are proposed to have been deposited (Bethke, 1988) or are remnants of a larger early hydrothermal

system. If other early hydrothermal cells with similar characteristics were present in structures of the central and southern parts of the district, they may have been replaced or overprinted by later assemblages, or they remain to be discovered. Early-stage paragenetic mineral assemblages may hold the greatest potential for vein-related gold mineralization in structures of the central caldera cluster of the San Juan Mountains.

4. The correlations of mineral assemblages described above have important implications for hydrologic modeling of the northern, central, and southern parts of the Creede district. The extensive correlation of base-metal-, silver-, and silica-rich assemblages suggests a similar source of fluids and metals for the ore mineralization and implies that the minerals were deposited in the veins by similar mechanisms and under similar conditions of ore formation.

REFERENCES CITED

- Abrecht, Jürgen, 1989, Manganiferous phyllosilicate assemblages: Occurrences, compositions, and phase relations in metamorphosed Mn deposits: *Contributions to Mineralogy and Petrology*, v. 103, p. 228-241.
- Baars, D.L., and Stevenson, G.M., 1984, The San Luis uplift, Colorado and New Mexico—An enigma of the ancestral Rockies: *The Mountain Geologist*, v. 21, no. 2, p. 57-67.
- Baedecker, P.A., ed., 1987, *Methods for geochemical analysis*: U.S. Geological Survey Bulletin 1770, 132 p.
- Barton, Mark, 1978, The Ag-Au-S system: Blacksburg, Va., Virginia Polytechnic Institute and State University, unpublished M.S. thesis, 75 p.
- Barton, M.D., Kieft, C., Burke, E.A.J., and Oen, I.S., 1978, Uytendogaardtite, a new silver-Au sulfide: *Canadian Mineralogist*, v. 16, pt. 4, p. 651-657.
- Barton, P.B., Jr., and Bethke, P.M., 1987, Chalcopyrite disease in sphalerite: Pathology and epidemiology: *American Mineralogist*, v. 72, p. 451-467.
- Barton, P.B., Jr., Bethke, P.M., and Roedder, Edwin, 1977, Environment of ore deposition in the Creede mining district, San Juan Mountains, Colorado; Part III, Progress toward interpretation of the chemistry of the ore-forming fluid for the OH vein: *Economic Geology*, v. 72, no. 1, p. 1-24.
- Bethke, P.M., 1988, The Creede, Colorado ore-forming system: A summary model: U.S. Geological Survey Open-File Report 88-403, 29 p.
- Bethke, P.M., Barton, P.B., Jr., Lanphere, M.A., and Steven, T.A., 1976, Environment of ore deposition of the Creede mining district, San Juan Mountains, Colorado; Part II, Age of mineralization: *Economic Geology*, v. 71, no. 6, p. 1006-1011.
- Bethke, P.M., and Lipman, P.W., 1987, Deep environment of volcanogenic epithermal mineralization: Proposed research drilling at Creede, Colorado: *Eos, Transactions, American Geophysical Union*, v. 68, no. 13, p. 177, 187-189.
- Bethke, P.M., and Rye, R.O., 1979, Environment of ore deposition of the Creede mining district, San Juan Mountains, Colorado; Part IV, Source of fluids from oxygen, hydrogen, and carbon isotope studies: *Economic Geology*, v. 74, no. 8, p. 1832-1851.

- Bickford, M.E., 1988, The accretion of Proterozoic crust in Colorado: Igneous, sedimentary, deformational, and metamorphic history, *in* Ernst, W.G., ed., *Metamorphism and crustal evolution of the Western United States*: Prentice Hall, Rubey Volume 7, p. 411-430.
- Capobianco, C.J., and Navrotsky, Alexandra, 1987, Solid solution thermodynamics in $\text{CaCO}_3\text{-MnCO}_3$: *American Mineralogist*, v. 72, no. 3-4, p. 312-318.
- Craig, J.R., and Vaughan, D.J., 1981, *Ore microscopy and ore petrography*: New York, John Wiley and Sons, 406 p.
- deCapitani, Christian, and Peters, Tjerk, 1981, The solvus in the system $\text{MnCO}_3\text{-CaCO}_3$: *Contributions to Mineralogy and Petrology*, v. 76, no. 4, p. 394-400.
- Emmons, W.H., and Larsen, E.S., 1913, A preliminary report on the geology and ore deposits of Creede, Colorado: U.S. Geological Survey Bulletin 530, p. 42-65.
- , 1923, Geology and ore deposits of the Creede district, Colorado: U.S. Geological Survey Bulletin 718, 198 p.
- Foley, N.K., 1990, Petrology of gold-, silver-, and base-metal ores of the North Amethyst vein system, San Juan Mountains, Mineral County, Colorado: Blacksburg, Va., Virginia Polytechnic Institute and State University, unpublished Ph.D. thesis, 325 p.
- Foley, N.K., and Ayuso, R.A., in press, Paragenetic constraints on Pb isotopic evolution of the North Amethyst Au-Ag vein system, Creede mining district, San Juan volcanic field: *Economic Geology*.
- Foley, N.K., Bethke, P.M., and Rye, R.O., 1990, A reinterpretation of the $\delta\text{D}_{\text{H}_2\text{O}}$ of inclusion fluids in contemporaneous quartz and sphalerite, Creede mining district, Colorado: A generic problem for shallow orebodies?: *Economic Geology*, v. 84, no. 7, p. 1966-1977.
- Foley, N.K., and Vardiman, D.M., 1988, Paragenesis and mineral chemistry of ores of the Au-, Ag-, and base-metal-bearing North Amethyst property, San Juan Mountains, Colorado [abs.]: *Geological Society of America, Abstracts with Programs*, v. 20, p. A276.
- Goldsmith, J.R., and Graf, D.L., 1957, The system CaO-MnO-CO_2 : Solid solution and decomposition relations: *Geochimica et Cosmochimica Acta*, v. 11, no. 4, p. 310-334.
- Gries, R.R., 1985, San Juan Sag: Cretaceous rocks in a volcanic covered basin, south-central Colorado: *The Mountain Geologist*, v. 22, no. 4, p. 167-179.
- Guidice, P.M., 1981, Mineralization at the convergence of the Amethyst and OH fault systems, Creede district, Mineral County, Colorado: Tucson, Ariz., University of Arizona, unpublished M.S. thesis, 95 p.
- Haas, J.L., 1971, The effect of salinity on the maximum thermal gradient of a hydrothermal system at hydrostatic pressure: *Economic Geology*, v. 66, no. 6, p. 940-946.
- Hayba, D.O., Bethke, P.M., Heald, Pamela, and Foley, N.K., 1985, Geologic, mineralogic, and geochemical characteristics of volcanic-hosted epithermal precious-metal deposits: *Reviews in Economic Geology*, v. 2, p. 129-167.
- Heald, P.W., Foley, N.K., and Hayba, D.O., 1987, Comparative anatomy of volcanic-hosted epithermal deposits: Acid-sulfate and adularia-sericite types: *Economic Geology*, v. 82, no. 1, p. 1-26.
- Hon, Ken, and Mehnert, H.H., 1983, Compilation of revised ages of volcanic units in the San Juan Mountains, Colorado: Recalculated K-Ar age determinations using IUGS constants: U.S. Geological Survey Open-File Report 83-668, 14 p.
- Horton, D.G., 1983, Argillic alteration associated with the Amethyst vein system, Creede mining district, Colorado: Urbana, Ill., University of Illinois, unpublished Ph.D. thesis, 337 p.
- Hurford, A.J., and Hammerschmidt, K., 1985, $^{40}\text{Ar}/^{39}\text{Ar}$ and K/Ar dating of the Bishop and Fish Canyon Tuffs: Calibration ages for fission-track dating standards: *Chemical Geology*, v. 58, p. 23-32.
- Lanphere, M.A., 1987, High-resolution $^{40}\text{Ar}/^{39}\text{Ar}$ geochronology, central San Juan caldera complex, Colorado [abs.]: *Geological Society of America, Abstracts with Programs*, v. 19, no. 5, p. 288.
- , 1988, High resolution $^{40}\text{Ar}/^{39}\text{Ar}$ chronology of Oligocene volcanic rocks, San Juan Mountains, Colorado: *Geochimica et Cosmochimica Acta*, v. 52, p. 1425-1434.
- LeMaitre, R.W., 1989, A classification of igneous rocks and glossary of terms, *in* LeMaitre, R.W., ed., *Recommendations of the International Union of Geological Sciences Subcommittee on the Systematics of Igneous Rocks*: Blackwell Scientific Publications, 35 p.
- Lipman, P.W., Doe, B.R., Hedge, C.E., and Steven, T.A., 1978, Petrologic evolution of the San Juan volcanic field, southwestern Colorado: Pb and Sr isotope evidence: *Geological Society of America Bulletin*, v. 89, no. 1, p. 59-82.
- Lipman, P.W., and Sawyer, D.A., 1988, Preliminary geology of the San Luis Peak quadrangle and adjacent areas, San Juan volcanic field, southwestern Colorado: U.S. Geological Survey Open-File Report 88-359, 32 p.
- Lipman, P.W., Steven, T.A., and Mehnert, H.H., 1970, Volcanic history of the San Juan Mountains, Colorado, as indicated by potassium-argon dating: *Geological Society of America Bulletin*, v. 81, no. 8, p. 2329-2352.
- Maresch, W.V., and Mottana, A., 1976, The pyroxmangite-rhodonite transformation for the MnSiO_3 composition: *Contributions to Mineralogy and Petrology*, v. 55, no. 1, p. 69-79.
- Ohashi, Y., Kato, A., and Matsubana, S., 1975, Pyroxenoids: A variation in chemistry of natural rhodonites and pyroxmangites: *Carnegie Institute of Washington Year Book*, v. 74, p. 561-564.
- Peacor, D.R., Essene, E.J., Brown, P.E., and Winter, G.A., 1978, The crystal chemistry and petrogenesis of a magnesian rhodonite: *American Mineralogist*, v. 63, no. 11-12, p. 1137-1142.
- Peacor, D.R., Essene, E.J., and Gaines, A.M., 1987, Petrologic and crystal-chemical implications of cation order-disorder in kutnahorite $[\text{CaMn}(\text{CO}_3)_2]$: *American Mineralogist*, v. 72, no. 3-4, p. 319-328.
- Peters, T.J., Trommsdorff, V., and Sommerauer, J., 1978, Manganese pyroxenoids and carbonates: Critical phase relations in metamorphic assemblages from the Alps: *Contributions to Mineralogy and Petrology*, v. 66, no. 4, p. 383-388.
- Peters, T.J., Valarelli, J.V., Coutinho, J.M., Sommerauer, J., and Von Raumer, J., 1977, The manganese deposits of Buritirama (Para, Brazil): *Schweizerische Mineralogische und Petrographische Mitteilungen*, v. 57, no. 3, p. 313-327.
- Plouff, Donald, and Pakister, L.C., 1972, Gravity study of the San Juan Mountains, Colorado, *in* Geological Survey Research 1972: U.S. Geological Survey Professional Paper 800-B, p. B183-B190.
- Plumlee, G.S., 1989, Processes controlling epithermal mineral distribution in the Creede mining district, Colorado: Cambridge, Mass., Harvard University, unpublished Ph.D. thesis, 378 p.
- Plumlee, G.S., Caddey, S.W., and Byington, C.B., 1989, Geology and ore deposits of the Creede mining district, Colorado, *in* Bryant, Bruce, and Beaty, D.W., eds., *Mineral deposits and geology of central Colorado: Field trip guidebook T129*, 23th International Geological Congress, American Geophysical Union, p. 54-62.
- Ramdohr, Paul, 1969, *The ore minerals and their intergrowths*: Braunschweig, Germany, Pergamon Press, 1,175 p.
- Robinson, R.W., 1981, Ore mineralogy and fluid inclusion study of the southern Amethyst vein system, Creede mining district, Colorado: Socorro, N.Mex., New Mexico Institute of Mining and Technology, unpublished M.S. thesis, 85 p.
- Robinson, R.W., and Norman, D.I., 1984, Mineralogy and fluid inclusion study of the southern Amethyst vein system, Creede mining district, Colorado: *Economic Geology*, v. 79, no. 3, p. 439-337.
- Roedder, E., 1977, Changes in ore fluid with time, from fluid inclusion studies at Creede, Colorado: *International Association on the*

- Genesis of Ore Deposits Proceedings (IAGOD), 4th Symposium, Problems of ore deposition, Varna, Bulgaria, 1974, v. 2, p. 179-185.
- Sawyer, D.A., Sweetkind, D., Rye, R.O., Siems, D.F., Reynolds, R.L., Rosenbaum, J.G., and others, 1989, Potassium metasomatism in the Creede mining district, San Juan volcanic field, Colorado [abs.]: Continental magmatism, International Association of Volcanology and Chemistry of the Earth's Interior, New Mexico Bureau of Mines and Mineral Resources, Bulletin 131, p. 234.
- Scarpelli, W., 1973, The Serra do Navio manganese deposit (Brazil): Paris, Unesco, Earth Sciences no. 9 (Genesis of Precambrian iron and manganese deposits, Proceedings of the Kiev Symposium, 20-25 August, 1970), p. 217-228.
- Skinner, B.J., 1966, The system Cu-Ag-S: *Economic Geology*, v. 61, p. 1-26.
- Skinner, B.J., Jambor, J.L., and Ross, Malcolm, 1966, Mckinstryite, a new copper-silver sulfide: *Economic Geology*, v. 61, no. 8, p. 1383-1389.
- Steven, T.A., 1968, Ore deposits in the central San Juan Mountains, Colorado, in Ridge, J.D., ed., *Ore deposits of the United States 1933-1967*, Graton-Sales volume: American Institute of Mining and Metallurgy, v. 1, p. 706-713.
- 1975, Middle Tertiary volcanic field in the southern Rocky Mountains, in Curtis, B.F., ed., *Cenozoic history of the southern Rocky Mountains*: Geological Society of America Memoir 144, p. 75-94.
- Steven, T.A., and Eaton, G.P., 1975, Environment of ore deposition of the Creede mining district, San Juan Mountains, Colorado; Part I, Geologic, hydrologic, and geophysical setting: *Economic Geology*, v. 70, no. 6, p. 1023-1037.
- Steven, T.A., and Lipman, P.W., 1976, Calderas of the San Juan volcanic field, southwestern Colorado: U.S. Geological Survey Professional Paper 958, 35 p.
- Steven, T.A., and Ratté, J.C., 1960, Relation of mineralization to caldera subsidence in the Creede district, San Juan Mountains, Colorado, in *Short papers in the geological sciences*: U.S. Geological Survey Professional Paper 400-B, p. B14-B17.
- 1965, Geology and structural control of ore deposition in the Creede district, San Juan Mountains, Colorado: U.S. Geological Survey Professional Paper 487, 90 p.
- Van Loenen, R.E., 1980, Inesite, a new U.S. occurrence near Creede, Mineral County, Colorado: *Mineralogical Record*, v. 11, no. 1, p. 35-36.
- Vergo, Norma, 1987, Wall rock alteration at the Bulldog Mountain Mine, Creede, Colorado [abs.]: *Geological Society America, Abstracts with Programs*, v. 19, no. 5, p. 340.
- Wetlaufer, P.H., 1977, Geochemistry and mineralogy of the carbonates of the Creede mining district, Colorado: U.S. Geological Survey Open-File Report 77-706, 134 p.
- Winter, G.A., Essene, E.J., and Peacor, D.R., 1981, Carbonates and pyroxenoids from the manganese deposit near Bald Knob, North Carolina: *American Mineralogist*, v. 66, p. 278-298.

SELECTED SERIES OF U.S. GEOLOGICAL SURVEY PUBLICATIONS

Periodicals

- Earthquakes & Volcanoes** (issued bimonthly).
Preliminary Determination of Epicenters (issued monthly).

Technical Books and Reports

Professional Papers are mainly comprehensive scientific reports of wide and lasting interest and importance to professional scientists and engineers. Included are reports on the results of resource studies and of topographic, hydrologic, and geologic investigations. They also include collections of related papers addressing different aspects of a single scientific topic.

Bulletins contain significant data and interpretations that are of lasting scientific interest but are generally more limited in scope or geographic coverage than Professional Papers. They include the results of resource studies and of geologic and topographic investigations, as well as collections of short papers related to a specific topic.

Water-Supply Papers are comprehensive reports that present significant interpretive results of hydrologic investigations of wide interest to professional geologists, hydrologists, and engineers. The series covers investigations in all phases of hydrology, including hydrogeology, availability of water, quality of water, and use of water.

Circulars present administrative information or important scientific information of wide popular interest in a format designed for distribution at no cost to the public. Information is usually of short-term interest.

Water-Resources Investigations Reports are papers of an interpretive nature made available to the public outside the formal USGS publications series. Copies are reproduced on request unlike formal USGS publications, and they are also available for public inspection at depositories indicated in USGS catalogs.

Open-File Reports include unpublished manuscript reports, maps, and other material that are made available for public consultation at depositories. They are a nonpermanent form of publication that may be cited in other publications as sources of information.

Maps

Geologic Quadrangle Maps are multicolor geologic maps on topographic bases in 7.5- or 15-minute quadrangle formats (scales mainly 1:24,000 or 1:62,500) showing bedrock, surficial, or engineering geology. Maps generally include brief texts; some maps include structure and columnar sections only.

Geophysical Investigations Maps are on topographic or planimetric bases at various scales; they show results of surveys using geophysical techniques, such as gravity, magnetic, seismic, or radioactivity, which reflect subsurface structures that are of economic or geologic significance. Many maps include correlations with the geology.

Miscellaneous Investigations Series Maps are on planimetric or topographic bases of regular and irregular areas at various scales; they present a wide variety of format and subject matter. The series also includes 7.5-minute quadrangle photogeologic maps on planimetric bases that show geology as interpreted from aerial photographs. Series also includes maps of Mars and the Moon.

Coal Investigations Maps are geologic maps on topographic or planimetric bases at various scales showing bedrock or surficial geology, stratigraphy, and structural relations in certain coal-resource areas.

Oil and Gas Investigations Charts show stratigraphic information for certain oil and gas fields and other areas having petroleum potential.

Miscellaneous Field Studies Maps are multicolor or black-and-white maps on topographic or planimetric bases for quadrangle or irregular areas at various scales. Pre-1971 maps show bedrock geology in relation to specific mining or mineral-deposit problems; post-1971 maps are primarily black-and-white maps on various subjects such as environmental studies or wilderness mineral investigations.

Hydrologic Investigations Atlases are multicolored or black-and-white maps on topographic or planimetric bases presenting a wide range of geohydrologic data of both regular and irregular areas; principal scale is 1:24,000, and regional studies are at 1:250,000 scale or smaller.

Catalogs

Permanent catalogs, as well as some others, giving comprehensive listings of U.S. Geological Survey publications are available under the conditions indicated below from the U.S. Geological Survey, Map Distribution, Box 25286, Bldg. 810, Federal Center, Denver, CO 80225. (See latest Price and Availability List.)

“**Publications of the Geological Survey, 1879–1961**” may be purchased by mail and over the counter in paperback book form and as a set of microfiche.

“**Publications of the Geological Survey, 1962–1970**” may be purchased by mail and over the counter in paperback book form and as a set of microfiche.

“**Publications of the U.S. Geological Survey, 1971–1981**” may be purchased by mail and over the counter in paperback book form (two volumes, publications listing and index) and as a set of microfiche.

Supplements for 1982, 1983, 1984, 1985, 1986, and for subsequent years since the last permanent catalog may be purchased by mail and over the counter in paperback book form.

State catalogs, “List of U.S. Geological Survey Geologic and Water-Supply Reports and Maps For (State),” may be purchased by mail and over the counter in paperback booklet form only.

“**Price and Availability List of U.S. Geological Survey Publications,**” issued annually, is available free of charge in paperback booklet form only.

Selected copies of a monthly catalog “New Publications of the U.S. Geological Survey” are available free of charge by mail or may be obtained over the counter in paperback booklet form only. Those wishing a free subscription to the monthly catalog “New Publications of the U.S. Geological Survey” should write to the U.S. Geological Survey, 582 National Center, Reston, VA 22092.

Note.—Prices of Government publications listed in older catalogs, announcements, and publications may be incorrect. Therefore, the prices charged may differ from the prices in catalogs, announcements, and publications.

